NTNU – Trondheim
Norwegian University of
Science and Technology

Earthquake Induced Behavior of Submerged Floating Tunnels with Tension Leg Anchorage

Birgir Indridason

Civil and Environmental Engineering (2 year)
Submission date: June 2013
Supervisor: Ragnar Sigbjørnsson, KT
Co-supervisor: Svein N Remseth, KT

Norwegian University of Science and Technology
Department of Structural Engineering

Department of Structural Engineering
Faculty of Engineering Science and Technology
NTNU- Norwegian University of Science and Technology

ACCESSIBILITY

OPEN

MASTER THESIS 2013

SUBJECT AREA:	DATE: 10.06.2013	NO. OF PAGES:130
Structural dynamics		(20+58+52)

TITLE:

Earthquake Induced Behavior of Submerged Floating Tunnels with Tension Leg Anchorage

Jordskjelvindusert Oppførsel av Neddykkede Rørbruer med Strekkstagforankring

BY:

Birgir Indridason

SUMMARY:
The purpose of this study is to examine the behavior of a submerged floating tunnel (SFT) anchored by tension legs and subjected to seismic excitation. A proposal of a tunnel crossing the Høgsfjord in Norway is used as a case for the finite element model. The tunnel was proposed as 1345m long with a cross section diameter of 11.3 m. Furthermore, the tunnel should lie 25m under the sea surface to enable regular sea traffic.

A seismic analysis of the SFT is performed using a pseudo-excitation method (PEM), which is based within the framework of random vibration methods. The coherency between different supports is studied, in particular the incoherence and wave passage effects. A simple constant incoherence model is introduced, for coherency between inter-components of motion. Three cases of the incoherence are then examined: (i) fully coherent, (ii) incoherent and, (iii) non-coherent. The seismic analysis is carried out for different velocities and angles of the propagating earthquake waves.

The structure is modeled in Abaqus, by using beam elements for both the tunnel and the tension legs. The fluid/structure interaction is modeled and its effects on the structure are discussed. The SFT is modeled with both vertical and inclined tension legs and the behavior of the models are investigated, with regard to seismic events. The seismic analysis is performed in Matlab, by developing m-scripts based on the system matrices generated in Abaqus.

The results from the analysis confirm the importance of accounting for the stochastic nature of seismic waves. Furthermore, the results suggest that submerged floating tunnels with tension leg anchoring are reliable when subjected to earthquake excitation. It is unlikely that earthquake action will be taken as the design load case for Norwegian conditions.

RESPONSIBLE TEACHER: Ragnar Sigbjörnsson

SUPERVISOR(S): Ragnar Sigbjörnsson, Svein N. Remseth

CARRIED OUT AT: Department of Structural Engineering, NTNU

Preface

This thesis is written as a part of two year Master's program in structural engineering at the Norwegian University of Science and Technology (NTNU) in Trondheim.

In the process of completing the thesis many challenges have arisen and many obstacles needed to be overcome. However, with the good guidance and theoretical preparation from NTNU and University of Iceland, these challenges were eventually overcome.

Much gratitude goes to Professor Ragnar Sigbjörnsson for his inspirational support and invaluable contribution to the project. Also, many thanks go to Professors Svein N. Remseth and Bernt J. Leira for their input in the process.

During the course of the project I was introduced to new fields of engineering, in which I previously had little experience. These fields included hydrodynamics and earthquake engineering, which proved to be essential part for the project. Working in these fields of engineering has been eye-opening and generated much interest and I am enthusiastic about further opportunities of exploring these fields.

Trondheim, June 10, 2013

Birgir Indridason

Abstract - English

The purpose of this study is to examine the behavior of a submerged floating tunnel (SFT) anchored by tension legs and subjected to seismic excitation. A proposal of a tunnel crossing the Høgsfjord in Norway is used as a case for the finite element model. The tunnel was proposed as $1345\,m$ long with a cross section diameter of $11.3\,m$. Furthermore, the tunnel should lie $25\,m$ under the sea surface to enable regular sea traffic.

A seismic analysis of the SFT is performed using a pseudo-excitation method (PEM), which is based within the framework of random vibration methods. The coherency between different supports is studied, in particular the incoherence and wave passage effects. A simple constant incoherence model is introduced, for coherency between inter-components of motion. Three cases of the incoherence are then examined: (i) fully coherent, (ii) incoherent and, (iii) non-coherent. The seismic analysis is carried out for different velocities and angles of the propagating earthquake waves.

The structure is modeled in Abaqus, by using beam elements for both the tunnel and the tension legs. The fluid/structure interaction is modeled and its effects on the structure are discussed. The SFT is modeled with both vertical and inclined tension legs and the behavior of the models are investigated, with regard to seismic events. The seismic analysis is performed in Matlab, by developing m-scripts based on the system matrices generated in Abaqus.

The results from the analysis confirm the importance of accounting for the stochastic nature of seismic waves. Furthermore, the results suggest that submerged floating tunnels with tension leg anchoring are reliable when subjected to earthquake excitation. It is unlikely that earthquake action will be taken as the design load case for Norwegian conditions.

Abstrakt - Norsk

Formålet med denne forskningsoppgaven er å studere jordskjelvindusert respons av forankrede og neddykkede rørbruer. Forslaget til en rørbru over Høgsfjorden blir modellert og undersøkt. Dette foreslaget inneholder en $1345\,m$ lang rørbru med tversnitts diameter $D = 11,3\,m$. Dessuten må brua ligge $25\,m$ under havflaten, slik å skipstrafikken ikke skal hindres.

Responsanalysen bygger på teorien om stokastiske svingninger hvor de seismiske bølgene blir modellert som stokastisk felt. I modelleringen blir det tatt hensyn til bølgeforplantnings-hastigheten samt bølgenes koherensstruktur. En modifisert koherens-modell er introdusert hvor det tas hensyn til kryss-komponent koherens i tillegg til auto-komponent koherensen. Generelt avtar koherensen med økende avstand mellom konstruksjonens støtte- og forankringspunkter samt med økende frekvens. Tre tilfeller er studert nærmere: (i) full koherent bølgefelt, (ii) delvis koherent bølgefelt som antas å være den mest eksakte beskrivelse, og (iii) fullstendig random (inkoherent) bølgefelt.

Konstruksjonen er modellert i Abaqus ved å bruke bjelkeelementer både for rørbrua og forankringssystemet. Det tas hensyn til fluid-struktur interaksjon i modelleringen og de effekter som den fører med seg diskuteres. To forskjellig forankringssystemer blir undersøkt: (i) skrå forspente forankringslinjer og (ii) vertikale forspente forankringslinjer. Den stokastiske responsanalyse blir utført i Matlab basert på m-skripter som ble utviklet for denne oppgaven, og er basert på systemmatrisene fra Abaqus.

De essensielle resultatene fra denne undersøkelsen understreker nødvendigheten av å ta hensyn til jordskjelvsbølgenes stokastiske natur. Videre antyder resultatene at neddykkede rørbruer med vertikale forankringslinjer er seismisk robuste konstruksjoner. Det vurderes som lite sannsynlig at jordskjelvsindusert respons vil utgjøre et dimensjonsgivende lasttilfelle under Norske forhold.

Contents

List of Symbols

Latin letters

$\mathbf{M}$ - Mass matrix
$\mathbf{C}$ - Damping matrix
$\mathbf{K}$ - Stiffness matrix
$\mathbf{r}$ - Structural response vector (Displacement)
$\dot{\mathbf{r}}$ - Structural response vector (Velocity)
$\ddot{\mathbf{r}}$ - Structural response vector (Acceleration)
$\mathbf{Q}(t)$ - Environmental load vector
$\mathbf{Q}_s$ - Seismic action
$\mathbf{Q}_h$ - Hydrodynamic action
$\mathbf{r}_0$ - Structural vibration amplitude
$\tilde{\mathbf{M}}$ - Mass matrix of the hydrodynamic system
$\tilde{\mathbf{C}}$ - Damping matrix of the hydrodynamic system
$\tilde{\mathbf{K}}$ - Stiffness matrix of the hydrodynamic system
dF - Transverse force from the hydroelastic system
C_D - Coefficient of drag
C_M - Coefficient of added mass
D - Diameter of the tunnel
$\mathbf{N}$ - Shape function
$\mathbf{F}(t)$ - hydrodynamic load vector
$\tilde{Q}_M$ - Inertia term of the consistent load vector
$\tilde{Q}_C$ - Damping term of the consistent load vector
$\mathbf{H}(\omega)$ - Frequency response transfer function
$\mathbf{m}(t)$ - Mass of the hydroelastic system in time domain
$\mathbf{c}(\mathbf{t})$ - Damping of the hydroelastic system in time domain
$\mathbf{k}(t)$ - Stiffness of the hydroelastic system in time domain
(t) - Impulse response function
S_{xx} - Auto power spectral density
S_{xy} - Cross spectral density
R_{xx} - Autocorrelation function
R_{xy} - Cross-correlation function
p -peak factor
n_+ - Number of upcrossings

T_d - Period of the strong earthquake load portion
$\ddot{u}_g$ - Ground acceleration
g - modulation function
$Z_{\ddot{u}_g}$ - Unfiltered non-stationary random process describing an earthquake
a - Unfiltered non-stationary random process describing an earthquake
E - Expected value
$\tilde{a}$ - ground acceleration of a structure
$\vec{a}_i$ - ground acceleration at each support
$\mathbf{S}$ - Spectral density matrix
c - Apparent wave velocity
A - Transformation matrx
r - Structural degrees of freedom
r_e - Degrees of freedom at the supports
r_i - Inner degrees of freedom of the structure
r_t - Total displacements of the structure
$r^{(s)}$ - Pseudo-static displacement
$\mathbf{M}_{ii}$ - Mass matrix containing inner degrees of freedom
$\mathbf{C}_{ii}$ - Damping matrix containing inner degrees of freedom
$\mathbf{K}_{ii}$ - Stiffness matrix containing inner degrees of freedom
$\mathbf{M}_{ee}$ - Mass matrix containing support degrees of freedom
$\mathbf{C}_{ee}$ - Damping matrix containing support degrees of freedom
$\mathbf{K}_{ee}$ - Stiffness matrix containing support degrees of freedom
$\mathbf{B}$ - Transformation matrix
$\mathbf{E}_{mN}$ - Orientation matrix
$\mathbf{e}_\beta$ - Orientation vector
N - Number of supports
$S_{\ddot{u}_g}$ - Auto-power spectral density of the ground acceleration
$S_{\dot{u}_g}$ - Auto-power spectral density of the ground velocity
$S_{\ddot{u}_g\dot{u}_g}$ - Cross spectral density of the ground acceleration and velocity
r_c - Outer radius of the tunnel cross section
r_c - Radius of the tension leg cross section
t - Thickness
A_s - Area of the tension leg cross section
E_c - Young's modulus of concrete
E_s - Young's modulus of steel

M_s - Surface wave magnitude of earthquake
S_0 - Amplitude of white noise acceleration
f_0 - Natural frequency of the system
a_i, b_i, c_i - Constants for Oliveira coherency model

Greek letters

ω - Angular frequency
ρ - density of fluid
α, β - Rayleigh damping coefficients
ω_i - Natural frequency for Rayleigh damping
ζ_i - Damping ratio
τ - Time lag
σ - Standard deviation
ξ - Distance
γ_{jk} - Coherency between supports j and k
θ_{jk} - Phase spectrum
Δt_{jk} - time lag between supports j and k
σ_r - Standard deviation of the response
$\sigma_{r_j r_k}$ - Co-variance between the response in two points
ρ_c - Material density of the tunnel
ρ_s - Material density of the tension legs
ρ_w - Density of sea water
ν_c - Poisson ratio of concrete
ν_s - Poisson ratio of steel
$\Delta\omega$ - frequency step of the analysis
ω_{gk} - natural frequency of the first Kanai-Tajimi filter
ω_{fk} - natural frequency of the second Kanai-Tajimi filter
ξ_{gk} - damping ratio of the first Kanai-Tajimi filter
ξ_{fk} - damping ratio of the second Kanai-Tajimi filter
β_i - Constant for Oliveira coherency model
α_i - Function for Oliveira coherency model

Abbreviations

NPRA - Norwegian Public Road Administration

SFT - Submerged floating tunnel
PEM - Pseudo excitation method
PSD - Power spectral density
DOF - Degrees of freedom
PGA - Peak ground acceleration

List of Figures

List of Tables

1 Introduction

In the modern society, the demand of direct and efficient transportation is continuously increasing. Long span bridges and tunnels are being constructed all around the world and there are more to come. In Norway there is particularly much interest in improving transportation. Due to the difficult landscapes these improvements can often be technically challenging. However, there are plans of connecting the coastal highway route from Trondheim to Kristiansand (NPRA, 2012), which would mean constructing links over fjords that are so wide and deep that they could require groundbreaking technology. The concept of a submerged floating tunnel (SFT) could be a solution for these crossings.

A submerged floating tunnel is, like bridges and tunnels, a direct connection between two locations separated by water. However, the SFT is a tube which floats submerged in water, deep enough so it doesn't effect ship traffic but not so deep that water pressure becomes an issue. A 25-30m clearance from the water surface is commonly suggested. While bridges are somewhat limited in length due to gravity, the buoyancy of the SFT counterparts gravity and enables longer crossings. However, SFTs are subjected to many kinds of environmental actions, generated by phenomena such as traffic, currents, waves, earthquakes, corrosion and marine growth. The impact these actions make on SFTs need to be carefully researched before such a structure can be realized. In this study special attention is given to earthquake actions, which could turn out to be problematic for such structures.

1.1 Submerged floating tunnel concepts

Floating submerged in water over long distances, the SFTs are generally vulnerable to environmental loads. Therefore, some kind of anchoring is essential to ensure required stiffness of the structure. Three main components of such structures can be acknowledged (FEHRL, 1996): The tube, anchoring, and shore connections.

The tube accommodates the traffic and needs to be held waterproof. The anchoring is responsible for preventing to much transverse movement, which could pose much uncomfort to passengers travelling through the tunnel. Two anchoring methods are commonly proposed, pontoons that connect the tunnel straight to the sea surface

Figure 1: The submerged floating tunnel concept (NPRA, 2012)

and tension legs that anchor the tunnel straight to the seabed. Both methods are effective of ensuring sufficient vertical stiffness, while leaving the tunnel vulnerable to horizontal movement. It is possible to address this issue partly by curving the tunnel or more efficiently by inclining the tension legs. This study examines a SFT anchored by tension legs, both vertical and inclined.

1.2 Literature survey

The concept of a submerged floating tunnel has been discussed for over a century. Sir Edward James Reed (1886) wrote a paper on his invention and gave rather detailed explanation of the concept. Andrew (1951) proposed a SFT crossing the Puget sound near Seattle, USA, which received much critique from scientists overseas. In the late 1960's increased interest was shown in the subject. A committee of recognized engineers was formed in Norway, which explored the possibility for SFT as a crossing method for Norwegian fjords (Brandtzæg *et al.* , 1971). The committee came to the conclusion that SFTs can be a suitable method for crossing many wide and deep fjords, which otherwise could hardly be crossed. Despite doing extensive work on the study, they suggested that further study was advisable. They recommended finding a location as a potential construction site for such tunnels. In 1971 a British proposal of a SFT, lead by Alan Grant, won first price in a competition of methods for crossing the Messina strait, Italy. To this day many studies have used this strait proposal as a case for their SFT analysis (Di Pilato *et al.* , 2008; Martire *et al.* , 2010, 2012; Fogazzi & Perotti, 2000). These studies examine the influence of seismic excitation, due to the high seismicity in the area. Furthermore, in the 1980's a project of crossing the Høgsfjord was started and

extensive research was carried out by four of the largest Norwegian contractors (Jakobsen, 2010). Which led the approval of SFTs as an feasible crossing method by the Norwegian Public Road Administration (Larssen & Jakobsen, 2010).

Remseth *et al.* (1999) performed stochastic dynamic response analysis of a SFT subjected to wave loading, where various methods are presented. They reached the conclusion that modeling the correct structural and hydrodynamic damping is crucial, as well as choosing the optimal buoyancy. Mazzolani *et al.* (2008) introduced a proposed 100 m prototype of a SFT in Qiandao lake (PR of China), he illustrated the type of actions generally subjected to such structures and performed a numerical analysis of the prototype's model. Martinelli *et al.* (2011) performed a seismic analysis of a SFT anchored by cables by addressing the spatial variability with a single coherency function. Martire *et al.* (2012) carried out a finite element analyses of SFTs differing in length and anchoring systems. Di Pilato *et al.* (2008) performed a dynamic analysis of a tension leg anchored SFT, subjected to hydrodynamic and seismic action. Where he used extreme cases of both hydrodynamic and seismic loading. Chen & Huang (2010) studied the wave passage effect on SFTs for low velocities of the seismic waves. They concluded that response was larger for multi-support excitation than uniform excitation of the seismic load. Xiao & Huang (2010) performed a seismic analysis of SFTs where they investigated effects of various shore connections to the seismic response. Their results suggest that the response for fixed shore connections is by far the largest. Furthermore, Zhang *et al.* (2009) used a psuedo-excitation method (PEM) to compute structural response for a suspension bridge, where he considered the effects of spatial variability of ground motions.

Numerous feasibility studies have been proposed (Kanie, 2010; Jakobsen, 2010; Larssen & Jakobsen, 2010; Skorpa, 2010; Tveit, 2010; Østlid, 2010), where various topics about SFTs are evaluated. These include anchoring alternatives, design challenges, safety considerations etc. Most of these studies came to the conclusion that SFT is a concept worth pursuing and many cited it as a suitable method for crossing the Norwegian fjords. A risk analysis study has also been performed regarding the SFT concept (Xiang *et al.* , 2010). The results of the study suggest that design, cost and management risk is of most concern, while the environmental risk is of less concern.

1.3 Selection of study case - The Høgsfjord tunnel proposal

In the 1980's a concept of crossing the 1400 m long Høgsfjord was brought to existence by politicians in Rogaland, Norway. The idea was to connect the districts of Ryfylke and Nord-Jæren for car traffic and thereby, replace the ferries operating on the site. The proposed crossing site was between Oanes and Lauvvik.

During the period of 1987-1999 the submerged floating tunnel concept was the preferred crossing method over the Høgsfjord. Tens of millions Norwegian kroner were put into research of the concept by the Norwegian authorities. Approval had been given to regard SFTs as a feasible crossing method by the Norwegian Public Road Administration. However, in the year of 2000 the Rogaland county dropped the idea and postponed all plans of crossing the fjord. The decision was to start over and investigate more alternatives for improvements of transportation in the area (Jøssang, 2005).

Although, the Høgsfjord tunnel has not yet been realized, there are still plenty of crossings all over the world where SFTs are a viable option. The deep and wide Sognefjord, often regarded as the ultimate Norwegian challenge, has generated discussions of a SFT being the possible solution (NPRA, 2011). The Messina strait in Italy has also been mentioned and even a transatlantic tunnel between Europe and America (Giotta, 2003), which would operate a train in vacuum traveling across the Atlantic ocean in the matter of hours.

While a transatlantic tunnel is an interesting concept, this study will focus on more realistic projects such as the Høgsfjord tunnel. A project of such manageable magnitude needs to be realized and tested before futuristic projects, like the transatlantic tunnel, can be further evaluated.

1.4 Objectives and research questions

This study examines the seismic response of the Høgsfjord tunnel by using the pseudo-excitation method and incorporating incoherence and wave passage effects in the seismic analysis. Three cases of incoherence are considered: (i) Fully coherent, (ii) incoherent and (iii) non-coherent. The incoherence effect is extended

to account for the incoherence between components of motion, at each given support. This effect is called the inter-component coherency which has up to now mostly been neglected in similar studies. In this study, a simple constant model is proposed using records from the 2008 earthquake in Ölfus, Iceland (Sigbjörnsson *et al.* , 2013).

The response of the model subjected to earthquake excitation is investigated for inclined versus vertical tension legs. The importance of structural and hydrodynamic damping is examined and the influence of added mass is discussed. The displacement, velocity and acceleration response are evaluated and the impact on both structural and public safety is discussed.

1.5 Limitations and organisation of the thesis

This study focuses on the behavior of SFTs undergoing seismic excitation. Other kinds of environmental actions are neglected. Including sea currents and waves, which could impact the structural behavior greatly. Furthermore, the performance of structural parts are not investigated. That includes the bending moment and axial force along the tunnel. Only one acceleration spectral density curve was created and excited to all supports, which could be regarded as a weakness in the modeling.

In the following chapters the theoretical background is presented, both regarding the fluid/structure interaction and the seismic action. Furthermore, detailed description of the modeling is provided. Where the program Abaqus (SIMULIA, 2011) was utilized for the geometric modeling and further evaluation was performed in Matlab (MATLAB, 2010). Finally, the results are presented and discussed and some further studies suggested.

2 Modelling of the fluid-structure system

Structural properties of a submerged floating tunnel have to be carefully modeled in order to correctly describe the behavior of the structure. The interaction between fluid and structure is an important factor in the modeling, as the water will generate forces proportional to the acceleration and velocity, against all motions of the structure. This chapter describes the representation of such effects, as well as some solution methods.

2.1 FE model of the submerged tunnel

The equation of motion within the framework of finite element modelling (Wilson, 2002) of the SFT can be described as follows:

$$\mathbf{M}\ddot{\mathbf{r}} + \mathbf{C}\dot{\mathbf{r}} + \mathbf{K}\mathbf{r} = \mathbf{Q}(t) \tag{2.1}$$

where $\mathbf{M}$, $\mathbf{C}$ and $\mathbf{K}$ are the structural system matrices, $\mathbf{r}$ is the structural response and $\mathbf{Q}$ is the environmental interaction vector, which includes seismic action $\mathbf{Q}_s$ and hydrodynamic action $\mathbf{Q}_h$:

$$\mathbf{Q}(t) = \mathbf{Q}_s(t) + \mathbf{Q}_h(t) \tag{2.2}$$

As discussed in the following, these interaction forces are depending on the structural response, i.e. the structural velocity and acceleration.

2.2 Hydrodynamic and hydroelastic action

The behavior of a structure changes significantly when it is submerged in water, due to the fluid-structure interaction. Since this study examines the dynamics of a fully submerged tunnel, this issue needs to be considered. The following expressions describe a method used to account for the hydrodynamic action (Wilson, 2003; Naess & Moan, 2013).

It is possible to express the fluid-structure interaction $\mathbf{Q}_h(t)$, induced by a "monochromatic" small amplitude harmonic vibration, as proportional to $exp(i\omega t)$ by the following linear equation:

$$\mathbf{Q}_h(t) = \left\{-\omega^2\,\mathbf{M}^{(h)}(\omega) + i\omega\,\mathbf{C}^{(h)}(\omega) + \mathbf{K}^{(h)}(\omega)\right\}\mathbf{r}_0 exp(i\omega t) \tag{2.3}$$

where ω is the frequency of the harmonic vibration; $\mathbf{M}^{(h)}$ is commonly denoted the hydrodynamic mass or added mass; $\mathbf{C}^{(h)}$ is the hydrodynamic damping originating from refracted waves; $\mathbf{K}^{(h)}$ is the restoring force and $\mathbf{r}_0$ is the structural vibration amplitude. It is noted that the added mass and hydrodynamic damping is in general frequency dependent (Faltinsen, 1990). Substituting Eq. 2.3 into Eq. 2.1 and rearranging the terms gives:

$$[\mathbf{M} - \mathbf{M}^{(h)}(\omega)]\ddot{\mathbf{r}} + [\mathbf{C} - \mathbf{C}^{(h)}(\omega)]\dot{\mathbf{r}} + [\mathbf{K} - \mathbf{K}^{(h)}(\omega)]\mathbf{r} = \mathbf{Q}_s exp(i\omega t) \tag{2.4}$$

Hence, the hydroelastic system can be modelled in terms of the classical dynamic equation (Eq. 2.1), by introducing $\tilde{\mathbf{M}} = [\mathbf{M} - \mathbf{M}^{(h)}(\omega)]$ as the system mass matrix; $\tilde{\mathbf{C}} = [\mathbf{C} - \mathbf{C}^{(h)}(\omega)]$ as the system damping matrix; $\tilde{\mathbf{K}} = [\mathbf{K} - \mathbf{K}^{(h)}(\omega)]$ as the system stiffness matrix; and $\mathbf{r} = \mathbf{r}_0 exp(i\omega t)$ is the system response. The complexity of this equation compared with Eq. 2.1 is apparently primarily related to the frequency dependence of the system matrices. However, within the framework of linear systems subjected to single harmonic excitation this does not pose any difficulties in the response analysis.

2.2.1 Morison's equation

The components of the hydrodynamic force vector (see Eq. 2.3), specifically the added mass and the hydrodynamic damping, have to be determined in order to solve the system equations of the submerged system. The most common way to do so is by using the Morison's equation (Morison *et al.* , 1950; Faltinsen, 1990). The transverse force dF on the strip dx of a cylindrical element, can be calculated using the modified Morison's equation:

$$dF = \frac{1}{2}C_D D dx\,(\dot{u} - \dot{r})|\dot{u} - \dot{r}| + \frac{\pi}{4}\rho C_M D^2\,dx\,\ddot{u} - \frac{\pi}{4}\rho(C_M - 1)D^2\,dx\,\ddot{r} \tag{2.5}$$

where ρ is the density of the fluid, D is the diameter of the tunnel, $\dot{r}$ and $\ddot{r}$ are the motions of the tunnel, $\dot{u}$ and $\ddot{u}$ are the motions of the surrounding water, C_M and C_D are the coefficients of inertia and drag. Since, no external water motions are assumed in this study, Equation 2.5 can be rewritten as:

$$dF = -\frac{1}{2}C_D D\, dx\, \dot{r}|\dot{r}| - \frac{\pi}{4}\rho(C_M - 1)D^2\, dx\, \ddot{r} \tag{2.6}$$

where fluid induced damping and inertia properties are expressed in the two distinct parts of Eq. 2.6. The latter part of describes added mass $\mathbf{M}^h(\omega)$ while the former describes the hydrodynamic damping $\mathbf{C}^h(\omega)$. It is noted that the damping part of Eq. 2.6 is nonlinear, which creates a problem carrying out the analysis. Therefore, it is convenient to linearize this property. Langen & Sigbjörnsson (1979) describe a stochastic linearization of the damping component, which leads to the following representation of the Morison's equation (2.5):

$$dF = -\frac{8}{3\pi}\omega C_D D r_0\, dx\, \dot{r} - \frac{\pi}{4}\rho(C_M - 1)D^2\, dx\, \ddot{r} \tag{2.7}$$

in which r_0 is the response amplitude. By means of Eq. 2.7 the force component dF can be integrated along the length of the structure to obtain the consistent load vector, which includes the added mass $\mathbf{M}(\omega)$ and the hydrodynamic damping $\mathbf{C}(\omega)$ (Liu & Quek, 2003):

$$\tilde{Q}(t) = \int_L \mathbf{N}^T \mathbf{F}(t) dx \tag{2.8}$$

where the force vector $\mathbf{F}(t)$ is:

$$\mathbf{F}(t) = \{dF_x \;\; dF_y \;\; dF_y \;\; dF_{\theta_x} \;\; dF_{\theta_y} \;\; dF_{\theta_z}\}^T \tag{2.9}$$

Here, $dF_i, (i = x, y, z)$ are the force components, and $\mathbf{N}$ is the shape function. The fluid-structure interaction for motions along, and rotations around, the axis of the tunnel are neglected, i.e. $dF_x = 0$ and $dF_{\theta_x} = 0$.

The response of the structure, as expressed in the Morison's equation (Eqs. 2.5-2.7), can be written as $\dot{r}(x) = \mathbf{N}(x)\dot{\mathbf{r}}$ and $\ddot{r}(x) = \mathbf{N}(x)\ddot{\mathbf{r}}$, (Liu & Quek, 2003). Including

this in Eq. 2.8 gives a full description of the consistent load vectors $\tilde{Q}_M(t)$ and $\tilde{Q}_C(t)$:

$$\tilde{Q}_M(t) = C_A(\omega) \int_L \mathbf{N}^T \mathbf{N}(t) dx \, \ddot{\mathbf{r}} = \mathbf{M}^{(h)}(\omega) \ddot{\mathbf{r}} \tag{2.10}$$

$$\tilde{Q}_C(t) = C_B(\omega) \int_L \mathbf{N}^T \mathbf{N}(t) dx \, \dot{\mathbf{r}} = \mathbf{C}^{(h)}(\omega) \dot{\mathbf{r}} \tag{2.11}$$

Here, $C_A(\omega) = -\pi\rho C_M D^2/4$ and $C_B(\omega) = -8\omega C_D D/3\pi$ are coefficients for inertia and damping properties. Since $K^{(h)}(\omega)$ is the restoring force, or in this particular case simply the buoyancy force of the tunnel, all terms in Eq. 2.4 have been introduced and a solution of the system can be obtained. Note, that the restoring force is written as frequency dependent. However, for this particular system it can be accurately expressed as frequency independent.

2.2.2 Random behavior

Up to now the motion has been treated as monochromatic single component harmonic motion. However, in real situation, random response characteristics must be modelled for all responding frequencies of the structure. Since the hydrodynamically modified system matrices are frequency dependent (see Eq. 2.4), the principle of superposition can be utilized in order to obtain structural response for the system. Utilizing this method is a common practice in dynamic analysis and it describes linear systems with excellent accuracy.

2.3 Damping properties

To represent damping in the structural model, Rayleigh damping can be considered. At a global level it is a linear combination of the mass and the stiffness matrix (Chopra, 2012; Cook *et al.* , 2002).

$$\mathbf{C} = \alpha\mathbf{M} + \beta\mathbf{K} \tag{2.12}$$

The coefficients α is mass proportional and β is stiffness proportional. The two coefficients can be determined by introducing two natural frequencies ω_i and appropriate critical damping ratios ζ_i.

$$\alpha = \frac{2\omega_1\omega_2(\zeta_2\omega_1 - \zeta_1\omega_2)}{\omega_1^2 - \omega_2^2} \tag{2.13}$$

$$\beta = \frac{2(\zeta_1\omega_1 - \zeta_2\omega_2)}{\omega_1^2 - \omega_2^2} \tag{2.14}$$

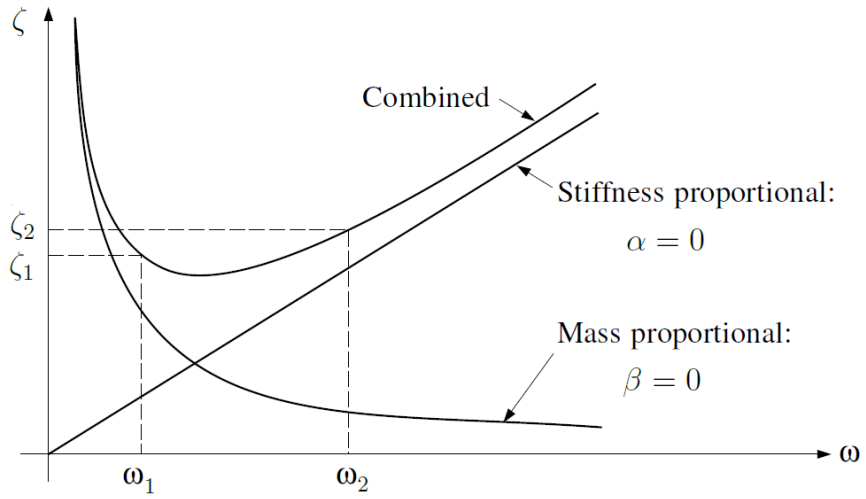

Figure 2: Rayleigh damping presented graphically (Clough & Penzien, 2010)

Alternative methods for modeling the structural damping exist. One of these is the Caughey damping and another is Wilson-Penzien damping, which uses superposition of modal damping matrices (Caughey, 1960; Wilson & Penzien, 1972).

2.4 Solution procedures

For a particular solution of the system, Eq. 2.4 needs to be solved. Solution procedures are generally represented either in the time domain or the frequency domain. These representations are expressed in the following sections.

2.4.1 Frequency domain solution

The easiest procedure is solving Eq. 2.4 in the frequency domain. This procedure is widely used. It describes the response as a harmonic function $\mathbf{r} = \mathbf{r}_0(\omega)exp(i\omega t)$, which by substitution into Eq. 2.4 gives the following equation:

$$[\tilde{\mathbf{K}}(\omega) - \omega^2\tilde{\mathbf{M}}(\omega) + i\omega\tilde{\mathbf{C}}(\omega)]\mathbf{r}_0(\omega) = \mathbf{Q}_s \tag{2.15}$$

Note that the response amplitude $\mathbf{r}_0(\omega)$ is a complex quantity to preserve the phase information of the response.

Furthermore, the matrices $\tilde{\mathbf{K}}$, $\tilde{\mathbf{M}}$ and $\tilde{\mathbf{C}}$ are the hydrodynamically modified system matrices introduced with Eq. 2.4. The particular solution of the response is obtained by solving:

$$\mathbf{r}_0(\omega) = \mathbf{H}(\omega)\mathbf{Q}_s \tag{2.16}$$

where the frequency response function $\mathbf{H}(\omega)$ is:

$$\mathbf{H}(\omega) = [\tilde{\mathbf{K}}(\omega) - \omega^2\tilde{\mathbf{M}}(\omega) + i\omega\tilde{\mathbf{C}}(\omega)]^{-1} \tag{2.17}$$

It should be noted, that the above presentation is a linear solution method and only valid for the monochromatic harmonic waves. However, the environmental action is not described accurately by these harmonic waves, that includes the seismic action which is a non-stationary random process. However, it is possible to generalize the excitation into finite number of linear systems, using the principle of superposition, which represents the excitation as a sum of finite number of harmonic components.

This study will focus on solving the system equation in the frequency domain as it is associated with the pseudo-excitation method which is utilized to induce seismic action on the structure.

2.4.2 Time domain solution

While the frequency domain solution is practical and easy to use, it doesn't always give the most accurate results for nonlinear systems. For these problems a solution method in the time domain can be feasible. A short description of the time domain alternative is given in the following.

A general time domain representation can be expressed by taking the inverse Fourier transform of Equation 2.16 which leads to the integro-differential equation (Langen & Sigbjörnsson, 1980):

$$\int_{-\infty}^{\infty} \mathbf{m}(t-\tau)\ddot{\mathbf{r}}(\tau)d\tau + \int_{-\infty}^{\infty} \mathbf{c}(t-\tau)\dot{\mathbf{r}}(\tau)d\tau + \int_{-\infty}^{\infty} \mathbf{k}(t-\tau)\mathbf{r}(\tau)d\tau = \mathbf{q}(t) \quad (2.18)$$

where $\mathbf{q}(t)$ is the time dependent load vector. Furthermore, the mass, damping and stiffness of the hydroelastic system, in the time domain, can be described as:

$$\mathbf{m}(t) = \frac{1}{2\pi}\int_{-\infty}^{\infty} \left[\mathbf{M} - \mathbf{M}^{(h)}(\omega)\right] exp(i\omega t)d\omega \quad (2.19)$$

$$\mathbf{c}(t) = \frac{1}{2\pi}\int_{-\infty}^{\infty} \left[\mathbf{C} - \mathbf{C}^{(h)}(\omega)\right] exp(i\omega t)d\omega \quad (2.20)$$

$$\mathbf{k}(t) = \frac{1}{2\pi}\int_{-\infty}^{\infty} \left[\mathbf{K} - \mathbf{K}^{(h)}(\omega)\right] exp(i\omega t)d\omega \quad (2.21)$$

This leads to the particular solution of the system, which can be expressed as:

$$\mathbf{r}(t) = \int_{-\infty}^{\infty} \mathbf{h}(t-\tau)\mathbf{q}(\tau)d\tau \quad (2.22)$$

where the function $\mathbf{h}(t)$ is the impulse response function, which can be written as follows, in terms of the frequency dependent transfer function $\mathbf{H}(\omega)$ expressed in Eq. 2.17

$$\mathbf{h}(t) = \frac{1}{2\pi}\int_{-\infty}^{\infty} \mathbf{H}(\omega)exp(i\omega t)d\omega \quad (2.23)$$

Time domain solution can be seismic analysis. However, it is more computationally expansive than the frequency domain solution and does not necessarily give better results.

3 Seismic action

In areas of high seismic activity, the earthquake action can be critical for the design of a structure. Nevertheless, earthquakes of high magnitude will potentially cause great damage to a structure, even though the probability of such events occurring within the structures lifetime is minimal. Therefore, most structural design codes require only to prevent damage for medium sized earthquake during its lifetime. The seismic design of a structure accounts for the two following criteria (Clough & Penzien, 2010):

1. A moderate sized earthquake, expected to occur once during a lifetime of a structure, is taken to be the basis of design. The structure should survive the occurrence of such event without significant damages.

2. To measure the structural safety, the largest potential earthquake at the site is used as a benchmark. Due to the low probability of the incident, the structure is allowed to endure significant damages, while preventing injuries of people and total collapse.

The guidelines mentioned above are widely used in the world and are meant to account for both the low probability of a severe earthquake and the injuries of people. Furthermore, preventing severe damage for earthquakes of the second type, for expensive structures with long lifetimes, has become desirable in recent years. In order to prevent costly restorations and repairs. The design of a submerged floating tunnel could be characterized as a structure of such importance. Therefore, seismic analyses for SFTs are of high importance, even for areas of relatively low seismicity such as Norway.

3.1 Modeling of strong ground motions

Modeling of the strong ground motion is an important step in seismic analysis. In order to measure the response in a structure, a suitable representation of the ground acceleration needs to be implemented. This could either be by generating time series for the ground acceleration, if a solution method in the time domain is utilized, or by generating a power spectral density (PSD) curves for solutions in the frequency domain. This study focuses primarily on the latter. In the

following expressions the spectral density functions are presented and discussed briefly (Zerva, 2009; Vanmarcke, 2010; Lin & Zhang, 2007). The auto-PSD $S_{xx}(\omega)$ and the autocorrelation function $R_{xx}(\omega)$, of a stationary random process $x(t)$, are commonly written as a Fourier transform pair:

$$S_{xx}(\omega) = \frac{1}{2\pi} \int_{-\infty}^{\infty} R_{xx}(\tau) exp[-i\omega\tau] d\tau \tag{3.1}$$

$$R_{xx}(\omega) = \frac{1}{2\pi} \int_{-\infty}^{T} S_{xx}(\omega) exp[-i\omega\tau] d\omega \tag{3.2}$$

where $R_{xx}(\tau)$ is the smoothed auto-correlation function and ω is the frequency (in rad/s). Similarly the cross spectral density, of the ergodic stationary random processes $x(t)$ and $y(t)$ can be written as:

$$S_{xy}(\omega) = \frac{1}{2\pi} \int_{-\infty}^{\infty} R_{xy}(\tau) exp[-i\omega\tau] d\tau \tag{3.3}$$

where $R_{xy}(\tau)$ is the smoothed cross-correlation function, ω is the frequency (in rad/s) and τ is the time lag between the processes $x(t)$ and $y(t)$ respectively.

3.1.1 Probabilistic modeling

When inducing structures with environmental action, which can be characterized by a stochastic process, the statistical properties of the process are useful. These properties can be easily obtained for an Gaussian ergodic and stationary random process, which is described in more detail in (Lin & Zhang, 2007). The variance of a zero mean stationary random process $x(t)$ can be expressed as:

$$\sigma_x^2 = \int_{-\infty}^{\infty} S_{xx} d\omega \tag{3.4}$$

where S_{xx} is the auto-PSD introduced in Eq. 3.1. The peak factor is given as follows (Cartwright & Longuet-Higgins, 1956):

$$p = \sqrt{2\ln(2n_+T_d)} + \frac{0.5772}{\sqrt{2\ln(2n_+T_d)}} \tag{3.5}$$

Where T_d is the period of the earthquake load portion and n_+ is number of zero up-crossings:

$$n_+ = \frac{1}{2\pi}\sigma_{\dot{x}}/\sigma_x \tag{3.6}$$

Earthquake records are, strictly speaking, a non-stationary random process, i.e. their statistical properties vary with time. Even so, in most cases these records can be assumed to be both ergodic and stationary random processes, as most structures have fundamental periods that are much shorter than the duration of the earthquake. However, that is not necessarily the case for long span structures, such as the proposed SFT, which can have important periods in the time range of the earthquakes duration. For these structures, the seismic excitation, shows clear signs of a non-stationary random process. For these situations, the seismic response can be calculated efficiently by using PEM (Lin & Zhang, 2007), which includes both the wave-passage and the incoherence effect of the multi-support structure.

3.1.2 Evolutionary processes

Some non-stationary random processes, where statistical properties vary with time, can be approximated as an evolutionary processes (Priestley, 1965). An evolutionary process can be modeled by operating on stationary random processes, and is commonly expressed in terms of the Riemann-Steiljes integral (Langen & Sigbjörnsson, 1979):

$$\ddot{u}_g(t) = \int g(\omega, t) exp(i\omega t) dZ_{\ddot{u}_g}(\omega) \cong g(t)a(t) \tag{3.7}$$

To avoid computational complexities, the evolutionary process is often handled by a uniform modulation function $g(t)$, instead of the nonuniform frequency and time varying modulation process $g(\omega, t)$. Such modulation process is explained in Figure 3. This study will be focused on the uniform modulation assumption.

In Eq. 3.7, $\ddot{u}_g(t)$ and $Z_{\ddot{u}_g}(\omega)$ are non-stationary random processes that describe the ground motion of a typical earthquake event; $g(\omega, t)$ is deterministic modulating

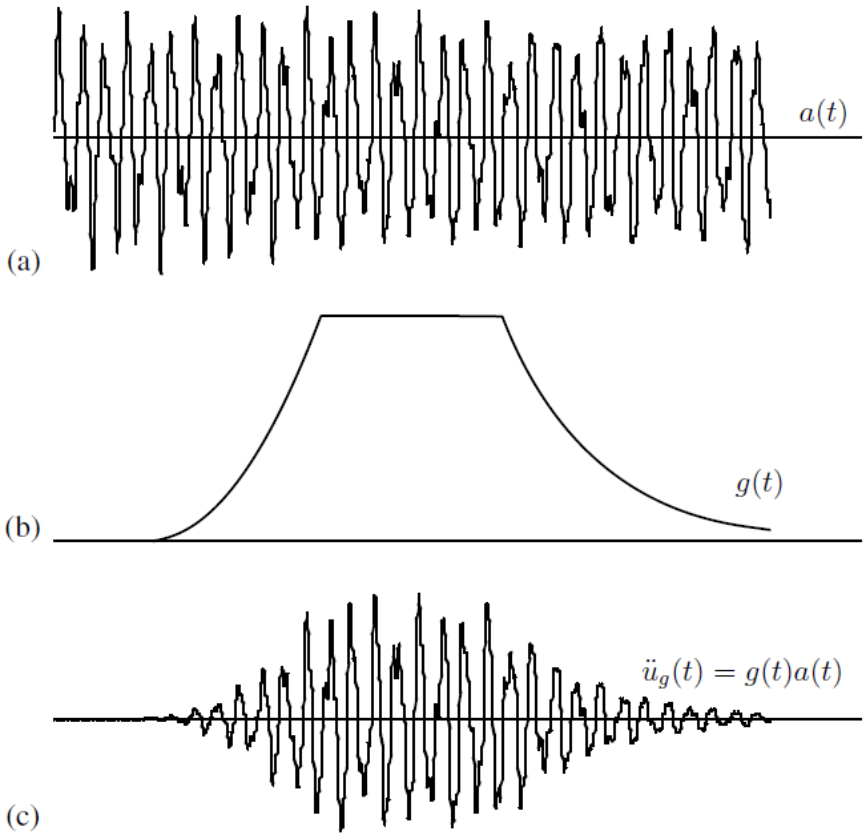

Figure 3: Uniformly modulated ground acceleration time series $\ddot{u}_g(t)$ (Lin & Zhang, 2007)

function varying with both time and frequency; and $a(t)$ is commonly described as follows:

$$a(t) = \int exp(i\omega t) dZ_{\ddot{u}_g}(\omega) \tag{3.8}$$

This process turns stationary and homogeneous if the increments of $Z_{\ddot{u}_g}(\omega)$ have zero mean and are orthogonal, which implies:

$$E[dZ_{\ddot{u}_g}(\omega)] = 0 \tag{3.9}$$

$$E[dZ_{\ddot{u}_g}(\omega_j) dZ^{T*}_{\ddot{u}_g}(\omega_k)] = S_{jk}(\omega)\delta_{jk} d\omega \tag{3.10}$$

Here, $S_{jk}(\omega)$ is the PSD function between the supports j and k, further described in Eq. 3.19 and δ_{jk} is the Kronecker delta function. The PSD function of the ground motion $\ddot{u}_g(t)$ is given by:

$$S_{\ddot{u}_g}(\omega, t) = |g(t)|^2 S_{jk}(\omega) \tag{3.11}$$

The velocity spectra is obtained by dividing by ω^2:

$$S_{\dot{u}_g}(\omega, t) = \frac{1}{\omega^2} S_{\ddot{u}_g}(\omega, t) \tag{3.12}$$

and the cross spectra $S_{\ddot{u}_g\dot{u}_g}$ and $S_{\dot{u}_g\ddot{u}_g}$ of the velocity and acceleration is:

$$S_{\ddot{u}_g\dot{u}_g}(\omega, t) = i\frac{1}{\omega^2} S_{\ddot{u}_g}(\omega, t) \tag{3.13}$$

$$S_{\dot{u}_g\ddot{u}_g}(\omega, t) = -i\frac{1}{\omega^2} S_{\ddot{u}_g}(\omega, t) \tag{3.14}$$

The the variance of the auto-PSD functions is expressed as:

$$\sigma^2_{\ddot{u}_g}(t) = \int_{-\infty}^{\infty} S_{\ddot{u}_g} d\omega = \int_{-\infty}^{\infty} |g(t)|^2 S_{jk}(\omega) \tag{3.15}$$

$$\sigma^2_{\dot{u}_g}(t) = \int_{-\infty}^{\infty} \frac{1}{\omega^2} S_{\ddot{u}_g} d\omega = \int_{-\infty}^{\infty} \frac{1}{\omega^2} |g(t)|^2 S_{jk}(\omega) \tag{3.16}$$

Statistical response for the seismic analysis can be computed using the variance functions expressed in Eqs. 3.15-3.16. The expected peak value can be obtained by utilizing the product of the peak factor (see Eq. 3.5) and the standard deviation derived from the variance functions.

3.2 Description of the spatial variability of ground motion

The seismic ground motion is assumed to be locally stationary and homogeneous random process. The ground acceleration of a structure with N supports can be written as:

$$\tilde{\mathbf{a}}(t) = [\vec{a}_1(t) \quad \vec{a}_2(t) \quad \dots \quad \vec{a}_N(t)]^T \tag{3.17}$$

where $\vec{a}_i(t)(i = 1, 2, ..., N)$ is the ground acceleration at each support and T denotes transpose. $\vec{a}_i(t)$ can be written as:

$$\vec{a}_i(t) = [a_i^{(x)}(t) \quad a_i^{(y)}(t) \quad a_i^{(z)}(t)]^T \tag{3.18}$$

where x, y and z are the coordinate axis directions. Let's consider supports j and k of the structure. The spatial variability of ground motion, between these two supports, can be characterized by the cross-spectral density function Eq. 3.3.

By the inclusion of all supports and components, S_{jk} takes the form of a complex spectral density matrix:

$$\mathbf{S}(\omega, \xi) = [\mathbf{S}_{jk}] = \begin{bmatrix} \mathbf{S}_1(\omega, \xi) & \mathbf{S}_{12}(\omega, \xi) & \cdots & \mathbf{S}_{1N}(\omega, \xi) \\ \mathbf{S}_{21}(\omega, \xi) & \mathbf{S}_2(\omega, \xi) & & \mathbf{S}_{2N}(\omega, \xi) \\ \vdots & & \ddots & \vdots \\ \mathbf{S}_{N1}(\omega, \xi) & \mathbf{S}_{N2}(\omega, \xi) & \cdots & \mathbf{S}_N(\omega, \xi) \end{bmatrix} \tag{3.19}$$

where ξ is the distance between supports, the off-diagonal terms are Hermitian symmetric, i.e. $\mathbf{S}_{jk} = \mathbf{S}_{kj}^{*T}$ and describe the coherency between supports j and k. The matrix $\mathbf{S}(\omega, \xi)$ is formed by 3×3 sub-matrices, which can be written as:

$$\mathbf{S}_{jk}(\omega) = [S_{mn}] = \begin{bmatrix} S_{xx} & S_{xy} & S_{xz} \\ S_{yx} & S_{yy} & S_{yz} \\ S_{zx} & S_{zy} & S_{zz} \end{bmatrix} \tag{3.20}$$

Each element of the sub-matrix describes the coherency of the ground motion between supports j and k in directions m and n. The spectral density functions contain effects due to wave passage and incoherence. These effects are discussed in the following sections.

3.3 Coherency

The complex coherency of the ground motions between the supports j and k is traditionally expressed as (Zerva, 2009):

$$\gamma_{jk}(\omega, \xi) = \frac{S_{jk}(\omega, \xi)}{\sqrt{S_{jj}(\omega) S_{kk}(\omega)}} \tag{3.21}$$

where $S_{jk}(\omega, \xi)$, $S_{jj}(\omega)$ and $S_{kk}(\omega)$ is the smoothed cross-spectrum between supports j and k and its corresponding auto-spectra. $\gamma_{jk}(\omega)$ is a complex function.

The absolute value of the coherency:

$$|\gamma_{jk}(\omega, \xi)| = \frac{|S_{jk}(\omega, \xi)|}{\sqrt{S_{jj}(\omega) S_{kk}(\omega)}} \tag{3.22}$$

commonly referred to as the lagged coherency is a real function with values in the range $0 \leq |\gamma_{jk}(\omega)| \leq 1$ according to definition. The coherency can be expressed in terms of the lagged coherency (Zerva & Zervas, 2002):

$$\gamma_{jk}(\omega, \xi) = |\gamma_{jk}(\omega, \xi)| exp[i\theta_{jk}(\omega, \xi)] \tag{3.23}$$

where $\theta_{jk}(\omega, \xi)$ is the phase spectrum and the complex term describes the wave passage effects.

3.3.1 Wave passage

The wave passage effect is the delay in arrival times of waves at different supports of the structure (Zerva, 2009).

$$\gamma_{jk}(\omega, \xi_{jk}) = exp\left[-i\frac{\omega\, \xi_{jk}}{c}\right] \tag{3.24}$$

where c is the apparent velocity of the seismic waves along a line between the two supports. The time lag between these two supports can by written as $\Delta t_{jk} = \xi_{jk}/c$, which leads to the following description of the wave passage:

$$\gamma_{jk}(\omega, t_{jk}) = exp[-i(\Delta t_{jk})] \tag{3.25}$$

It should be noted that observations from the SMART-1 array in Taiwan show random fluctuations around the wave passage delay (Zerva, 2009). These fluctuations will be neglected in this study.

3.3.2 Site effects

The soil conditions are often not uniform at the construction site of a long span structure. For sites containing more than one soil condition, a so called site response effect should be considered. This could include a structure that has different soil profile at support j and k. These different soil types are not likely to have the same filtering effects on the ground motion. Which implies that even though the ground motion is the same underneath these two layers, the same does not necessarily apply on top of these layers. However, a study suggests that the effects of site response are minimal for long span structures, while the contribution of wave passage is more significant (Der Kiureghian, 1996).

While it is important to discuss the site effects, this study estimates uniform soil layers and disregards the site response effects. The SFT is also considered a long span structure, so the soil effects are not likely to be a deciding factor.

3.4 Structural seismic analysis methods

The equation of motion for the structure, which is subjected to ground acceleration excitation $\ddot{u}_g(t)$, is commonly presented as follows (Lin & Zhang, 2007):

$$\mathbf{M}\ddot{\mathbf{r}} + \mathbf{C}\dot{\mathbf{r}} + \mathbf{K}\mathbf{r} = \mathbf{Q}(t) \tag{3.26}$$

where the load vector of the system can be written as:

$$\mathbf{Q}(t) = \mathbf{A}_a\ddot{\mathbf{u}}_g(t) + \mathbf{A}_v\dot{\mathbf{u}}_g(t) \tag{3.27}$$

in which $\mathbf{A}_a$ and $\mathbf{A}_v$ are transformation matrices described in further detail in Section 3.4.2; $\mathbf{M}$, $\mathbf{C}$ and $\mathbf{K}$ are the system matrices; and $\ddot{u}_g(t)$ and $\dot{u}_g(t)$ are a stationary random processes, introduced in Eq. 3.7, with known auto-PSD functions $S_{\ddot{u}_g}(\omega)$ and $S_{\dot{u}_g}(\omega)$. The auto-PSD represents acceleration excitation applied to a support of the SFT.

3.4.1 Equation of motion for multi-support excitation

Earthquake motion is generally induced to the supports of a structure. Furthermore, the action is induced on foundations which are assumed to sustain no displacement. To assess the motions of a multi-support structure, a method described by (Clough & Penzien, 2010; Lin & Zhang, 2007; Langen & Sigbjörnsson, 1979) is followed.

The structural degrees of freedom can be grouped as follows

$$\mathbf{r} = [\mathbf{r}_i \quad \mathbf{r}_e]^T \tag{3.28}$$

where $\mathbf{r}_e$ represents the degrees of freedom (DOF) of the supports and $\mathbf{r}_i$ describes the DOFs of the rest of the structure.

Total displacements $\mathbf{r}^{(t)}$ of the structure can be expressed as the sum of the two vectors:

$$\mathbf{r}^{(t)} = \mathbf{r}^{(s)} + \mathbf{r} \tag{3.29}$$

here, $\mathbf{r}^{(s)}$ is the pseudo-static displacement of the structure which is generated by the support motion $\mathbf{r}_e$ and $\mathbf{r}$ is the relative displacement, which characterizes the dynamic effects of the structure. Merging the two previous equations, Eq. 3.28 and Eq. 3.29 gives

$$\begin{bmatrix} \mathbf{r}_i^{(t)} \\ \mathbf{r}_e \end{bmatrix} = \begin{bmatrix} \mathbf{r}_i^{(s)} \\ \mathbf{r}_e \end{bmatrix} + \begin{bmatrix} \mathbf{r}_i \\ \mathbf{0} \end{bmatrix} \tag{3.30}$$

Inserting the total response (see Eq. 3.30) into the equation of motion (see Eq. 2.1), the following expression can be obtained

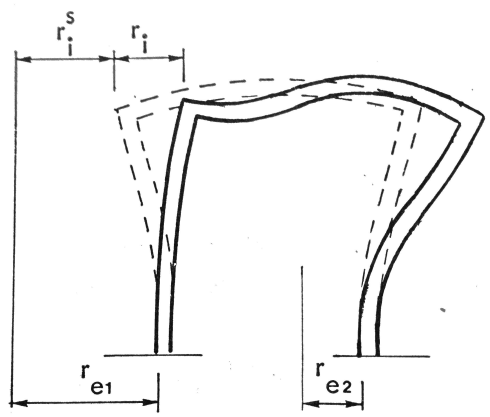

Figure 4: A simple frame, subjected to time dependent displacement on its supports (Langen & Sigbjörnsson, 1979)

$$\begin{bmatrix} \mathbf{M}_{ii} & \mathbf{M}_{ie} \\ \mathbf{M}_{ei} & \mathbf{M}_{ee} \end{bmatrix} \begin{Bmatrix} \ddot{\mathbf{r}}_i^{(t)} \\ \mathbf{r}_e \end{Bmatrix} + \begin{bmatrix} \mathbf{C}_{ii} & \mathbf{C}_{ie} \\ \mathbf{C}_{ei} & \mathbf{C}_{ee} \end{bmatrix} \begin{Bmatrix} \dot{\mathbf{r}}_i^{(t)} \\ \mathbf{r}_e \end{Bmatrix} + \begin{bmatrix} \mathbf{K}_{ii} & \mathbf{K}_{ie} \\ \mathbf{K}_{ei} & \mathbf{K}_{ee} \end{bmatrix} \begin{Bmatrix} \mathbf{r}_i^{(t)} \\ \mathbf{r}_e \end{Bmatrix} = \begin{Bmatrix} \mathbf{0} \\ \mathbf{Q}_e \end{Bmatrix} \quad (3.31)$$

Since the support motion is assumed, the first line of Eq. 3.31 can be separated from the equation and rewritten as follows:

$$\mathbf{M}_{ii}\ddot{\mathbf{r}}_i^{(t)} + \mathbf{C}_{ii}\dot{\mathbf{r}}_i^{(t)} + \mathbf{K}_{ii}\mathbf{r}_i^{(t)} = -\mathbf{M}_{ie}\ddot{\mathbf{r}}_e - \mathbf{C}_{ie}\dot{\mathbf{r}}_e - \mathbf{K}_{ie}\mathbf{r}_e \quad (3.32)$$

This can also be described in terms of the relative motions with the introduction of Eq. 3.30:

$$\mathbf{M}_{ii}\ddot{\mathbf{r}}_i + \mathbf{C}_{ii}\dot{\mathbf{r}}_i + \mathbf{K}_{ii}\mathbf{r}_i = \mathbf{Q}_i \quad (3.33)$$

where

$$\mathbf{Q}_i = -(\mathbf{M}_{ii}\ddot{\mathbf{r}}_i^{(s)} + \mathbf{M}_{ie}\ddot{\mathbf{r}}_e) - (\mathbf{C}_{ii}\dot{\mathbf{r}}_i^{(s)} + \mathbf{C}_{ie}\dot{\mathbf{r}}_e) - (\mathbf{K}_{ii}\mathbf{r}_i^{(s)} + \mathbf{K}_{ie}\mathbf{r}_e) \quad (3.34)$$

To calculate the displacement $\mathbf{r}_i^{(s)}$ the following equilibrium condition obtained from Eq. 3.32 is used

$$\mathbf{K}_{ii}\mathbf{r}_i^{(s)} + \mathbf{K}_{ie}\mathbf{r}_e = 0 \tag{3.35}$$

which gives

$$\mathbf{r}_i^{(s)} = -\mathbf{K}_{ii}^{-1}\mathbf{K}_{ie}\mathbf{r}_e \tag{3.36}$$

Then, substituting $\mathbf{r}_i^{(s)}$ into Eq. 3.33 and Eq. 3.34 and introducing $\mathbf{B} = -\mathbf{K}_{ii}^{-1}\mathbf{K}_{ie}$ (Langen & Sigbjörnsson, 1979) gives

$$\mathbf{M}_{ii}\ddot{\mathbf{r}}_i + \mathbf{C}_{ii}\dot{\mathbf{r}}_i + \mathbf{K}_{ii}\mathbf{r}_i = -(\mathbf{M}_{ii}\mathbf{B} + \mathbf{M}_{ie})\ddot{\mathbf{r}}_e - (\mathbf{C}_{ii}\mathbf{B} + \mathbf{C}_{ie})\dot{\mathbf{r}}_e \tag{3.37}$$

where, the right hand side of Eq. 3.32 describes the load vector of the system. Since the structure is fully submerged in water, both the inertia and damping parts of the load vector can be assumed to make significant contribution.

Now, the equation of motion has been described for ground motions in the system coordinates, i.e. $\ddot{\mathbf{r}}_e$, but when the earthquake waves arrive at an angle β, modifications need to be made. Hence, the ground motions are expressed as:

$$\ddot{\mathbf{r}}_e = \mathbf{E}_{mN}\ddot{\mathbf{u}}_g \tag{3.38}$$

where $\ddot{\mathbf{u}}_g$ is the ground acceleration that propagates with an angle β to the SFT. The matrix E_{mN} is a block-diagonal matrix that can be expressed as:

$$\mathbf{E}_{mN} = \mathrm{diag}[\mathbf{e}_\beta \quad \mathbf{e}_\beta \quad \dots \quad \mathbf{e}_\beta]_{m\times N} \tag{3.39}$$

in which the sub-matrix $\mathbf{e}_\beta$ is $[\cos\beta \quad 0 \quad \sin\beta]^T$; $[0 \quad 0 \quad 1]^T$ and $[-\sin\beta \quad 0 \quad \cos\beta]^T$, N is the number of supports and $m = 3n$. Note that only three translations are considered, as the rotational excitation is assumed to be zero.

Substituting Eq. 3.38 into Eq. 3.37 yields:

$$\mathbf{M}_{ii}\ddot{\mathbf{r}}_i + \mathbf{C}_{ii}\dot{\mathbf{r}}_i + \mathbf{K}_{ii}\mathbf{r}_i = -(\mathbf{M}_{ii}\mathbf{B} + \mathbf{M}_{ie})\mathbf{E}_{mN}\ddot{\mathbf{u}}_g - (\mathbf{C}_{ii}\mathbf{B} + \mathbf{C}_{ie})\mathbf{E}_{mN}\dot{\mathbf{u}}_g \tag{3.40}$$

Equation 3.40 can be regarded as the final version of the equation of motion (Eq. 2.1), which needs to be solved for the whole system, using a solution method described in the following section.

3.4.2 Power spectral density solution

Considering the right hand side of Eq. 3.40 as the seismic load vector Q_s, the spectral density of the seismic load can be computed as such (derived in Appendix B):

$$S_Q(\omega) = \mathbf{A}_a S_{\ddot{u}_g}(\omega)\mathbf{A}_a^T + \mathbf{A}_v S_{\dot{u}_g}(\omega)\mathbf{A}_v^T + \mathbf{A}_a S_{\ddot{u}_g \dot{u}_g}(\omega)\mathbf{A}_v^T + \mathbf{A}_v S_{\dot{u}_g \ddot{u}_g}(\omega)\mathbf{A}_a^T \quad (3.41)$$

where $\mathbf{A}_a = -(\mathbf{M}_{ii}\mathbf{B} + \mathbf{M}_{ie})\mathbf{E}_{mN}$ and $\mathbf{A}_v = -(\mathbf{C}_{ii}\mathbf{B} + \mathbf{C}_{ie})\mathbf{E}_{mN}$ are matrices that transform the ground acceleration and velocity spectral density matrices $\mathbf{S}_{\ddot{u}_g}(\omega)$ and $\mathbf{S}_{\dot{u}_g}(\omega)$ into the load spectral density matrix $\mathbf{S}_Q(\omega)$. The response spectral density matrix $\mathbf{S}_r(\omega)$ can then be obtained by multiplying the frequency response function $\mathbf{H}(\omega)$, in Eq. 2.17, with $S_Q(\omega)$:

$$\mathbf{S}_r(\omega) = \mathbf{H}(\omega) S_Q(\omega) \mathbf{H}^{T*}(\omega) \quad (3.42)$$

The response spectral density matrix $\mathbf{S}_r(\omega)$ contains both the auto-PSD of the response at each support, as well as the cross spectral density of the response between all supports.

3.4.3 Response Statistics

The spectral density matrix, $\mathbf{S}_r(\omega)$, obtained in the preceding section (Eq. 3.42) contains all the information about the response of the structure. The variance of the response is found by integrating the auto-PSD at each point being observed:

$$\sigma_r^2 = \int_{-\infty}^{\infty} S_r(\omega) d\omega \quad (3.43)$$

$$\sigma_{\dot{r}}^2 = \int_{-\infty}^{\infty} \omega^2 S_r(\omega) d\omega \tag{3.44}$$

$$\sigma_{\ddot{r}}^2 = \int_{-\infty}^{\infty} \omega^4 S_r(\omega) d\omega \tag{3.45}$$

Here, the variance describes the displacement, velocity and acceleration response of the structure. Furthermore, the co-variance of the response between two points can be expressed as:

$$\sigma_{r_j r_k} = \int_{-\infty}^{\infty} S_{r_j r_k}(\omega) d\omega \tag{3.46}$$

The standard deviation is attained by taking the square root of the variance. As demonstrated in Eqs. 3.44-3.45 the variance for the velocity and acceleration is found by multiplying the response spectra with ω^2 and ω^4, and then integrate it over all frequencies. Furthermore, the expected maximum value of the response is then calculated by using the peak factor, introduced in Eq. 3.5, as written in the following expression:

$$E[z_{max}] = p \times \sigma_r \tag{3.47}$$

The expected maximum of the velocity and acceleration is obtained with the same procedure but by multiplying the peak factor with $\sigma_{\dot{r}}$ or $\sigma_{\ddot{r}}$.

4 Case studies

The submerged floating tunnel over the Høgsfjord in Norway is used as a application for the methods described in preceding chapters. The supports of the model are excited with earthquake action and the wave passage and incoherence effects are studied. Three different scenarios, of the incoherence, are examined: Fully coherent ($\gamma = 1$), incoherent (see Section 3.3) and non-coherent ($\gamma = 0$). Furthermore, the influence of inter-component coherency is investigated with a simple coherency model (see Table 5). In addition, the wave passage effect is examined for apparent wave velocity ranging from $c = 400 - 1000\,m/s$, which are estimated values for soft soil conditions.

Two different versions of the structure are modeled. One where the tension legs anchoring the system are inclined, at an 30° angle. While the other case has vertical tension legs, which changes the behavior of the structure quite a lot, i.e. the natural frequencies and the natural modes. Most results are based on the former model, while the latter is used for comparison.

The response statistics of all motions in the tunnel are examined, i.e. the displacement, velocity and acceleration. The potential effects of the motions are discussed concerning structural and public safety.

4.1 Definition of the case - the Høgsfjord tunnel

The SFT concept was proposed to cross the approximately 1400 m wide and 160m deep Høgsfjord, in Norway. The bottom of the Høgsfjord is quite irregular in shape, as seen in Figure 5 with the deepest part close to the left end of the tunnel. Firm soil conditions are assumed at the shore connections. However, the The Norwegian fjords are usually filled with a deep layer of soft sediments. These sediments effect the velocity of the propagating wave, soft soil means generally low wave velocity. Hence, it would be inaccurate to assume firm soil conditions for the whole structure. However, for simplicity, the same filter was used to describe the soil structure interaction of all supports (see Section 4.3.1). The filter has relatively low frequency content which is typical for soft soil conditions. Although not performed in this study, it would be interesting to compare the response spectra of the structure with response spectra from Eurocode. This could lead to more

accurate description of the soil conditions. Assuming that the sediments in the Høgsfjord are of a particularly soft nature, the analyses is carried out for wave velocity of $c = 500m/s^2$ as the basis of the study. Nevertheless, the the effects of varying wave velocity is also studied.

The proposal suggested using concrete as the building material, with inclined tension legs of steel. The tunnel is designed with a slight vertical curvature which gives even more vertical stiffness, apart from what is obtained from the tension legs. The main goal of the study is to observe and understand the behavior of submerged floating tunnel under seismic events. Thus, some parts are not modeled exactly as proposed.

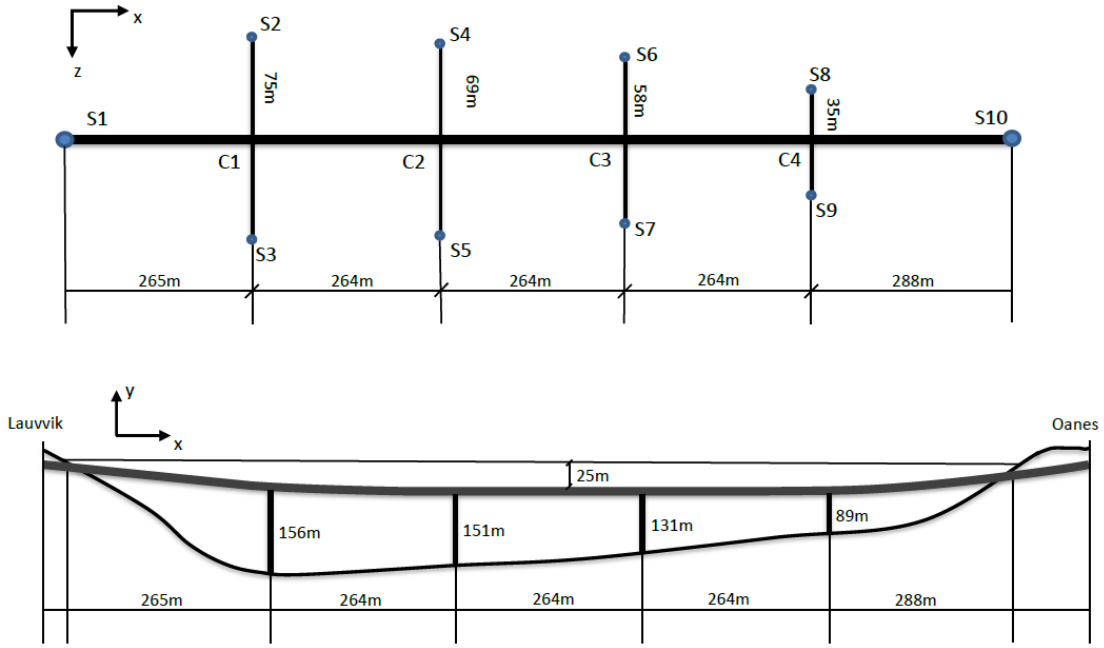

Figure 5: The Høgsfjord tunnel

The irregularity of the bottom shape, at the site, means that the anchoring will be much shorter on the right side, close to Oanes (Figure 5). Shorter cables should imply more stiffness, they also do not reduce the buoyancy force of the tunnel as they weigh less. This results in higher pretension and more stiffness for the shorter cables. At mid span the tunnel lies 25 m under the sea surface, which enables even the most deep cut sea traffic.

4.2 FE modeling of the study structure

The finite element model of the SFT is modeled based on a report from SINTEF (Holmås & Fergestad, 1988). It is modeled in two parts (the tunnel and the tension legs), using 3D Euler-Bernoulli beam elements. The crossing length of the tunnel is taken to be 1345 m between rigid ends, as drawings from the SINTEF report suggest. All supports are considered fixed. The model consists of 65 nodes, 64 elements and 390 degrees of freedom (DOFs), which can be decoupled into 60 foundation- and 330 inner DOFs. This controllable number of elements is chosen to avoid unnecessary computing time.

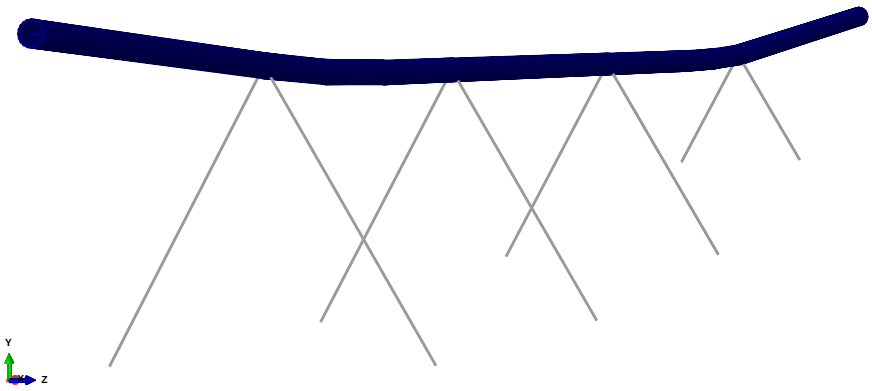

Figure 6: 3D picture of the Abaqus model

The finite element model is assembled in Abaqus, where all material properties and static loads are applied. Since, Abaqus is primarily a powerful tool for solutions in the time domain, the system matrices are extracted out of the program and further evaluated in Matlab. However, when extracting, the program generated 128 extra DOFs, in which the author has no explanation. In order to continue the study, these elements were simply removed. It was then observed that the removal did not effect the natural frequencies significantly (see Table 1), nor did it impact the natural modes. Therefore, it was decided to continue without them.

As observable in Tables 1 and 2 the natural frequencies are closely spaced, it can also be noticed that the "wet" natural frequencies are significantly lower than their "dry" counterparts. This can be explained by the added mass of the hydrodynamic system, while the stiffness stays unchanged.

Table 1: First 15 natural frequencies of the SFT model anchored with inclined tension legs and their corresponding mode shapes. Where H denotes horizontal, V vertical and C cable mode shapes.

Mode number	1	2	3	4	5
Mode shape	H	H	V	H	V
Dry natural frequency Abaqus [Hz]	0.255	0.269	0.289	0.295	0.328
Dry natural frequency (reduced) [Hz]	0.263	0.276	0.290	0.305	0.331
Deviation (%)	3.4%	2.6%	0.5%	3.3%	1.2%
Wet natural frequency [Hz]	0.207	0.217	0.230	0.239	0.264
Mode number	6	7	8	9	10
Mode shape	H	V	H	VC	C
Dry natural frequency Abaqus [Hz]	0.348	0.371	0.381	0.388	0.434
Dry natural frequency (reduced) [Hz]	0.353	0.378	0.391	0.392	0.434
Deviation (%)	1.3%	1.8%	2.8%	0.8%	0.0%
Wet natural frequency [Hz]	0.283	0.303	0.305	0.332	0.360
Mode number	11	12	13	14	15
Mode shape	C	V	C	C	HC
Dry natural frequency Abaqus [Hz]	0.435	0.448	0.480	0.481	0.483
Dry natural frequency (reduced) [Hz]	0.435	0.456	0.480	0.481	0.488
Deviation (%)	0.0%	1.6%	0.0%	0.0%	0.9%
Wet natural frequency [Hz]	0.434	0.434	0.436	0.451	0.480

Table 2: First 15 natural frequencies of the SFT model anchored with vertical tension legs and their mode shapes.

Mode number	1	2	3	4	5
Mode shape	H	H	H	H	V
Dry natural frequency [Hz]	0.028	0.066	0.127	0.208	0.292
Wet natural frequency [Hz]	0.022	0.051	0.099	0.163	0.232
Mode number	6	7	8	9	10
Mode shape	H	V	V	H	C
Dry natural frequency [Hz]	0.310	0.344	0.412	0.433	0.459
Wet natural frequency [Hz]	0.246	0.273	0.325	0.348	0.374
Mode number	11	12	13	14	15
Mode shape	C	C	C	V	V
Dry natural frequency [Hz]	0.459	0.459	0.460	0.476	0.494
Wet natural frequency [Hz]	0.387	0.455	0.456	0.459	0.459

4.2.1 Modeling of structural parts

The cross section of the tunnel (Figure 7) has a outer radius of $r_c = 5.65\,m$ and thickness of $t = 0.9\,m$. For simplicity, the cross section was considered to be a perfect circle. However, in a real situation the section would likely have a ballast to stabilize the tunnel and control the weight. The tension legs were connected to the outside of the tunnel, pointing straight to the shear center of the cross section.

The tension legs were designed with a circular cross section and a radius of $r_s = 0.2\,m$, which gives cross sectional area $A_s = 0.126\,m^2$. It should be noted that by using tension legs with a cross sectional area of $A_s = 0.4\,m^2$, as proposed by Holmås & Fergestad (1988), increased mass of the tension legs had significant effects on the buoyancy of the tunnel.

4.2.2 Material properties and structural damping

Concrete is used as the main building material. However, the material density is taken as $\rho_c = 3,179\,kg/m^3$, to control the net buoyancy of the tunnel. The elastic properties of concrete are used for the material in the tunnel, i.e. Young's modulus

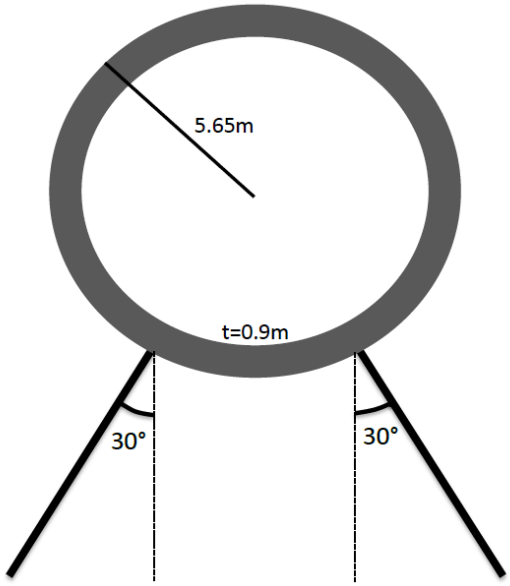

Figure 7: Cross section of the Høgsfjord tunnel, with inclined tension legs.

of $E_c = 33\,GPa$ and Poisson ratio of $\nu_c = 0.2$. For the tension legs the material density was taken as $\rho_s = 7,850\,kg/m^3$, the Young's modulus $E_s = 33\,GPa$ and Poisson ratio $\nu_s = 0.3$.

The structural damping is represented by mass and stiffness proportional Rayleigh damping (see Section 2.3). The damping coefficients, α and β are obtained by using Eqs. 2.13−2.14, selecting the frequencies and damping ratios as $\omega_1 = 1.3$, $\omega_2 = 2.3$, $\zeta_1 = 0.9$ and $\zeta_2 = 1$. Solving Eqs. 2.13 − 2.14 gives $\alpha = 0.0064$ and $\beta = 0.0031$. The effects of increased damping was also studied, by increasing the damping ratio to about $\zeta = 2\%$.

4.2.3 Loads and pretension in tension legs

The tunnel is considered to lie submerged in still water, i.e. with no streams and no waves. The restoring force is expressed by gravity and the buoyancy of the tunnel. Which is expressed in the following:

$$b_y = g \times \frac{\rho_w A_w - \rho_c A_c}{\rho_c A_c} = 0.1\,g \tag{4.1}$$

Table 3: Pretension in tension legs

$\sigma_{c1}[MPa]$	$\sigma_{c2}[MPa]$	$\sigma_{c3}[MPa]$	$\sigma_{c4}[MPa]$
90	92	95	120

Here, $A_w = 100.3\,m^2$ denotes the area of water repelled by the structure; $\rho_w = 1,025\,kg/m^3$ is the density of salt water; $A_c = 29.4\,m^2$ is the cross sectional area of the tunnel; and ρ_c is the density of concrete, described in the preceding section.

When applied, the buoyancy force results in small vertical displacement of the structure. To ensure that the tunnel keeps in place, the tension legs must be subjected to pretension. Table 3 describes the pretension assigned to the tension legs, which are supporting each connection ($C1 - C4$) shown in Figure 5.

The only environmental action covered in this study is the seismic ground acceleration, which is induced to all ten supports. Response in the structure is calculated for each given frequency. The modeling of the seismic excitation is described in detail in Section 4.3. However, when the SFT is put in motion by the seismic action, a hydrodynamic action is generated, which can be calculated using the Morison's equation (Eq. 2.7). The coefficients of drag and added mass are chosen as $C_D = 1$ and $C_M = 2$. These values are commonly recommended for offshore structures (Wilson, 2003; Naess & Moan, 2013). Even so, the coefficient of added mass is presumably a little smaller than the recommended value, which has been confirmed by experiments on large diameter cylinders (Kunisu, 2010). However, assuming the tunnel will eventually be covered with marine growth, the coefficient of added mass C_M is expected to approach the recommended value. On the other hand, the experiments show scattering results of the drag coefficient C_D. Even so, the study suggests that the force generated by added mass dominates the drag force for cylinders with large diameters. It could also be argued that if the response velocity of the SFT is assumed to be relatively small. Then, the drag part of Equation 2.7 will have small effects on the structure, and could therefore easily be neglected.

4.2.4 Solution strategies

Response in the structure was calculated for each given frequency. The total response was then established using the principle of superposition. Angular frequencies on the interval $\omega\epsilon[0, 15]\, rad/s$ were utilized in the analysis, with $\Delta\omega = 0.05$. Observing the response spectra at each node along the tunnel unveils that the first ten mode shapes, i.e. in the frequency range of $[1.30, 2.30]\, rad/s$ contribute the most to the structural response (see Figures 12-13.

4.3 Modelling of earthquake excitation at the site of the structure

Although Norway is a area of relatively low seismicity, earthquakes with the magnitude of $M_s = 5$ can occur (Bungum *et al.* , 2010). The earthquake excitation is created with a moderately sized earthquake in mind. Peak ground acceleration of $0.2\, g$ is used as a benchmark for the study and the period of the strong earthquake portion is taken as $T_d = 10\, s$. Earthquake size is expected to be an important parameter in determining the seismic response. However, the frequency content of earthquake is also of high importance.

4.3.1 Spectral density of the ground acceleration

The ground acceleration spectrum was obtained using a modified Kanai-Tajimi spectral density function (Clough & Penzien, 2010):

$$S_{\ddot{u}_g}(\omega) = S_0 \frac{1 + 4\xi_{gk}^2(\omega/\omega_{gk})^2}{[1 - (\omega/\omega_{gk})^2]^2 + 4\xi_{gk}^2(\omega/\omega_{gk})^2} \times \frac{(\omega/\omega_{fk})^4}{[1 - (\omega/\omega_{fk})^2]^2 + 4\xi_{fk}^2(\omega/\omega_{fk})^2} \tag{4.2}$$

where ω_{gk} and ξ_{gk} is the resonant frequency and the damping ratio of the first filter; ω_{fk} and ξ_{fk} are those of the second filter and S_0 is the amplitude of white noise acceleration in the bedrock. The parameters chosen in this study are presented in Table 4.

Table 4: Filter parameters for the Kanai-Tajimi spectral density function

Parameters	Values
S_0	0.05
ω_{gk}	15.6
ξ_{gk}	0.7
ω_{fk}	4
ξ_{fk}	0.5

Implementing the aforementioned parameters into Equation 4.2 gives the spectral density function used for this study (Figure 8). It should be noted that the same acceleration spectral density was used for all the supports, which may be regarded as a weakness in the modeling. The spectrum in Figure 8 describes an medium sized earthquake event with an estimated PGA of $0.2\,g$. The PGA was estimated by calculating the standard deviation of the PSD curve (see Eq. 3.4) and multiplying it with the peak factor expressed in the following (Vanmarcke & Lai, 1980):

$$p \cong \sqrt{2\ln(2.8T_d f_0/2\pi)} \tag{4.3}$$

where T_d is the duration of earthquake and f_0 is the natural frequency of the system.

4.3.2 Coherency Model

Finding a model that characterizes the coherency of seismic ground motion between two locations has been the objective of earthquake engineers for over three decades. Various models have been proposed and fall into one of the tree categories: empirical, semi-empirical or analytical. In Appendix A, a few of these models are presented. Therein, a clear difference between the models can be noticed. It can in fact be assumed that the coherency can vary significantly with different events, since the majority of proposed models have utilized acceleration records from the SMART-1 array in Taiwan (Figure 9).

One of these is an empirical model proposed by Oliveira *et al.* (1991), which will be utilized for all coherency calculations in this study (see Section 3.2). The strength

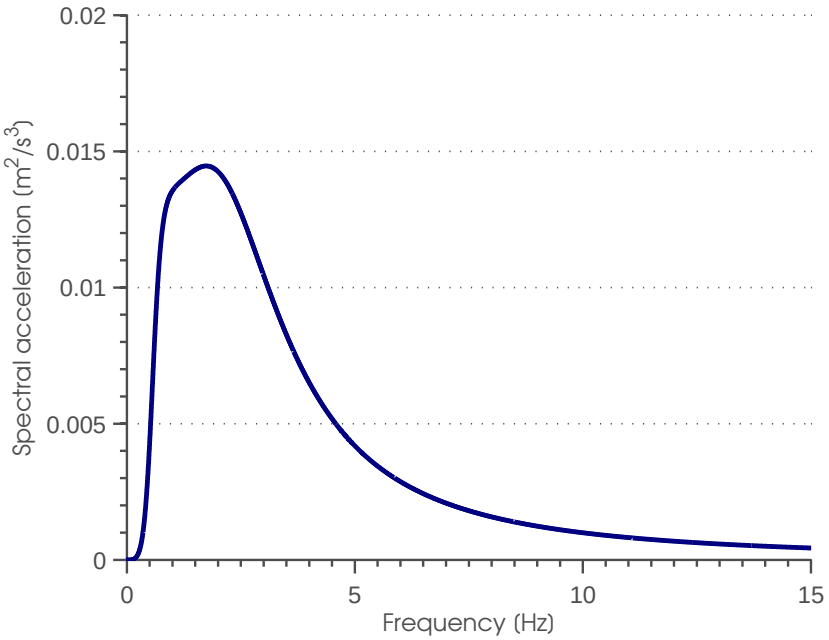

Figure 8: Acceleration spectral density curve

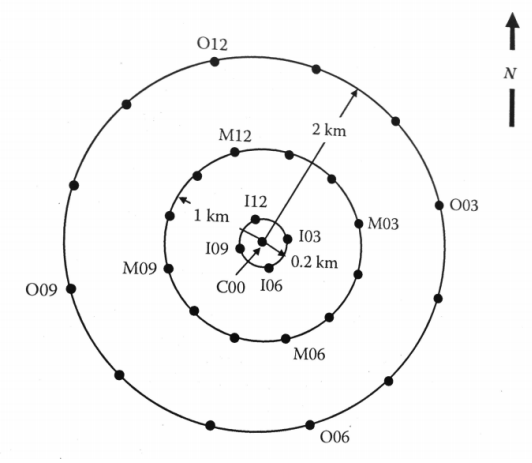

Figure 9: The SMART-1 array. The figure shows the arrangement of 37 force balanced triaxial accelerometers (Zerva, 2009).

of the model, is that it is based on the entire records of each component of the motion. Furthermore, it accounts for the direction of the propagating wave and considers that the ground motions are anisotropic. The model can be expressed as:

$$|\gamma_{jk}(\xi_{jk}^l, \xi_{jk}^t, \omega)| = exp(-\beta_1 \xi_{jk}^l - \beta_2 \xi_{jk}^t) exp[(\alpha_1 \sqrt{\xi_{jk}^l} - \alpha_2 \sqrt{\xi_{jk}^t})(\omega/2\pi)^2] \quad (4.4)$$

where $\alpha_i = 2\pi a/\omega + b\omega/2\pi + c, (i = 1, 2)$, ξ_{jk}^l and ξ_{jk}^t are the separation distances in the longitudinal and tangential direction of the propagating wave. The constants β_i, a_i, b_i and c_i, $(i = 1, 2)$ are obtained from least square fitting of 17 recorded SMART-1 array events (Oliveira *et al.* , 1991). It is noted that the coherency of the model is quite high, for both high and low frequencies, in comparison with other models. This, however is not far from what is observed from the coherency records of the ICEARRAY, for the 2008 Ölfus earthquake in Iceland (Sigbjörnsson *et al.* , 2013).

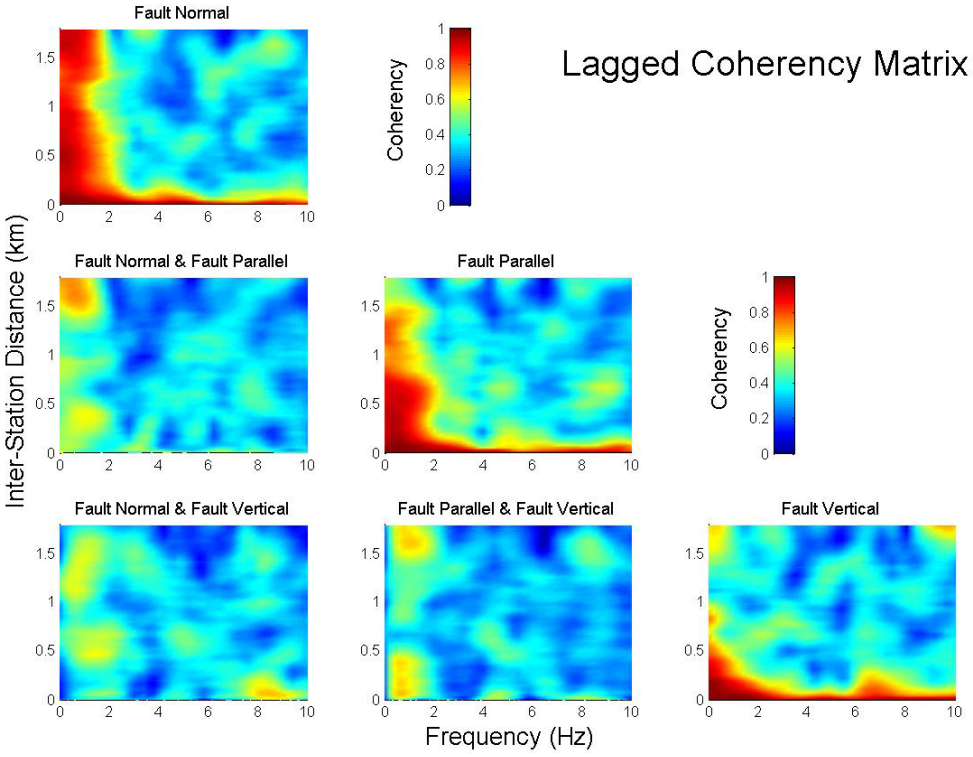

Figure 10: The lagged coherency from the ICEARRAY (Sigbjörnsson *et al.* , 2013)

As an addition to the coherency model, the inter-component coherency is studied. Where the coherency between each component at the same support is considered. Results from the ICEARRAY (Figure 10), where used to generate a simple model between components. Note that the light blue color from Figure 10 is prominent,

Table 5: Inter-component coherency model

Components	Lagged coherency
γ_{xy}	0.3537
γ_{xz}	0.3506
γ_{yz}	0.3295

which are values in the range of $0.3 - 0.4$. Therefore, utilizing a constant model is deemed sufficient, which led to using the mean value of the ICEARRAY lagged coherency records as the inter-component model Table 5.

4.4 Limitations in the modeling

The overall finite element modeling of the structure is considered a success. However, few limitations in the modeling can be mentioned and are presented in the following:

A little uncertainty surrounds the structural damping in the model, as different methods for determining damping, were not studied sufficiently and the damping ratio was simply assumed to be $\zeta = 1\%$ and up to $\zeta = 2\%$. However, these ratios are commonly used in finite element modeling and the structural damping is not far from what was utilized in earlier studies regarding the Høgsfjord tunnel (Remseth *et al.* , 1999).

As mentioned before the ground acceleration spectral density function is exactly the same for all supports. That effects the analysis of the spatial variability of ground motions. The model could be easily improved by generating unique functions for the ground acceleration for each component at each support. Also, the soil-structure interaction model needs to be investigated further, to match the soil conditions on the side. Introducing non-linearity in the modeling could be useful for that matter.

Ultimately, although it did not effect the study greatly, the system matrices retrieved from Abaqus were not understood thoroughly. The author recommends using Matlab for generating the system matrices, in order to fully understand the finite element model. Especially for random vibration analysis of a stochastic system in the frequency domain.

5 Numerical results and discussion

In the following chapter the results from the analyses are presented and discussed. The relevance of all the different parameters in the study is evaluated and the behavior of the structure is discussed in terms of the response.

5.1 Response statistics

The response statistics are obtained using Eqs. 3.43−3.47. In the following sections peak displacement, velocity and acceleration for the model is presented, concerning both vertical and horizontal motions. The incoherence and wave passage effects are evaluated and the inter-component coherency is studied. Furthermore, the response of the inclined and vertical tension leg models are compared and the seismic wave velocity is studied. Ultimately, the influence of increased structural damping is investigated.

5.1.1 Peak structural response

The peak structural response is examined to get insight into structural and public safety. The displacement will give information about the structural safety, while the velocity and acceleration will effect the traffic inside the tunnel, and thus potentially have effects on public safety. The main focus is on the horizontal response, as it is significantly greater than the vertical response. The peak vertical displacement is about $1\,m$, which implies that the expected peak horizontal displacement is about 50% greater (Figure 12). However, different results are obtained when the tension leg anchoring is vertical, then the vertical displacement is greater (Figures $20 - 21$).

A peak displacement in the range of $1 - 2\,m$ (Eq. 11) is not considered large for a $1400\,m$ long tunnel. Therefore, it is safe to assume that structural safety is unlikely to be at risk during medium sized seismic events. However, it is of more importance to identify which frequencies the displacement is associated with, as the higher the frequency the larger the acceleration.

The frequencies can be identified from the response spectra of the analysis (Eqs.

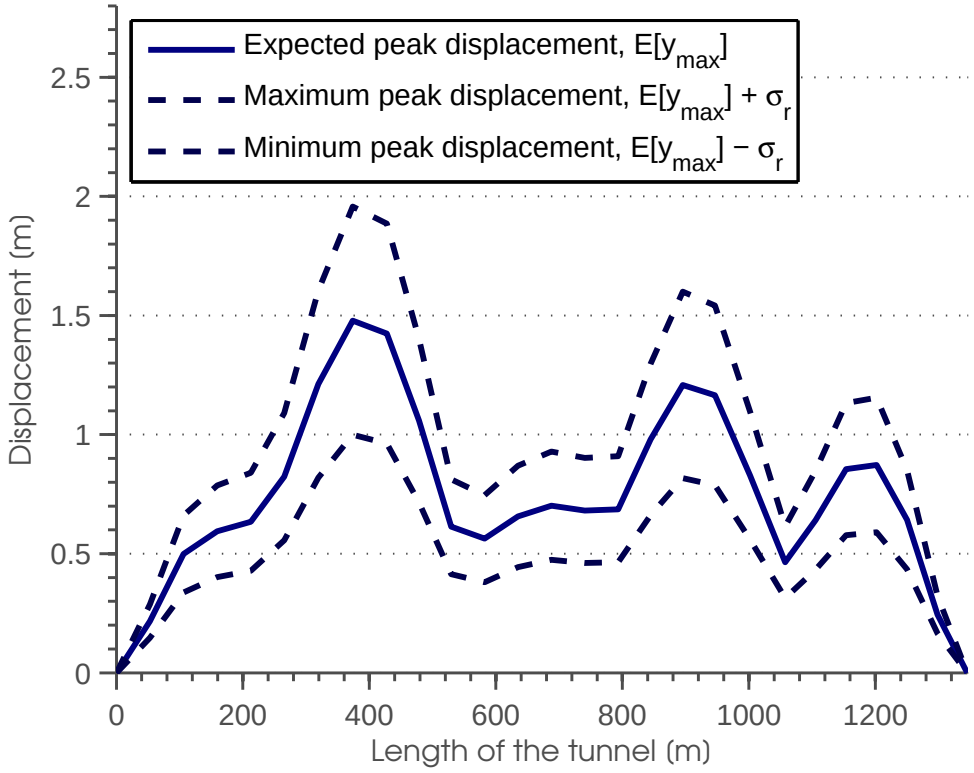

Figure 11: Peak *horizontal* displacement, with seismic waves arriving at 0° angle. Velocity of seismic waves is $500\,m/s$.

$12-13$). It is observed that most of the frequencies generating response lie between $0.2-0.4Hz$. By looking at the acceleration spectral density curve (Eq. 8), it is noticeable that the spectral density starts to increase rapidly around the frequencies in question.

To further evaluate the seismic hazard, in particular to traffic safety, velocity and acceleration response are presented (Figures 14-15). The acceleration is observably high, close to $1g$, which is something that could effect traffic dramatically. It is fair to assume that the tunnel will accommodate traffic at all times, which implies strong probability for traffic inside when the earthquake strikes.

Comparing the peak acceleration (Figure 14) to the peak velocity and displacement implies that the duration of the high acceleration is short, which means that the acceleration could be felt like a series of impacts, during the period of the earthquake. It is safe to assume that accelerations in the range of $1\,g$ will only

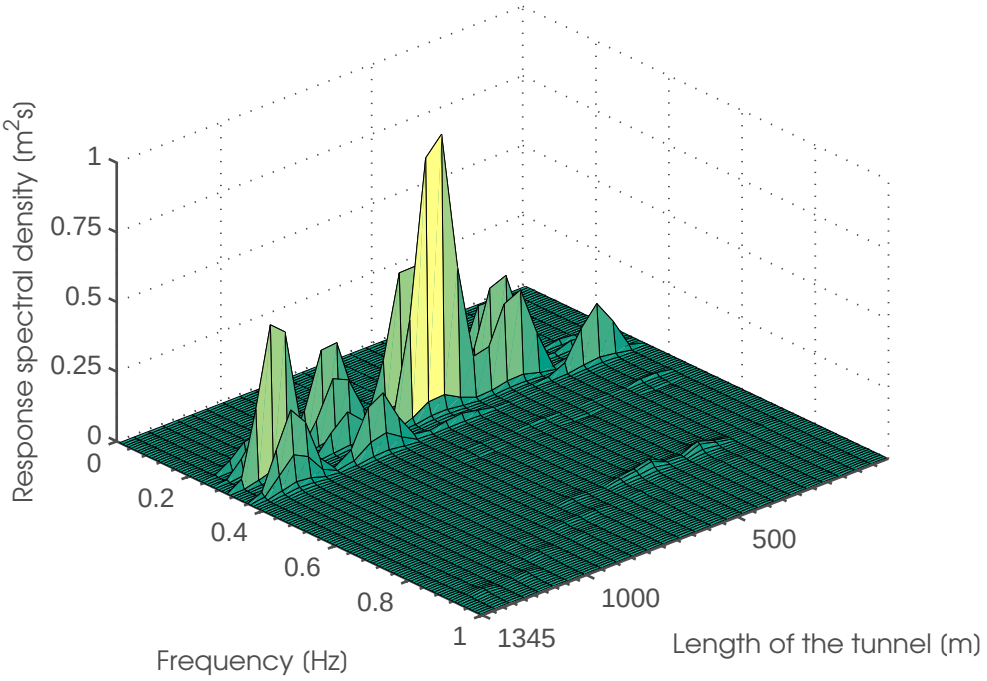

Figure 12: Response spectral density over the length of the tunnel for *vertical* displacement, with seismic waves arriving at a 90° angle.

occur during a small time period, which implies smaller acceleration for the most part during the earthquake.

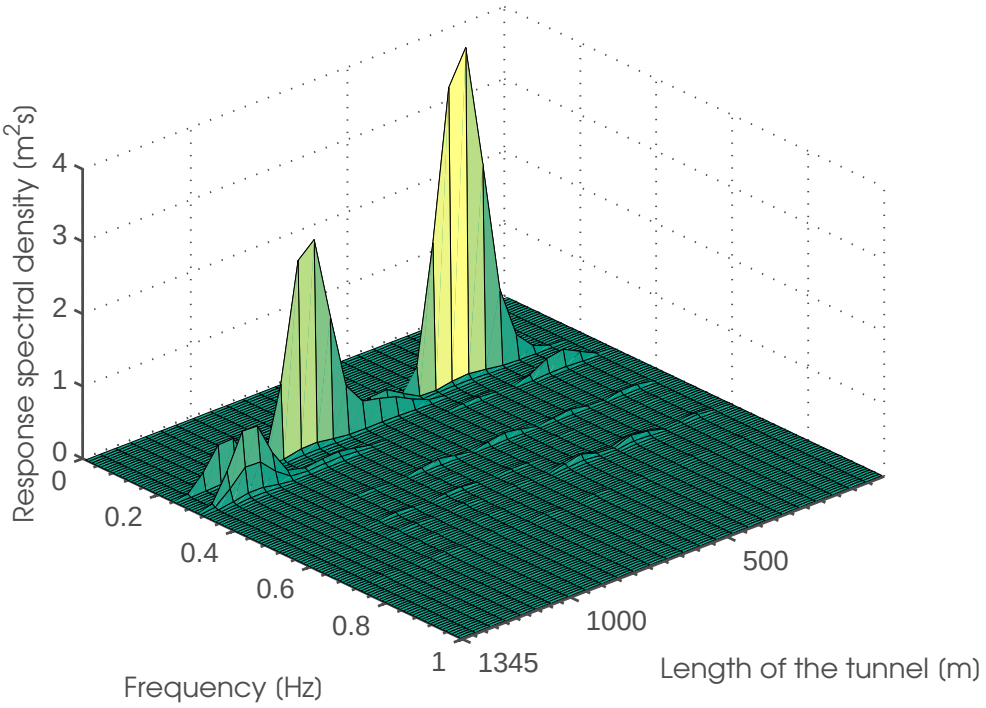

Figure 13: Response spectral density over the length of the tunnel for *horizontal* displacement, with seismic waves arriving at a 90° angle.

5.1.2 Incoherence and wave passage

The incoherence was studied by looking at three examples. The first example utilizes both the (Oliveira *et al.* , 1991) coherency model and the inter-component coherency (see Section 4.3.2) in addition to the wave-passage model, the second only utilizes the wave passage model and is termed fully coherent, the third example is assuming zero coherency, which eliminates the wave passage effects. Two scenarios are observed, differing in direction of the propagating wave, i.e. parallel and perpendicular to the tunnel.

For the case presented in Figure 16 the seismic waves travel in the direction perpendicular to the tunnel. It is visible that the fully coherent model gives the largest response. It is also noticeable that the behavior seems to change significantly for the three different coherency examples, as the fully coherent model does not result in highest displacement all along the tunnel. This implies that the coherency effects, including wave passage and incoherence are complex in nature. Moreover,

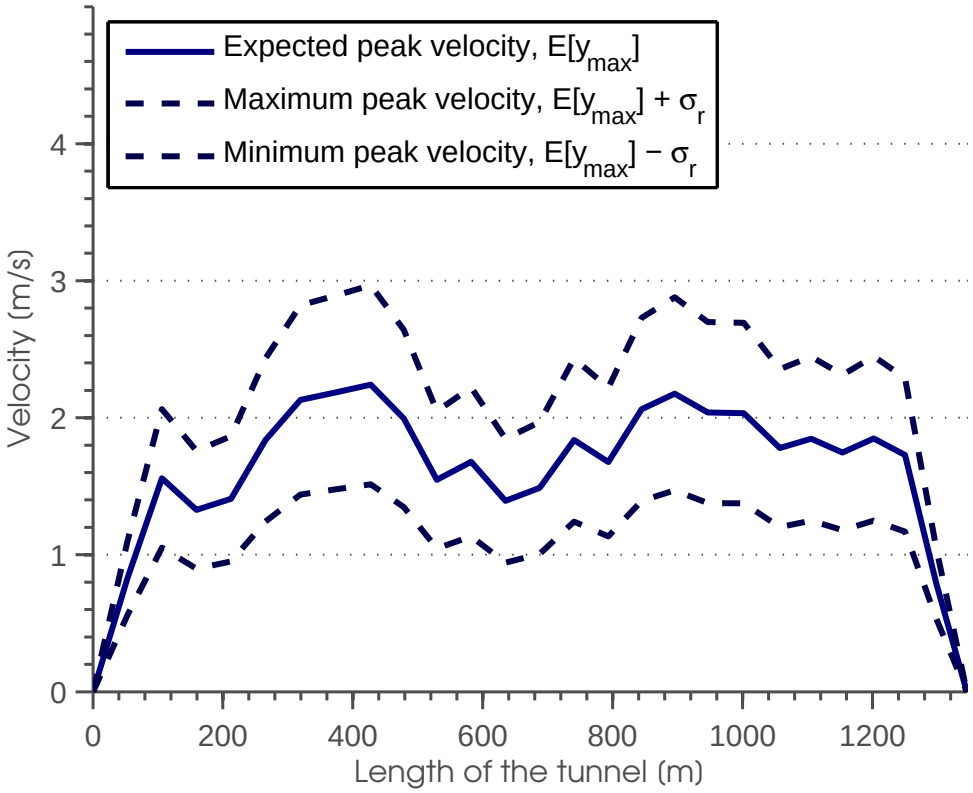

Figure 14: Peak *horizontal* velocity, with seismic waves arriving at 0° angle. Velocity of seismic waves is $500\,m/s$.

in Figure 17, where the waves travel along the tunnel, the incoherent model gives the largest response. For this scenario, both the incoherence and the wave passage are effected by the increased distances between support, which yields to different effects from the coherency model, compared to the results from the other scenario. This underlines the complexity of the subject.

It is evident that the incoherence and wave passage effects change the behavior of the structure. However, it is not obvious whether it increases or decreases the response of the tunnel, depending on at what angle the waves arrive, the distance between the supports and the velocity of the seismic waves.

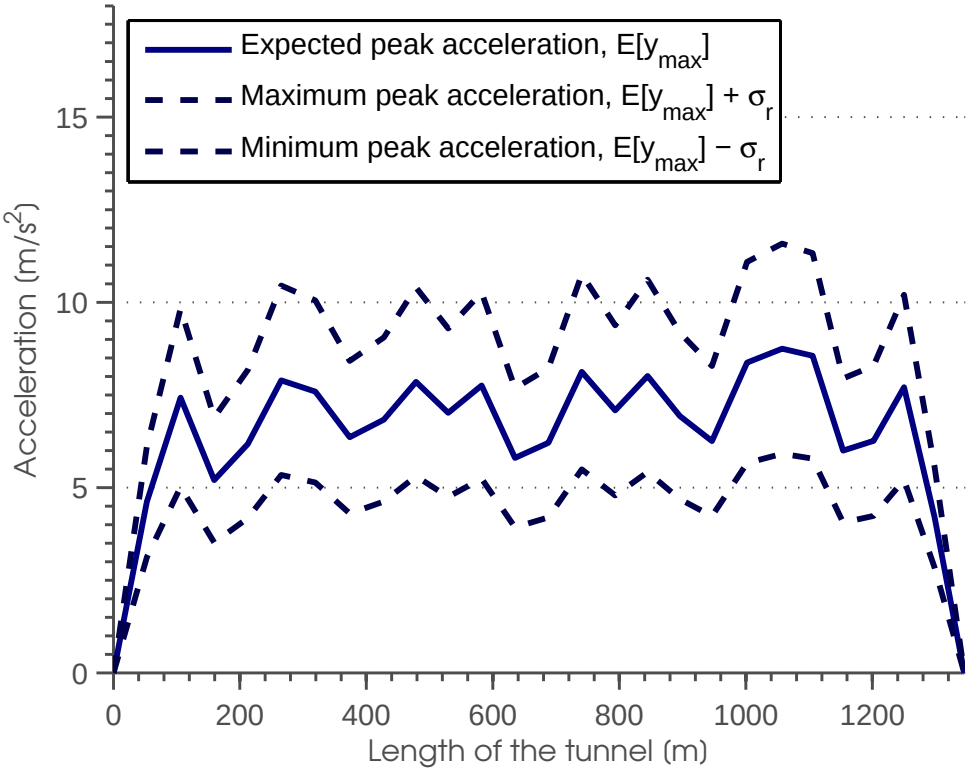

Figure 15: Peak horizontal acceleration, with seismic waves arriving at 0° angle. Velocity of seismic waves is $500\,m/s$.

5.1.3 Inter-component coherency

To estimate the importance of coherency between components, the analysis is performed with the inter-component and inter-support coherency model. The outcome is then compared with results from only the inter-support model and the fully coherent model analyses. This will give a good sense on the importance of the inter-component model.

In Figure 18 it is visible how much influence the inter-component coherency has on the structural response, while the inter-support incoherence does hardly effect the response at all. It should be noted that all the examples include the wave passage, but since the wave passage is dependant on the distance between supports, it has no influence on the inter-component incoherence for the diagonal blocks, i.e. the incoherence between components in an individual support. Therefore, it can

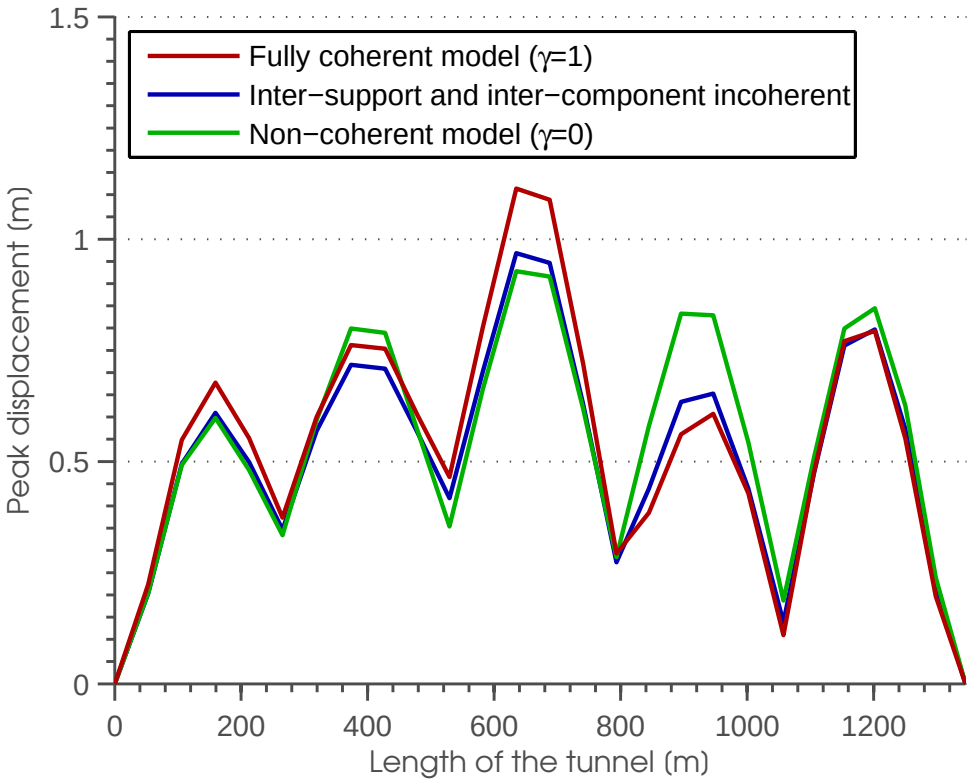

Figure 16: Expected maximum vertical displacement of the tunnel for three incoherence examples, with seismic waves arriving at a 90° angle. The velocity of seismic waves is $500\,m/s$.

be safely assumed that the wave passage effect is the dominating factor for the inter-support incoherence, while the the inter-component incoherence should not be neglected like it has in many previous studies.

5.1.4 Seismic wave velocity

The seismic analysis is carried out for varying wave velocity. The purpose is to examine the effects of wave passage in the analyses. Different scenarios are evaluated and they are all presented in Appendix D. However, one example is selected and presented in Figure 19

As can be seen in Appendix D, the vertical response is more effected by both the direction of the incoming wave and the variation in wave velocity. The horizontal

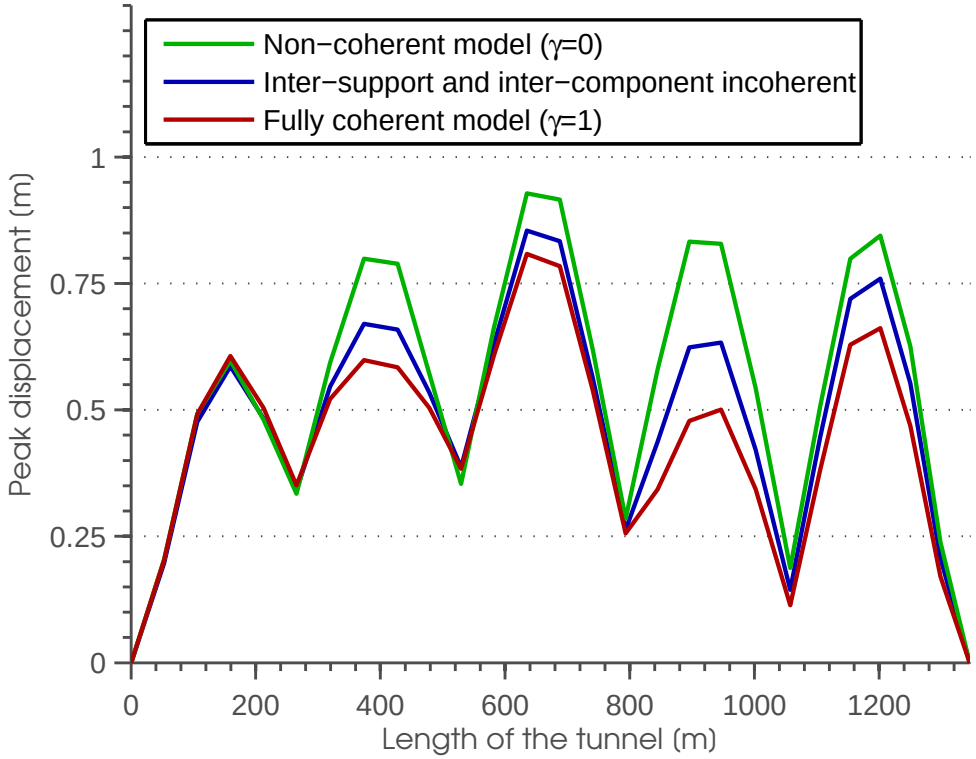

Figure 17: Expected maximum vertical displacement of the tunnel for three incoherence examples, with seismic waves arriving at a 0° angle. The velocity of seismic waves is $500\,m/s$.

response for different angles of the incoming wave is almost exactly the same, but some differences can be noticed for the vertical displacement. When the model is non-coherent, Figures $38 - 41$ shows neither variations in response from different angles nor variations from different wave velocities, since the non-coherence eliminates the wave passage and incoherence effects.

It is apparent that the variation in seismic wave velocities has complex relationship with the structural response. For two different wave velocities, the response can vary significantly in shape and magnitude. In order to carry out accurate seismic analysis, the apparent wave velocity needs to be carefully selected for the site of the structure.

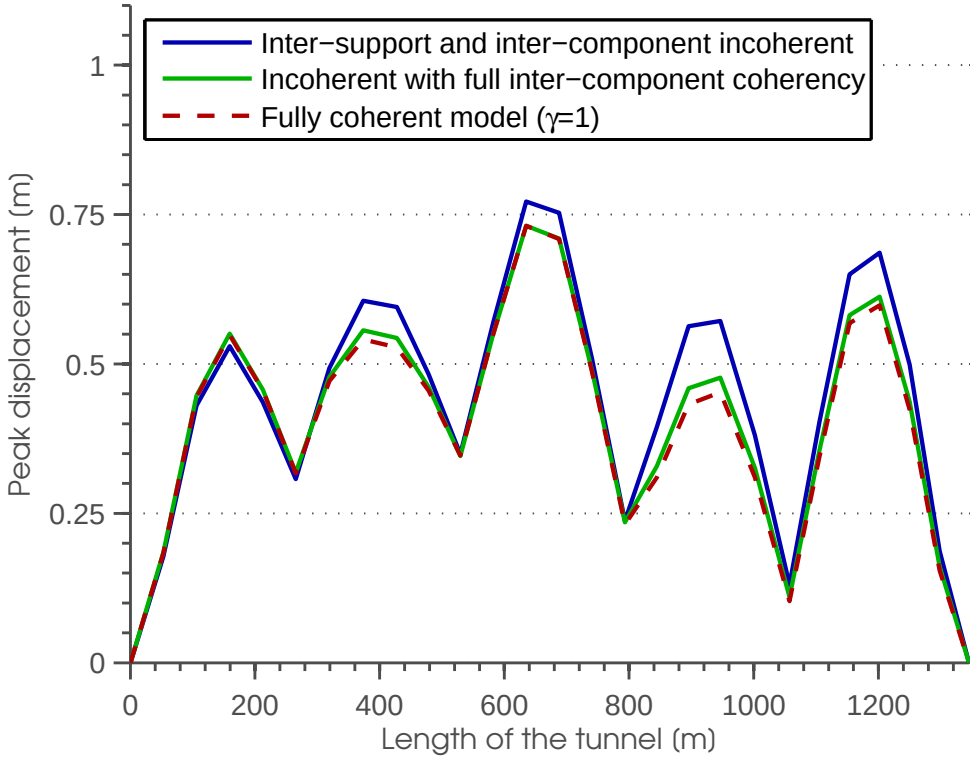

Figure 18: Expected maximum vertical displacement of the tunnel for three inter-component incoherence examples, with seismic waves arriving at a 0° angle. Velocity of seismic waves is 500 m/s and the incoherence between supports are estimated by the Oliveira *et al.* (1991) coherency model (see Eq. 4.4.

5.1.5 Tension leg anchoring and damping

Choosing the best possible anchoring method is essential for a structure of this caliber and many variables are relevant in the design. Sea states and currents could be the controlling factor. However, this study investigates two methods of tension leg anchoring for a SFT subjected to seismic excitation.

From Figure 20 it is evident that the anchoring method does not effect the vertical response heavily. There are small changes, but similar response can be assumed for both inclined and vertical tension legs. However, the horizontal response (Figure 21) shows dramatic differences. It is apparent that the horizontal response is much smaller for the vertical tension leg system. This is due to the fact that

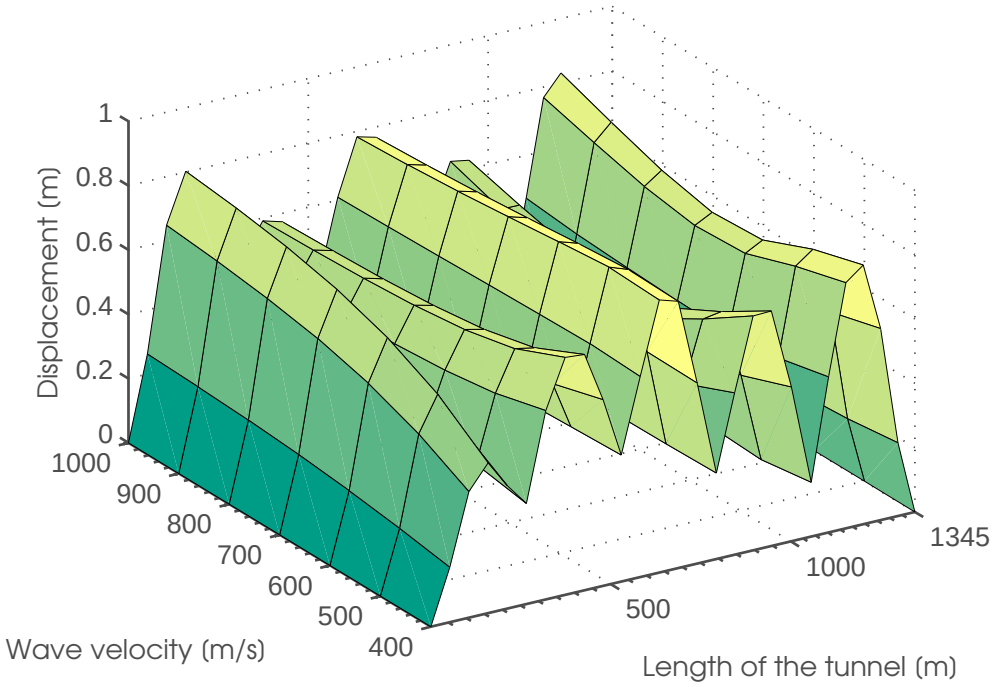

Figure 19: Expected maximum *vertical* displacement of the tunnel for different wave velocities, with seismic waves arriving at a 0° angle and the incoherence estimated by the Oliveira *et al.* (1991) coherency model(see Eq. 4.4.

the decreased stiffness puts the most important horizontal natural frequencies out of range of the ground acceleration frequency content (Figure 8), as the natural frequencies are close to zero (see Table 2).

Increasing the structural damping in the system, decreases the response in the tunnel (Figure 22). However, the differences still hold almost proportional to what was observed in Figure 21, apart from the highest peaks seem to have started to damp out just a little. It is still apparent that vertical tension legs result in much smaller horizontal response, and therefore much smaller total response.

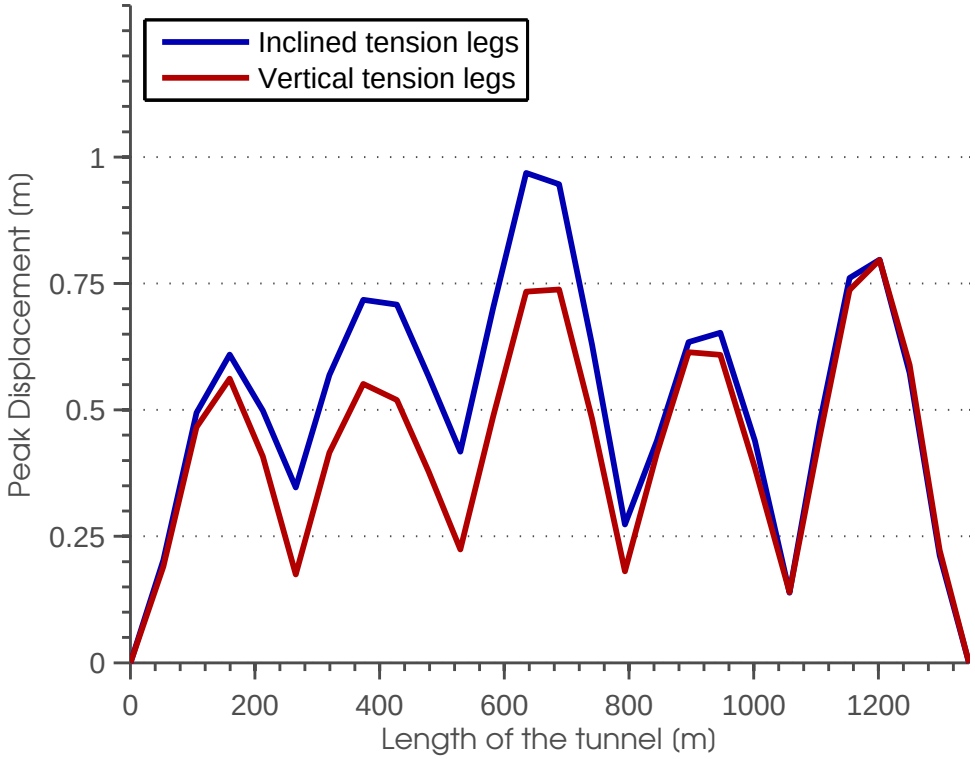

Figure 20: Expected peak value of the *vertical* response for vertical and inclined tension legs. Seismic waves arrive at 90° angle.

5.2 Further discussion

This section, discusses a few matters that have yet to be addressed.

The seismic load vector plays in important role in the modeling. This study uses acceleration and velocity spectra to generate the load vector (see Eq. 3.41), including their cross spectra. However, the inertia term generated by the acceleration spectra, in Eq. 3.41, contributes the most to the load vector. In fact, it it could be reasoned that they are negligible.

The effects of the fluid/structure interaction seems to help the performance of the tunnel during seismic events. It decreases the natural frequencies, which might bring them farther from the main frequency content of the earthquake. Also, the effects of hydrodynamical damping is small in comparison with the effects of added mass, which could be explained by the small motions in the structure. However,

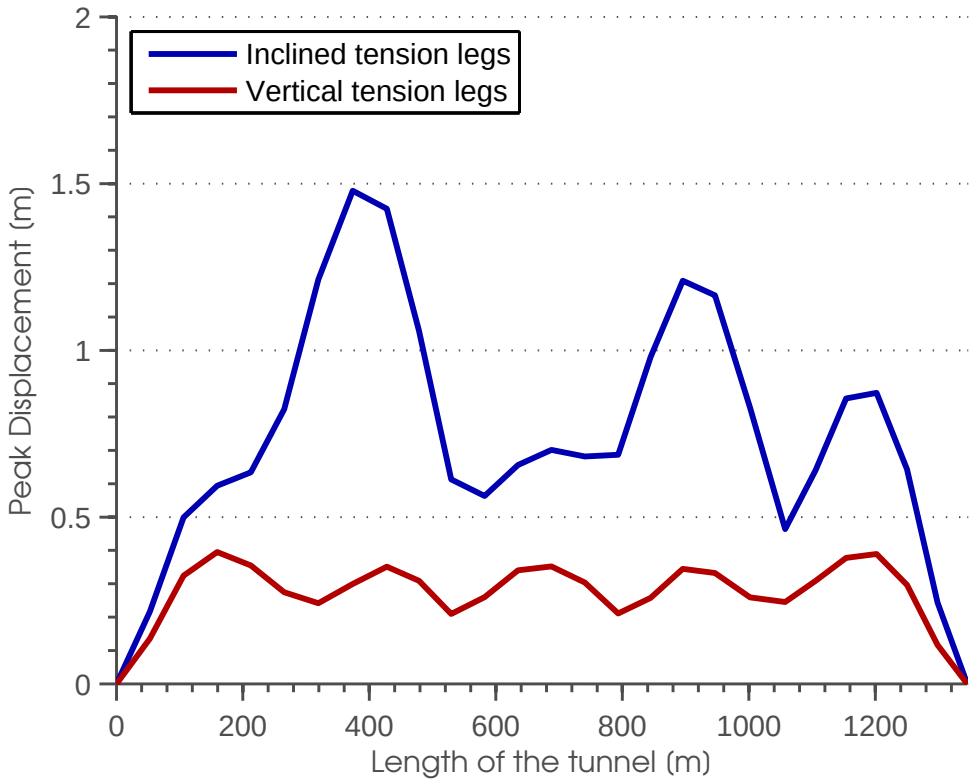

Figure 21: Expected peak value of the *horizontal* response for vertical and inclined tension legs. With $\zeta = 1\%$ damping ratio and seismic waves arrive at 90° angle.

including a steady current in the surrounding water could increase the hydrodynamical damping, since the damping increases non-linearly with the velocity of the surrounding water.

The results suggest that by inclining the tension legs the overall stiffness of the structure increases, which puts the structure into the frequency range of the structure. One can only suggest that by increasing the number of tension legs could increase the stiffness even further and result in larger response from seismic events. This is important to consider in the design of a SFT.

Ultimately, due the complexity of the incoherence and wave passage effect. All parameters and assumptions need to be carefully reasoned, in order to model the structural behavior accurately. Since the response is significantly influenced by the incoherence effects between supports, it would be interesting to implement different excitations for each component at each support of the structure. This would

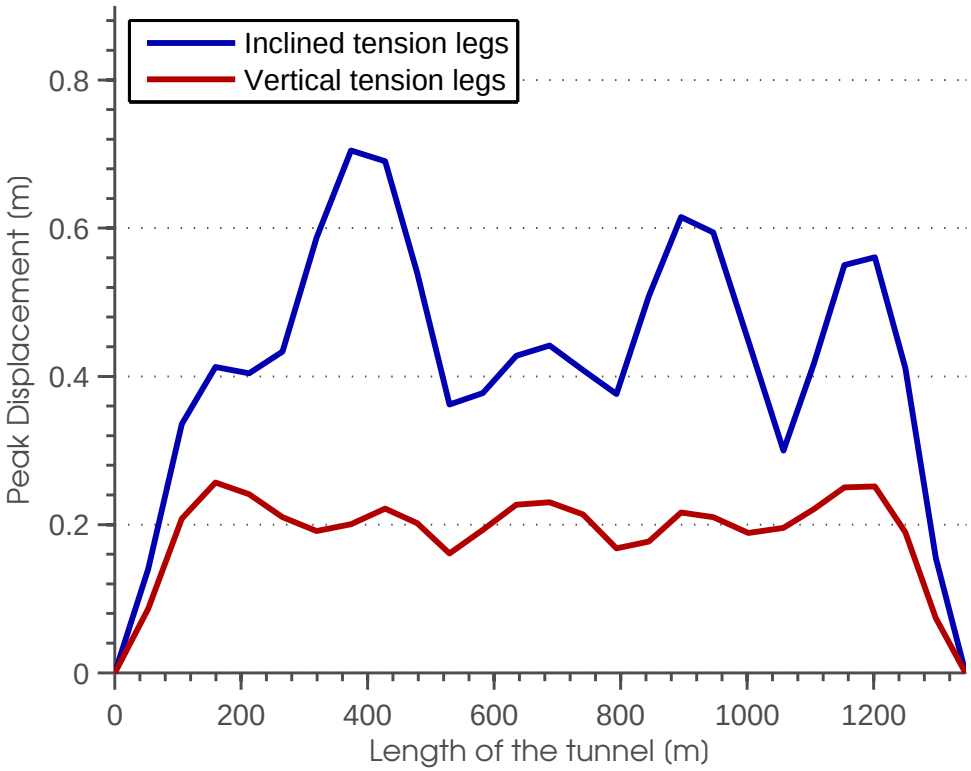

Figure 22: Expected peak value of the *horizontal* response for vertical and inclined tension legs. With $\zeta = 2\%$ damping ratio and seismic waves arrive at 90° angle.

probably increase the complexity of the structural behavior even further.

6 Conclusion

Submerged floating tunnels induced with seismic excitation are not likely to impose any major structural damages, as the response is small relative to the length of the structure. However, the traffic inside the tunnel could be subjected to strong accelerations. A structure of that importance should tolerate a seismic event without any risk of injuries to people. Therefore, acceleration effects on car traffic, needs to be studied and evaluated before any conclusions can be made.

The coherency between supports does have influence on the structural behavior. The wave passage effect seems to have more influence than the incoherence effect, the inter-component coherency also seems to matter. These effects seem increase the complexity of the structural behavior, as there are many parameters of relevance. The wave passage effect depends strongly on the seismic wave velocity, and as it varies it has often quite complex relationships with the response in the tunnel (Appendix D). For long span structure of such importance, it is essential to examine the coherency, as its effects on the structural behavior is not easily predictable.

For the seismic analysis, vertical tension legs are better suited to withstand large responses. Though they might not be particularly efficient in resisting the various sea loads. To avoid potential accidents as a cause of an earthquake, the structure should be designed with natural frequencies that do not match the frequency content of common seismic events. It should be mentioned that increased structural damping is also quite efficient in reducing the seismic response.

Ultimately, SFT can be regarded as earthquake resilient structures and earthquake load is probably not going to be the design load case for Norwegian requirements.

7 Further studies

Even though the analysis are termed successful and have given good insight in the behavior of SFTs subjected to seismic loading, it is important to identify areas where the modeling can be improved. In this chapter a few suggestions regarding further studies are mentioned and presented as follows:

- Introducing non-linearity to the finite element model and investigating the non-linear and inelastic effects to the structural stiffness and damping; especially due to soil properties, which is crucial in the soil-structure interaction. This could give better insight in the behavior of the structure.
- Utilizing different ground acceleration spectral density functions for each component at each support of the structure, which would give better description of the incoherence and the wave passage effects.
- Introducing site response effect, if the site of the structure has significant variations in soil conditions. This would add another dimension to the coherency model.
- Generating a improved inter-component coherency model. Possibly by considering more earthquake records than the ones considered in this study.
- Studying the structural and hydrodynamic damping. As the damping is an important factor in controlling the response of SFTs due to various environmental loads.

The current study has focused on the Norwegian seismic environments. It would be worthwhile to extent the study to more intensive earthquake prone areas to test the resilience of this type of structure.

A Coherency Models

A few coherency models are presented in the following section, with lagged coherency figures from some of the models.

A.1 Hindy-Novak model

The first to coherency model was introduced by Hindy & Novak (1980) and was based on wind engineering:

$$|\gamma_{jk}(\xi,\omega)| = exp\left[-\kappa\left(\frac{\omega\,\xi}{V_s}\right)^{\nu}\right] \tag{A.1}$$

where κ and ν are constants and V_s is shear wave velocity.

A.2 Harichandran-Vanmarcke model

Harichandran & Vanmarcke (1986) introduced a model based on 4 recorded events from the SMART-1 array. They noted that isotropy could be assumed for these records. The model took the form of the following expression:

$$|\gamma_{jk}(\xi_{jk},\omega)| = Aexp\left[-\frac{2\xi_{jk}}{\alpha\theta(\omega)}(1-A+\alpha A)\right]+(1-A)exp\left[-\frac{2\xi_{jk}}{\alpha\theta(\omega)}(1-A+\alpha A)\right] \tag{A.2}$$

where $\theta(\omega) = k[1+(\omega/\omega_0)^b]^{-1/2}$ and A, α, k, f_0, b are the model parameters which were estimated by a weighted least-square procedures and are listed in Table 6 for event 20.

Table 6: Proposed parameters for event 20 from the SMART-1 array (Harichandran & Vanmarcke, 1986).

	A	α	$k[m]$	$f_0[Hz]$	b
Event 20	0.736	0.147	5210	1.09	2.78

A.3 Loh-Yeh model

The method is based on 40 recordings of the SMART-1 array and takes the following form Loh & Yeh (1988):

$$|\gamma_{jk}(\xi_{jk},\omega)| = exp\left[-\alpha\frac{\omega\,\xi_{jk}}{2\pi v_{app}}\right] \tag{A.3}$$

in which v_{app} is the apparent velocity of the seismic waves and α is the wave-number of the seismic waves.

A.4 Oliveira-Hao-Penzien model

$$|\gamma_{jk}(\xi^l_{jk},\xi^t_{jk},\omega)| = exp(-\beta_1\xi^l_{jk}-\beta_2\xi^t_{jk})exp[(\alpha_1\sqrt{\xi^l_{jk}}-\alpha_2\sqrt{\xi^t_{jk}})(\omega/2\pi)^2] \tag{A.4}$$

where $\alpha_i = 2\pi a/\omega + b\omega/2\pi + c, (i = 1, 2)$, ξ^l_{jk} and ξ^t_{jk} are the separation distances in the longitudinal and tangential direction of the propagating wave. The constants β_i, a_i, b_i and c_i, $(i = 1, 2)$ are obtained from least square fitting of 17 recorded SMART-1 array events (Oliveira *et al.* , 1991).

A.5 Luco-Wong model

$$|\gamma_{jk}(\xi_{jk},\omega)| = exp\left[-\left(\frac{v\omega\xi_{jk}}{V_s}\right)^2\right] \tag{A.5}$$

in which $v = \mu(R/r_0)^{1/2}$, V_s is the shear velocity of the seismic wave, R is the distance traveled by the wave in random medium, r_0 is the scale length of random inhomogeneities along the path and μ is a measure of the relative variation of the elastic properties.

A.6 Der Kiureghian model

Der Kiureghian (1996) introduced a semi-empirical model that describes the incoherent effect of the coherency in a probabilistic sense using the theory of random

processes. He assumed that the time histories at two locations j and k where were stationary and expressed as:

$$a_j(t)^d = \sum_{i=1}^{n} A_i \cos(\omega_i t + \phi_i) \tag{A.6}$$

$$a_k(t)^d = \sum_{i=1}^{n} (p_{jk} A_i + q_{jk} B_i) \cos(\omega_i t + \phi_i + \varepsilon_{jk,i}) \tag{A.7}$$

Equation A.6 is the discrete Fourier series of the acceleration time history at support j. Eq. A.7 introduces variables that describe the incoherence between supports j and k. B_i are zero-mean, uncorrelated random variables with mean square values σ^2 describing the incoherent part of the amplitudes, $\varepsilon_{jk,i}$ are independent random phase differences with zero mean and variance $\alpha^2_{jk,i}$. p_{jk} and q_{jk} are deterministic coefficients with values assumed on the interval (0,1) with $p_{jk} + q_{jk} = 1$. The subscript jk, i denotes that the parameters are dependant on the separation distance ξ_{jk} and the frequency ω_i. The lagged coherency was then expressed as (Der Kiureghian, 1996):

$$|\gamma_{jk}(\xi_{jk}, \omega)| = \cos[\beta(\xi_{jk}, \omega)] exp\left[-\frac{1}{2}\alpha^2(\xi_{jk}, \omega)\right] \tag{A.8}$$

where $\beta(\xi_{jk}, \omega) = \tan^{-1}(q_{jk}/p_{jk}))$ and $\alpha^2(\xi_{jk}, \omega)$ is introduced above. Since then, Yang & Chen (2000) has provided functional forms for the functions $\beta(\xi_{jk}, \omega)$ and $\alpha^2(\xi_{jk}, \omega)$ which gives the lagged coherency the following form:

$$|\gamma_{jk}(\xi_{jk}, \omega)| = \left[1 + a_1 \xi_{jk} + a_2 \left(\frac{\xi_{jk}\omega}{2\pi}\right)^{1/2}\right]^{-1/2} exp\left[-\frac{1}{2}\left(\frac{a_3 \xi_{jk}^{a_4} \omega^{a_5}}{2\pi}\right)\right] \tag{A.9}$$

The parameters in Eq.A.9 were obtained by utilizing records from the SMART-1 array. The parameters are listed in Table 7

Table 7: Parameters introduced by Yang & Chen (2000) for the coherency model developed by Der Kiureghian (1996).

a_1	a_2	a_3	a_4	a_5
0.1151	-0.2249×10^{-2}	0.0762	0.3784	0.2206

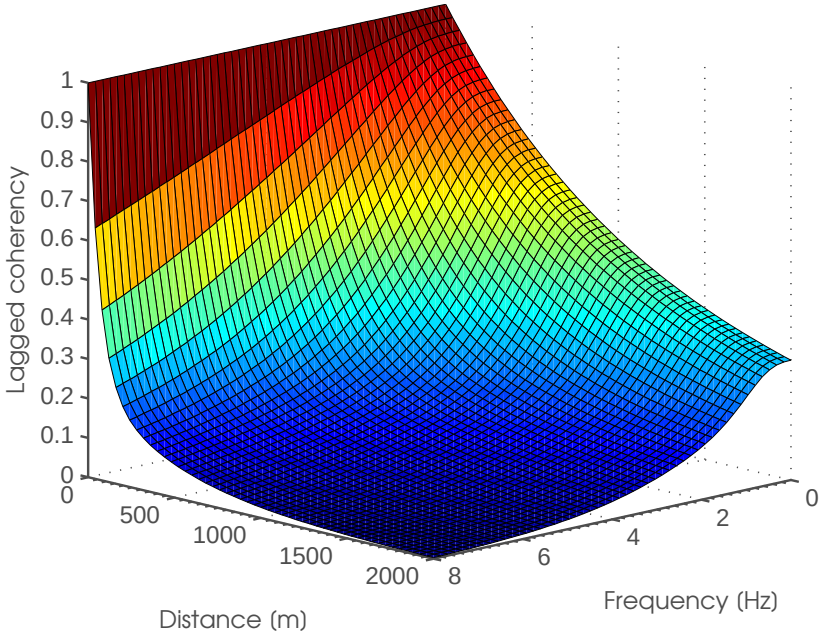

Figure 23: Lagged coherency as a function of distance and frequency. A coherency model developed by Harichandran & Vanmarcke (1986).

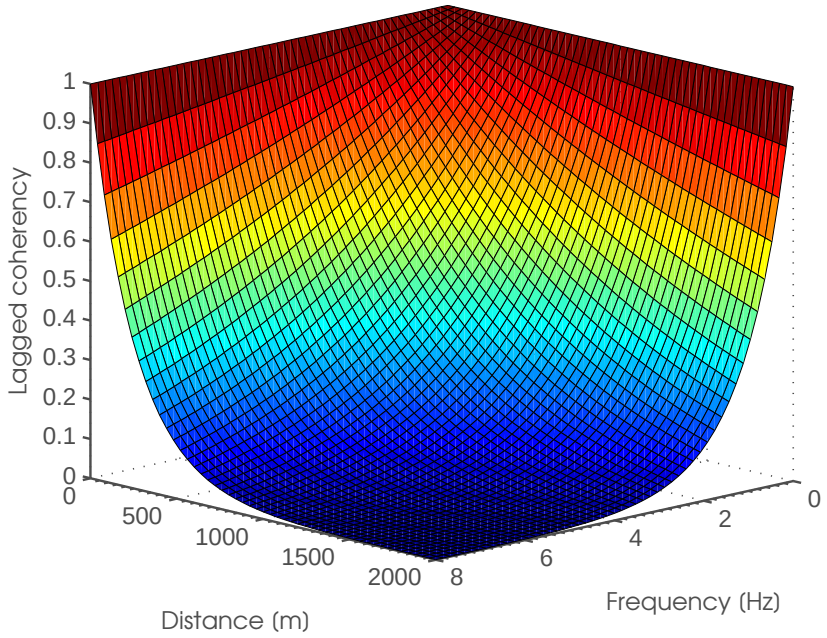

Figure 24: Surface plot of Loh & Yeh (1988) coherency model.

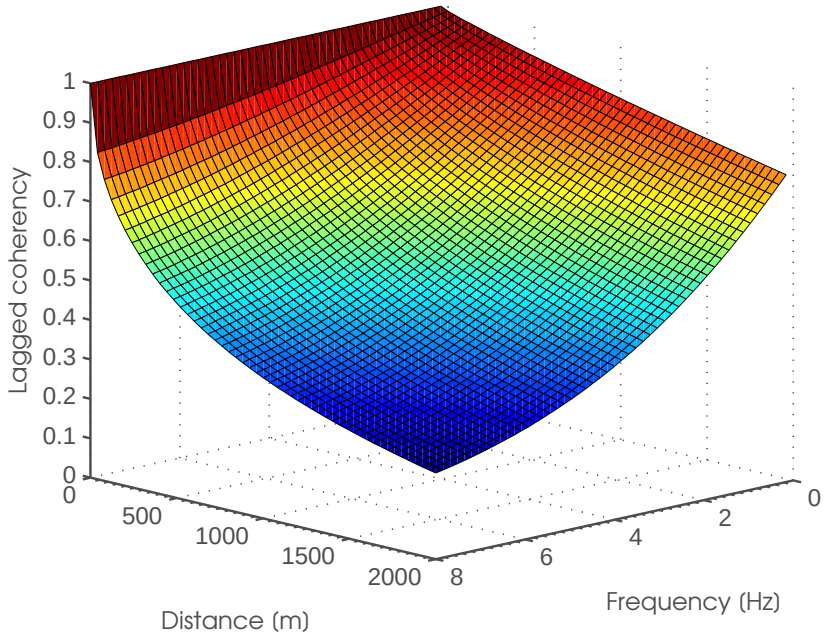

Figure 25: Variation of the lagged coherency (Oliveira *et al.* , 1991), when separation distance normal to the propagation of the wave equals zero $\xi_{jk}^{t} = 0$.

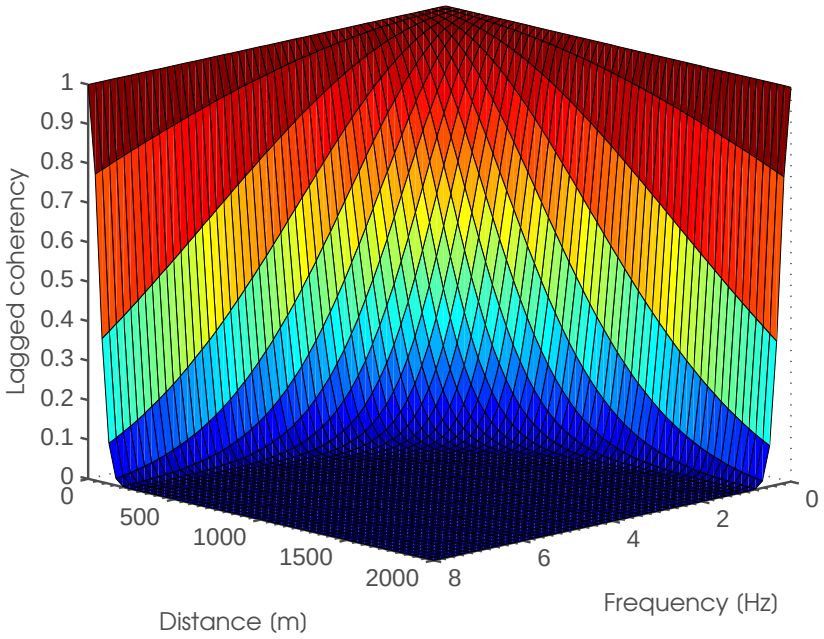

Figure 26: Variation of the lagged coherency. A model developed by Luco & Wong (1986).

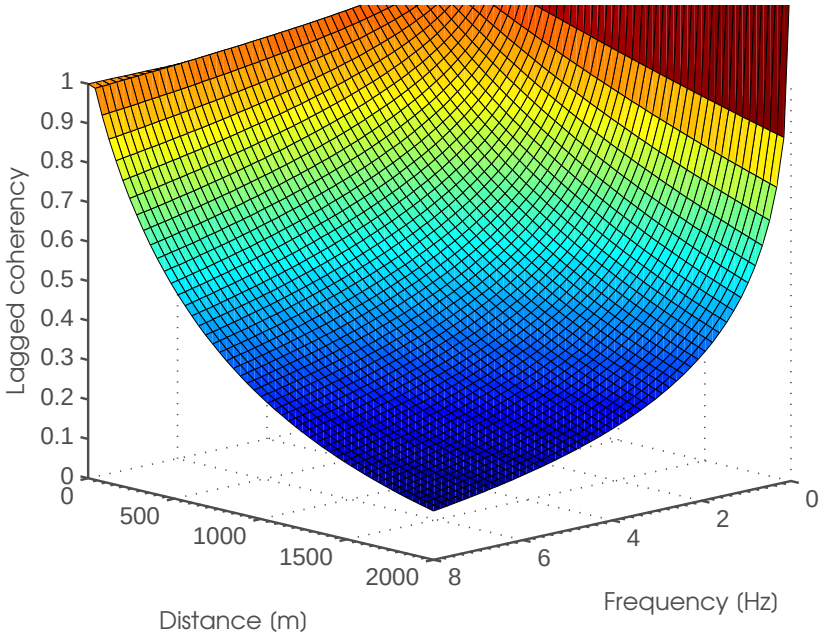

Figure 27: Variation of the lagged coherency. A model developed by Der Kiureghian (1996)

B PSD of the seismic load vector

The consistent load vector for the system described in Eq. 3.40 is written in two parts, i.e. for the acceleration and the velocity of the ground motion. The load vector can be written as:

$$Q(t) = \mathbf{A}_a \ddot{\mathbf{u}}_g(t) + \mathbf{A}_v \dot{\mathbf{u}}_g(t) \tag{B.1}$$

where $\mathbf{A}_a$ and $\mathbf{A}_v$ are transformation matrices of the load system introduced in Section 3.4.2. The auto-correlation function of the load vector can be expressed as:

$$R_Q(\tau) = E[\mathbf{Q}(t)\mathbf{Q}^T(t+\tau)] \tag{B.2}$$

Substituting Eq. B.1 into Eq. B.2 gives:

$$R_Q(\tau) = \mathbf{A}_a R_{\ddot{u}_g}(\tau)\mathbf{A}_a^T + \mathbf{A}_a R_{\ddot{u}_g \dot{u}_g}\mathbf{A}_v^T + +\mathbf{A}_v R_{\dot{u}_g \ddot{u}_g}\mathbf{A}_a^T + \mathbf{A}_v R_{\dot{u}_g}(\tau)\mathbf{A}_v^T \tag{B.3}$$

where $R_{\ddot{u}_g}$ and $R_{\dot{u}_g}$ are the auto-correlation functions; whereas $R_{\ddot{u}_g \dot{u}_g}$ and $R_{\dot{u}_g \ddot{u}_g}$ are is the cross correlation function of the ground acceleration and velocity.

Since, the auto-correlation function $R_Q(\tau)$ and the auto-PSD function $S_Q(\omega)$ are a Fourier transform pair, as described in Eqs. 3.1-3.2, the auto-PSD function of the load vector can be written as:

$$S_Q(\omega) = \mathbf{A}_a S_{\ddot{u}_g}(\omega)\mathbf{A}_a^T + \mathbf{A}_v S_{\dot{u}_g}(\omega)\mathbf{A}_v^T + \mathbf{A}_a S_{\ddot{u}_g \dot{u}_g}(\omega)\mathbf{A}_v^T + \mathbf{A}_v S_{\dot{u}_g \ddot{u}_g}(\omega)\mathbf{A}_a^T \tag{B.4}$$

which is then used in the analysis (see Section 3.4.2).

C Mode shapes

In this section the natural mode shapes from Abaqus are presented

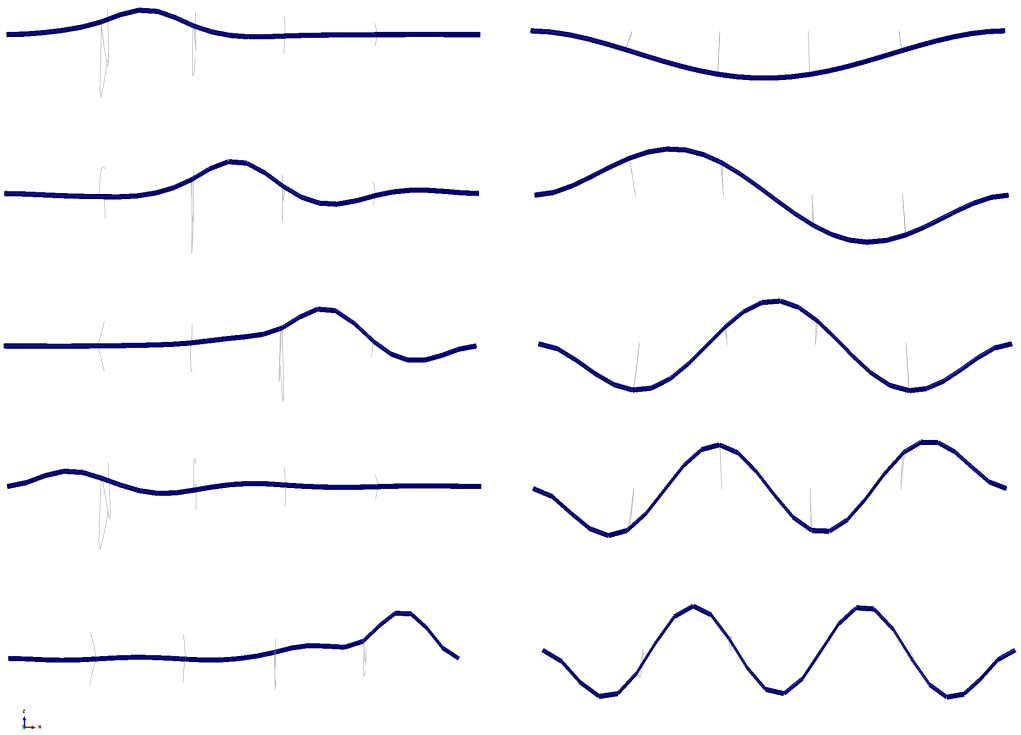

Figure 28: First five "dry" *horizontal* mode shapes for both the inclined (left) and the vertical (right) tension legs.

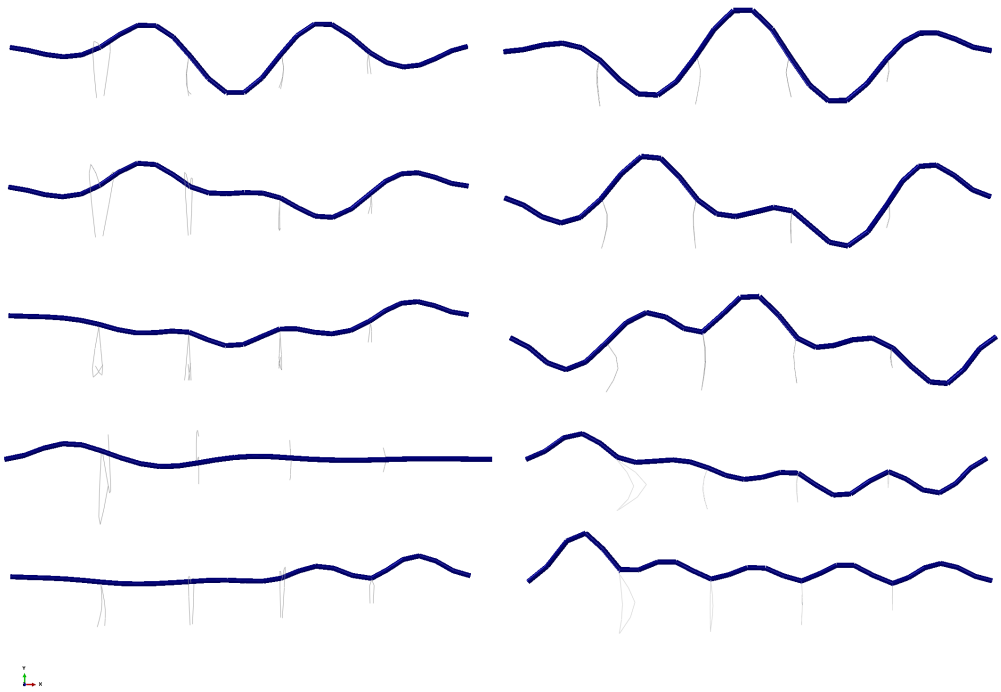

Figure 29: First five "dry" *vertical* mode shapes for both the inclined (left) and the vertical (right) tension legs.

D Response for varying seismic wave velocity

This section demonstrates plots of a the displacement response for varying velocity of the seismic waves:

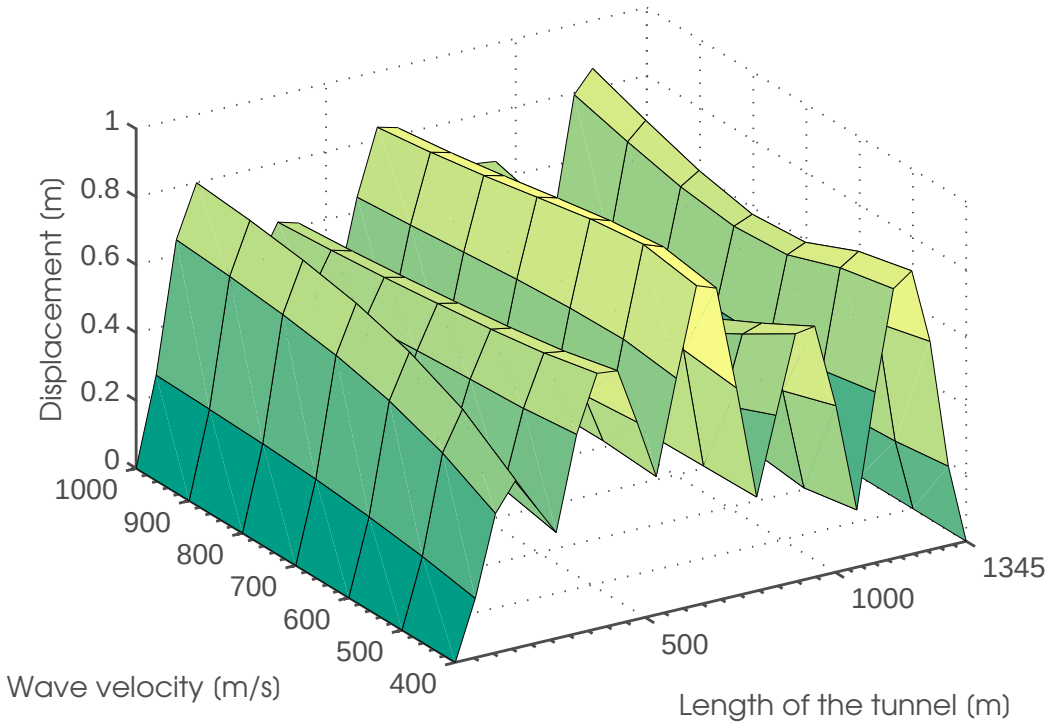

Figure 30: Expected maximum *vertical* displacement of the tunnel, with seismic waves arriving with 90° angle and incoherence modeled by Oliveira *et al.* (1991).

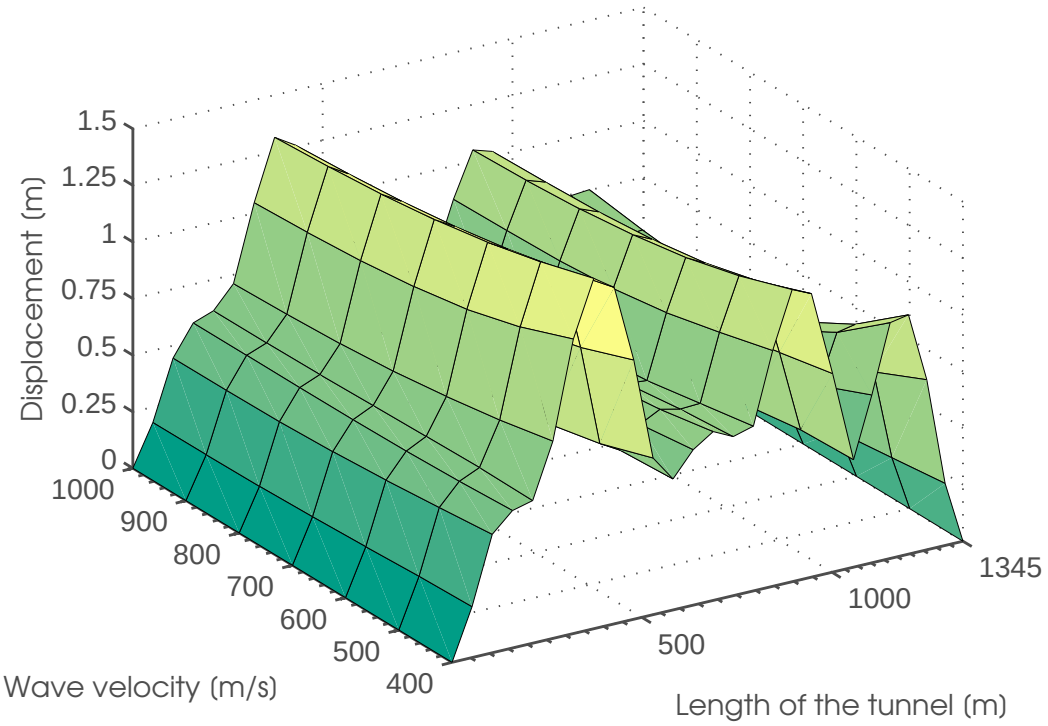

Figure 31: Expected maximum *horizontal* displacement of the tunnel for different wave velocities, with seismic waves arriving with 90° angle and incoherence modeled by Oliveira *et al.* (1991)

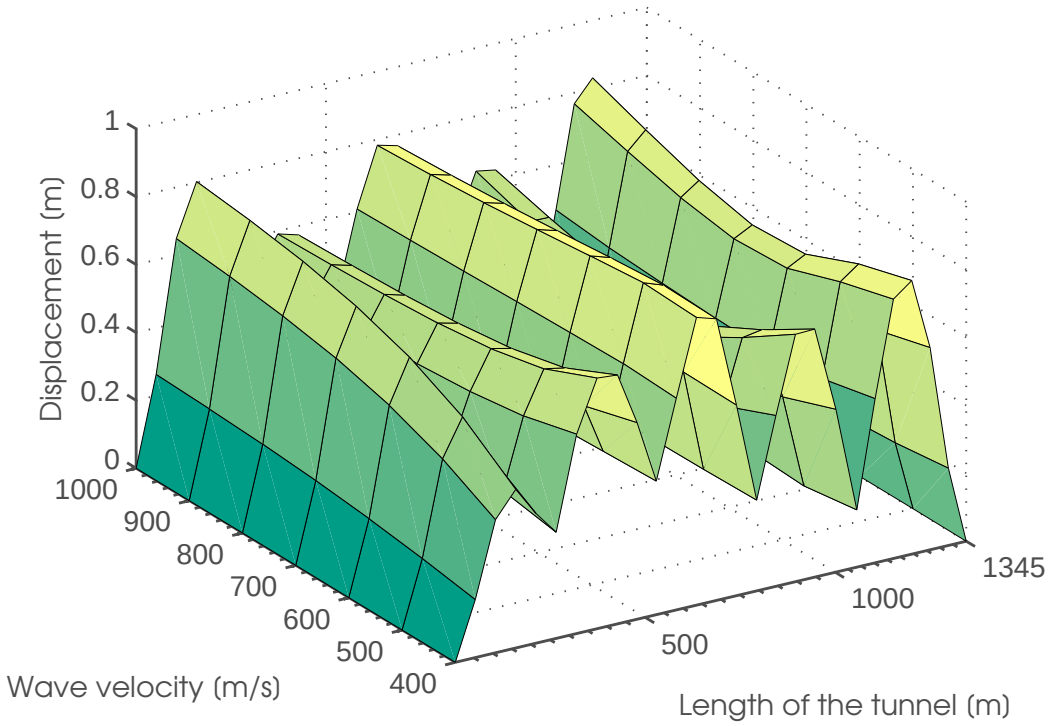

Figure 32: Expected maximum *vertical* displacement of the tunnel for different wave velocities, with seismic waves arriving with 0° angle and incoherence modeled by Oliveira *et al.* (1991)

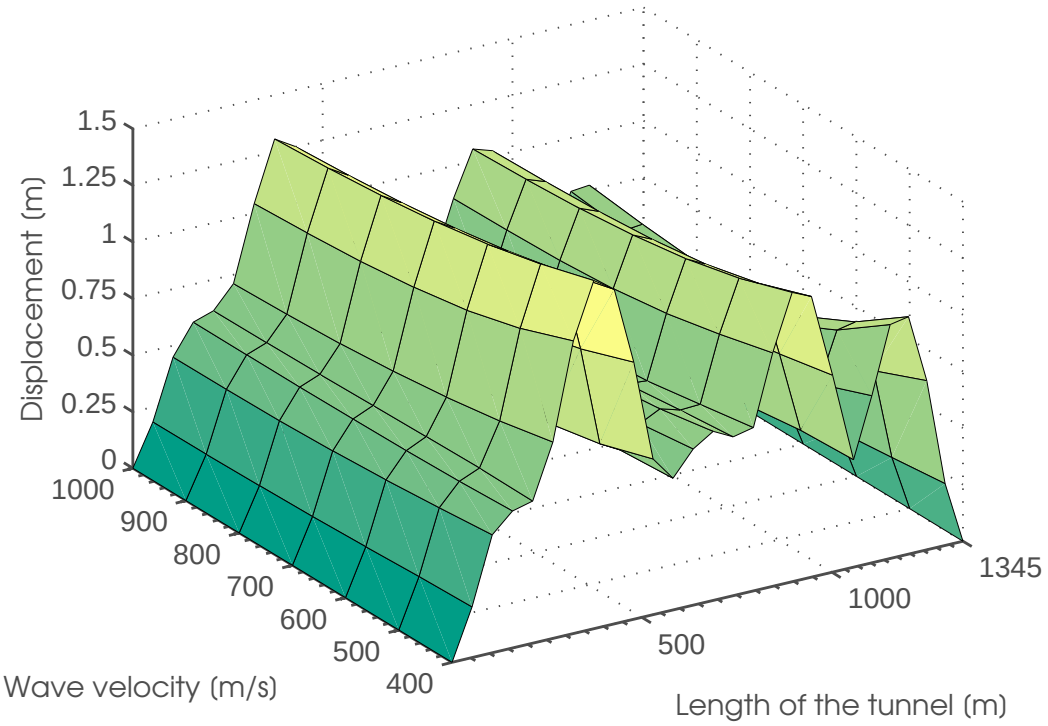

Figure 33: Expected maximum *horizontal* displacement of the tunnel for different wave velocities, with seismic waves arriving with 0° angle and incoherence modeled by Oliveira *et al.* (1991)

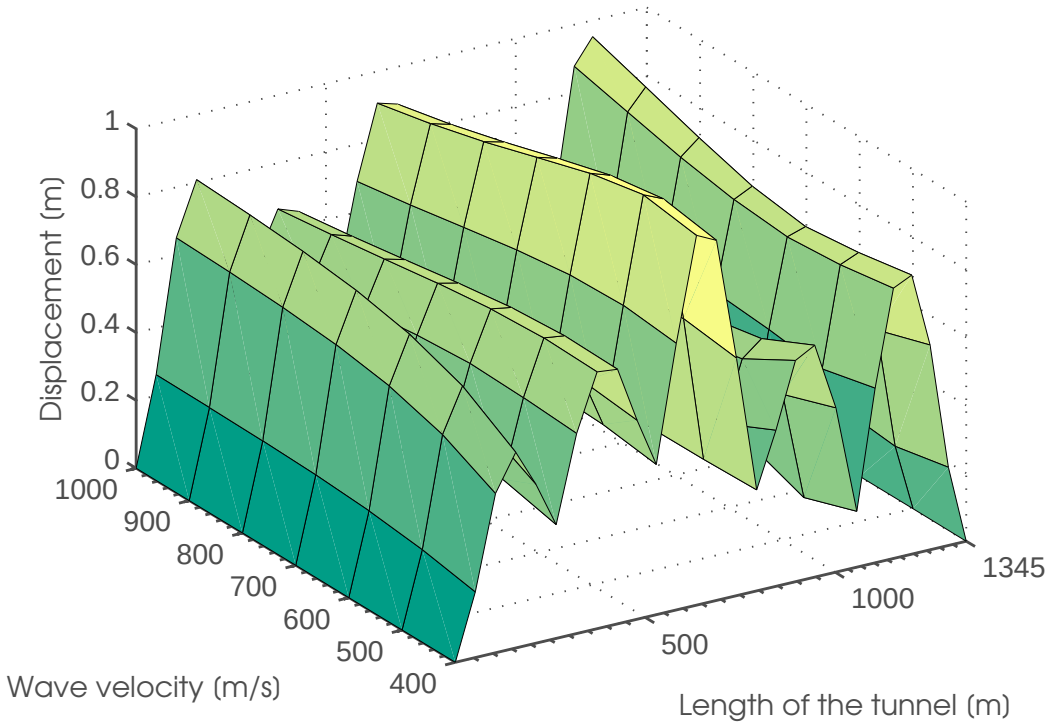

Figure 34: Expected maximum *vertical* displacement of the tunnel for different wave velocities, with seismic waves arriving with 90° angle for a fully coherent excitation ($\gamma = 1$).

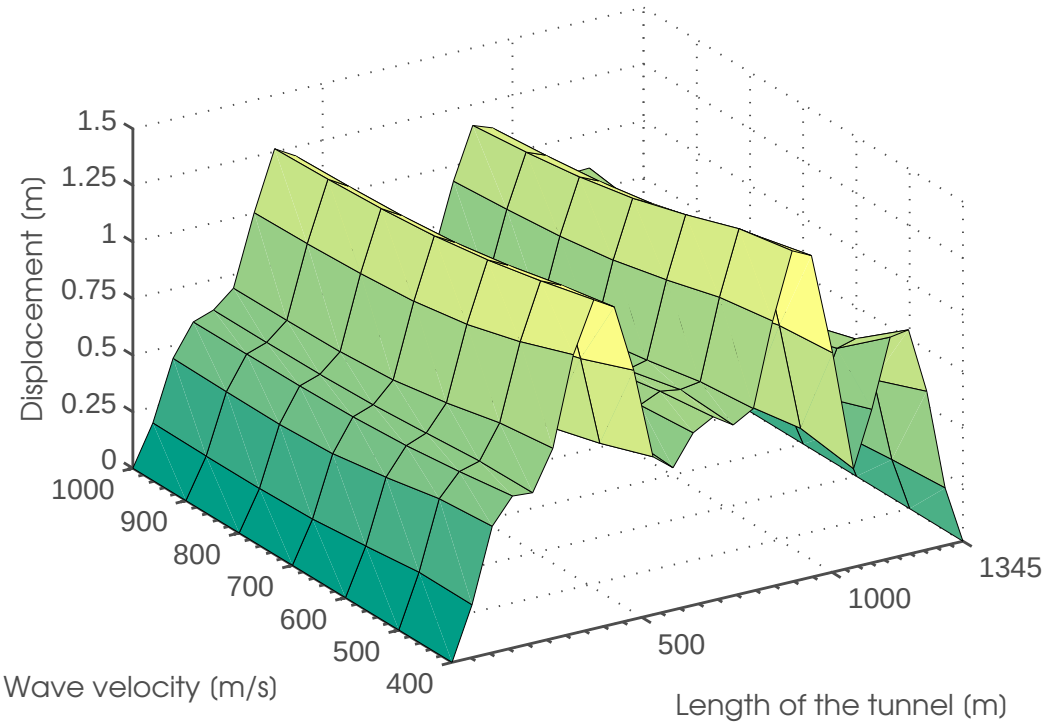

Figure 35: Expected maximum *horizontal* displacement of the tunnel for different wave velocities, with seismic waves arriving with 90° angle for a fully coherent excitation ($\gamma = 1$).

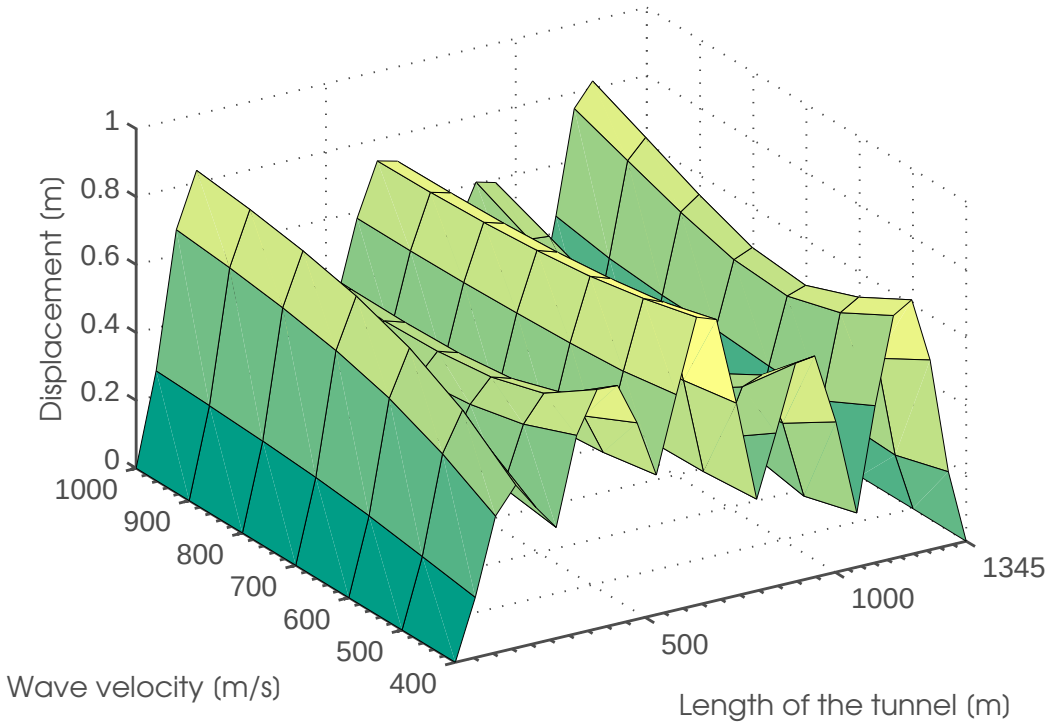

Figure 36: Expected maximum *vertical* displacement of the tunnel for different wave velocities, with seismic waves arriving with 0° angle for a fully coherent excitation ($\gamma = 1$).

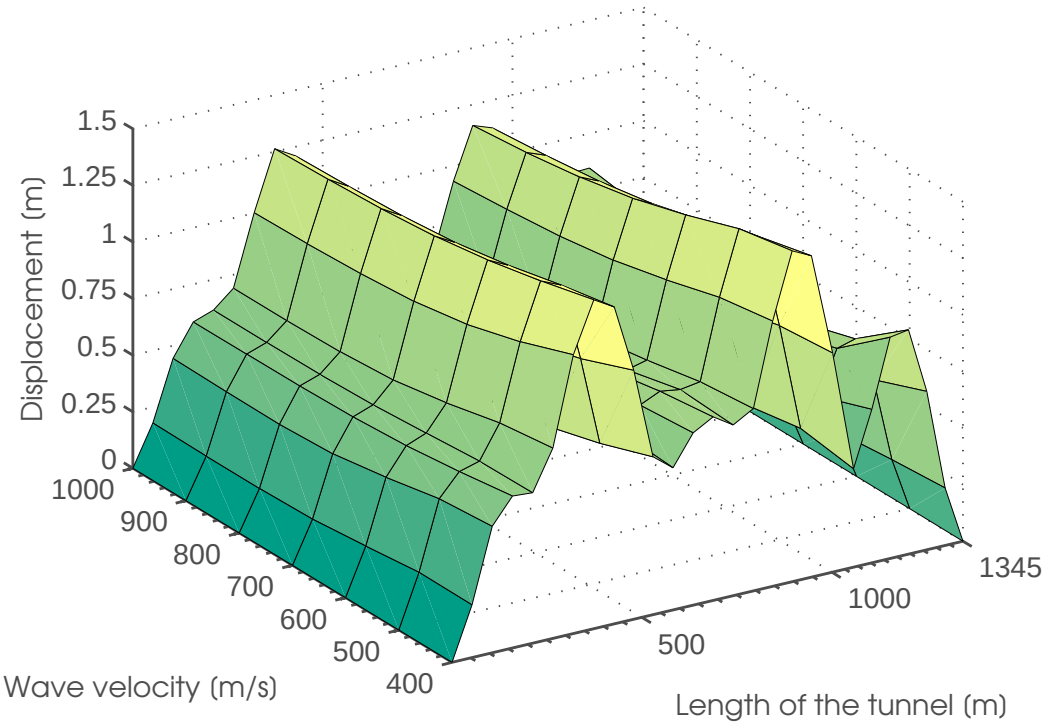

Figure 37: Expected maximum *horizontal* displacement of the tunnel for different wave velocities, with seismic waves arriving with 0° angle for a fully coherent excitation ($\gamma = 1$).

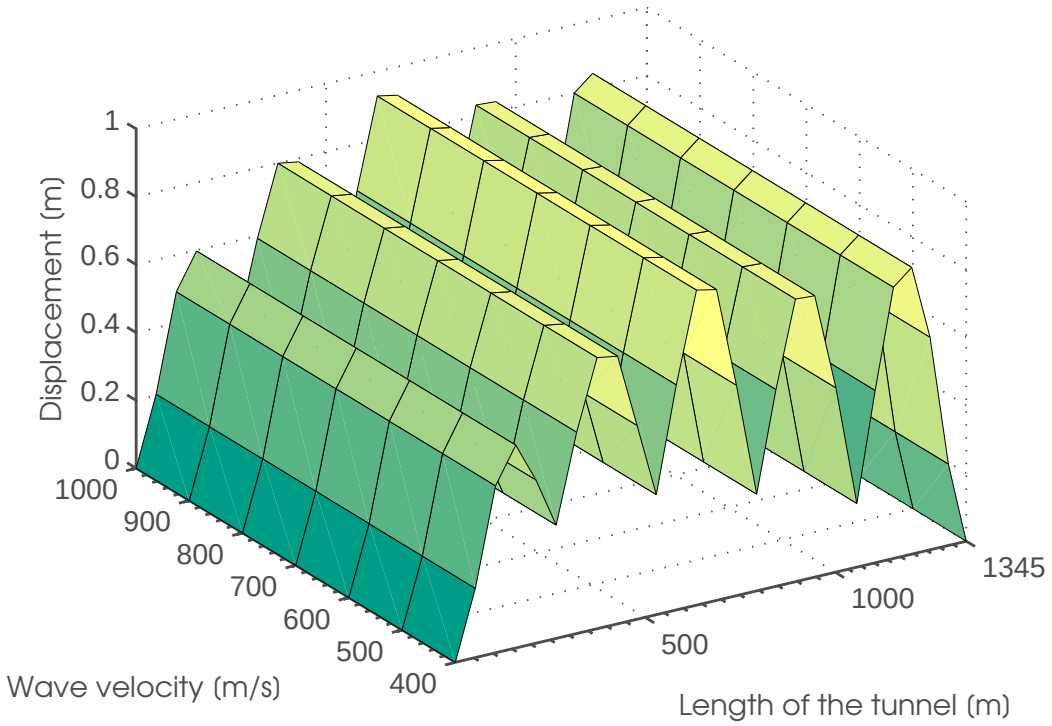

Figure 38: Expected maximum *vertical* displacement of the tunnel for different wave velocities, with seismic waves arriving with 90° angle for a non-coherent excitation ($\gamma = 0$).

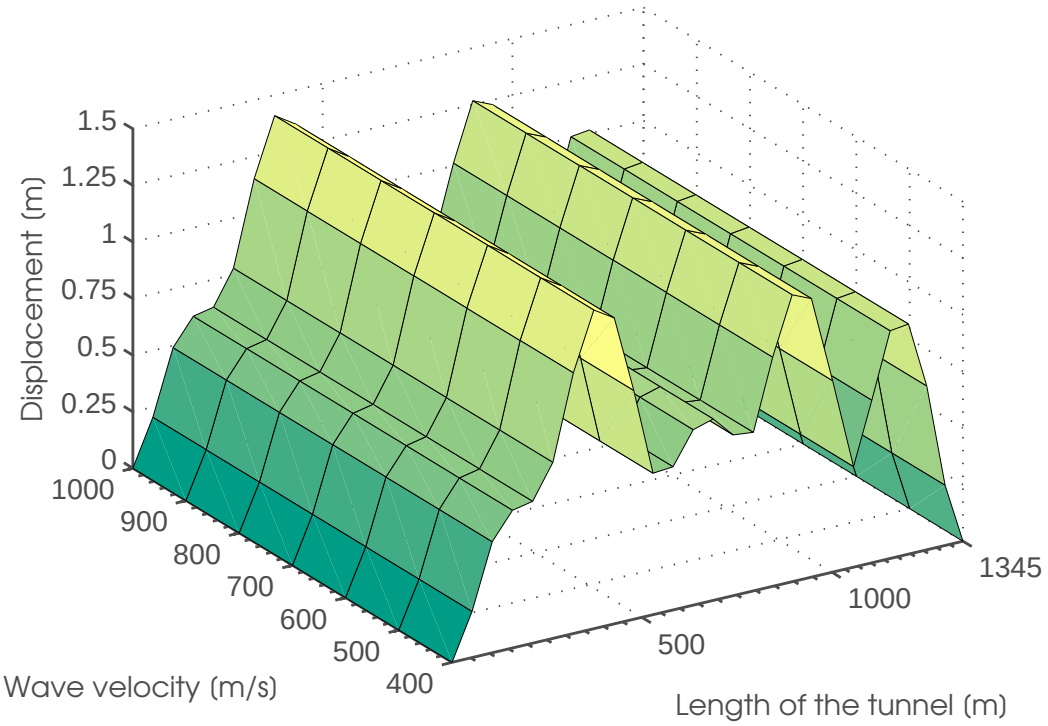

Figure 39: Expected maximum *horizontal* displacement of the tunnel for different wave velocities, with seismic waves arriving with 90° angle for a non-coherent excitation ($\gamma = 0$).

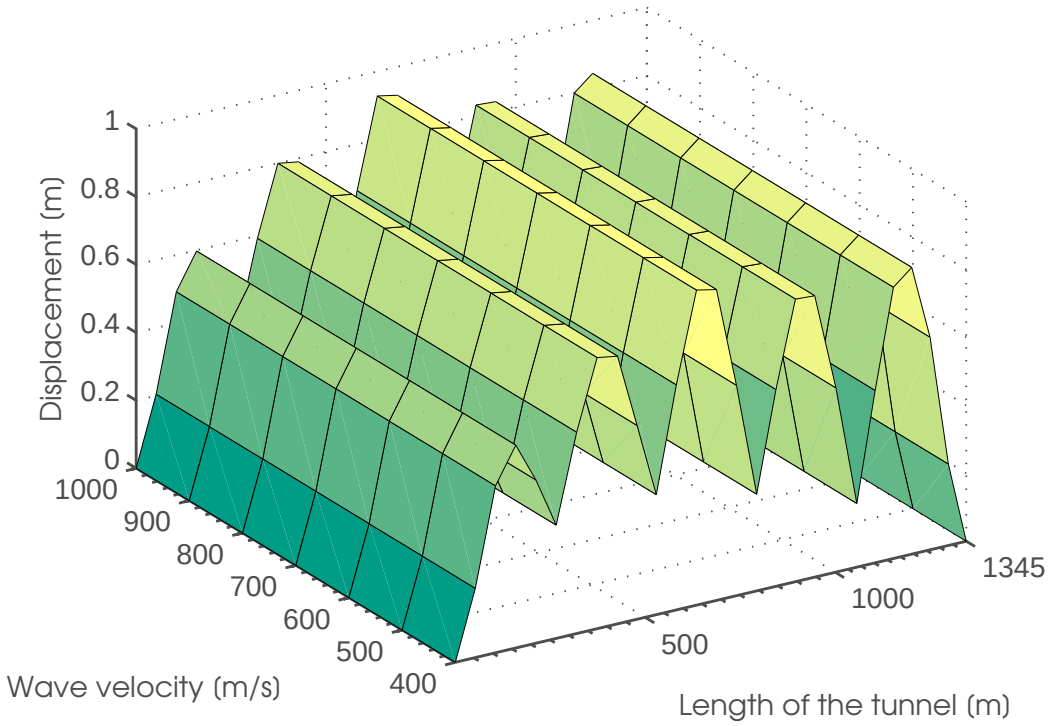

Figure 40: Expected maximum *vertical* displacement of the tunnel for different wave velocities, with seismic waves arriving with 0° angle for a non-coherent excitation ($\gamma = 0$).

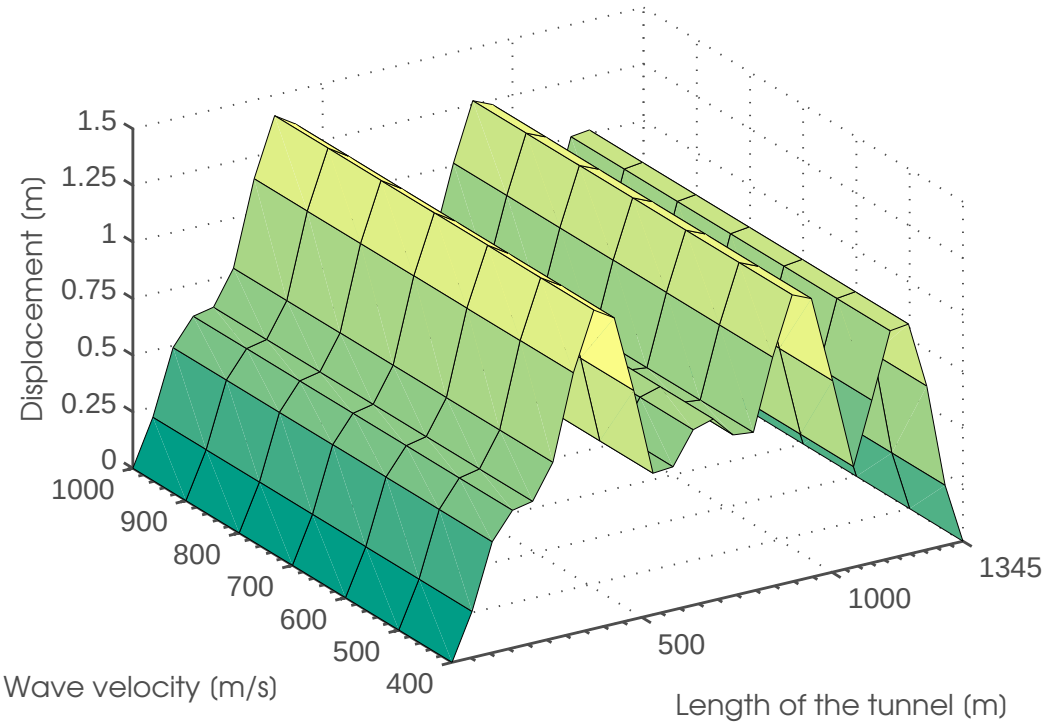

Figure 41: Expected maximum *horizontal* displacement of the tunnel for different wave velocities, with seismic waves arriving with 0° angle for a non-coherent excitation ($\gamma = 0$).

E Matlab codes

In this section the Matlab codes for the analysis are presented:

E.1 Main file

```
% m-file: Mainfile.m
%
% Purpose: Seismic analysis for SFT
%
% Note:
% Written by: Birgir Indridason, Spring 2013
%


MassData=load('bla_MASS2.mtx');
StifData=load('bla_STIF2.mtx');

NatFreqAba=load('NatFreqAbaqus.txt');

%Damping Properties
a=0.0230;         %Alfa coefficient for rayleigh damping
B=0.0087;        %Beta coefficient for rayleigh damping
eta=0.012;       %Damping coefficient for stiffness damping


%Generating system matrices for the system

[Mii,Cii,Kii,Mie,Kie,Cie]=MatrixGenerate2...
(MassData,StifData,a,B,eta);



Cm = 2;        %Coefficient of Mass (inertia)

p=1025;        %Density of the fluid
Cd = 1;        %Coefficient of Drag
D = 5.65*2;    %Diameter of cylinder
d = 0.1*2;     %Diameter of the tension leg
```

```
34
35 [Mh Ch]=hydrodynamics(p,Cd,Cm,D,d);
36
37
38 M=Mii-Mh;                    %Applying hydrodynamics to the element
39 C=Cii-Ch;                    %matrices
40 K=Kii;
41
42
43 beta=pi/2;                   %angle of the incoming wave to the ...
       tunnel
44
45 [fw,Two,f,Vw,Dw]=eigfreq(M,K,Mii,Kii); %Calculating "wet" and ...
       "dry"
46                                          %and wet frequencies
47
48
49 v=[400:100:1000];            %Wave propagation speed [km/s]
50 %v=500;
51 Td=10;              %Period of the strong earthquake portion
52
53
54 for i=1:length(v)
55
56     V1=v(i);
57
58
59
60 [sigmaR,maxDispl,Sr,Srv,Sra,maxvel,maxacc,sigmaRV,sigmaRa]...
61 =analysis1(K,Kie,M,Mie,C,Cie,beta,V1,Td);
62
63 Sr_mat(:,:,i)=Sr;        %Generating matrices for different ...
       wave velocities
64 sigma_r(i,:)=sigmaR;
65 MaxD(i,:)=maxDispl;
66
67 Srv_mat(:,:,i)=Srv;
68 sigma_rv(i,:)=sigmaRV;
69 MaxV(i,:)=maxvel;
70
71 Sra_mat(:,:,i)=Sra;
72 sigma_ra(i,:)=sigmaRa;
```

```
73 MaxA(i,:)=maxacc;
74
75 end
```

E.2 Matrix generation

```
1
2  function [Mii,Cii,Kii,Mie,Kie,Cie]...
3      =MatrixGenerate2(MassData,StifData,a,B)
4
5  %Importing mass matrix from data
6
7  for i=1:length(MassData)
8
9      j=MassData(i,1);
10     k=MassData(i,2);
11     Mii(j,k)=MassData(i,3);
12
13 end
14
15 %Importing Stiffness matrix from data
16
17 for i=1:length(StifData)
18
19     j=StifData(i,1);
20     k=StifData(i,2);
21     Kii(j,k)=StifData(i,3);
22
23 end
24
25 %Degrees of freedom which contain the foundations of the structure
26
27 y=[139:144 175:180 331:378];
28
29 %Rotational DOFs of the Kei and Mei matrices (will be eliminted)
30
31 z=[4:6 10:12 16:18 22:24 28:30 34:36 40:42 46:48 52:54 58:60];
32
33
34 Cii=a*Kii+B*Mii;        %Generating damping matrix
35
36
37 Kei1(1:length(y),1:length(Kii))=Kii(y,:);
38 Mei1(1:length(y),1:length(Mii))=Mii(y,:);
39 Cei1(1:length(y),1:length(Cii))=Cii(y,:);
```

```
40
41 Kii(y,:)=[];              %Subtracting the DOFs of the supports
42 Mii(y,:)=[];
43 Cii(y,:)=[];
44 Kii(:,y)=[];
45 Mii(:,y)=[];
46 Cii(:,y)=[];
47 Kei1(:,y)=[];
48 Mei1(:,y)=[];
49 Cei1(:,y)=[];
50 Kei1(z,:)=[];
51 Mei1(z,:)=[];
52 Cei1(z,:)=[];
53
54 %Subtracting into regular DOF matrices
55 Kii=Kii(121:end,121:end);
56 Mii=Mii(121:end,121:end);
57 Cii=Cii(121:end,121:end);
58
59 Kei1=Kei1(:,121:end);
60 Mei1=Mei1(:,121:end);
61 Cei1=Cei1(:,121:end);
62
63 %Transforming the matrices
64 Kie=Kei1';
65 Mie=Mei1';
66 Cie=Cei1';
67
68 end
```

E.3 Natural frequencies

```
1
2  function [fw,Tw,fd,Vw]=eigfreq(M,K,Mii,Kii)
3
4  [Vw,Dw]=eig(K,M);        %Wet natural frequencies and vectors
5
6  [Vd,Dd]=eig(Kii,Mii);    %Dry natural frequencies and vectors
7
8  ww=sqrt(diag(Dw));       %Wet angular natural frequencies
9
10 wd=sqrt(diag(Dd));       %Dry angular natural frequencies
11
12 fw=ww./(2*pi);           %Wet natural frequencies
13
14 fd=wd./(2*pi);           %Dry natural frequencies
15 end
```

E.4 Anlysis

```
1
2  function [sigmaR,maxDispl,Sr,maxvel,maxacc,sigmaRV,sigmaRa]...
3      =analysis1(K,Kie,M,Mie,C,Cie,beta,V1,Td)
4
5  %Kanai-Tajimi filter parameters
6  wg=15.6;
7  wh=4;
8  Lg=0.7;
9  Lh=0.5;
10 S0=0.05;       %Period of the strong earthquake portion
11
12
13 e1=[cos(beta);0;sin(beta)];         %orientation vectors
14 e2=[0; 1; 0];
15 e3=[-sin(beta);0;cos(beta)];
16 e=[e1 e2 e3];
17
18 EmN=zeros(30);           %Orientation matrix
19
20 for n=1:10
21
22     EmN(n*3-2:n*3,n*3-2:n*3)=e;
23 end
24
25 B=-(K\Kie);               %Transformation matrices
26 B1=-(M*B+Mie)*EmN;
27 B2=-(C*B+Cie)*EmN;
28
29 dw=0.05;
30 w=[0.05:dw:15];       %Frequency interval for the response ...
       calculations
31
32 %Oliveira coherency model parameters
33 B3=[1.109e-4 6.730e-5];
34 a=[3.853e-3 5.163e-3];
35 b=[-18.11e-6 -7.583e-6];
36 c=[11.77e-5 -1.905e-4];
37
38 %Nodes along thes tunnel
```

```
hp=[30 31 32 33 8 28 29 7 27 6 23 24 25 26 5 21 22 4 20 1 15 ...
    16 17 ...
     18 19]*6-3;

for m=1:length(hp)
for n=1:length(w)

    w1=w(n);
%Generation of acceleration spectra
[Sa, Sv, Sav, Sva]=AccelSpectra(w1,wg,wh,Lg,Lh,S0);

%Coherency model (Oliveira)
[Sc]=Oliveira(B3,a,b,c,w1,beta,V1);

Sa=Sc*Sa;       %auto spectral density of acceleration and
Sv=Sc*Sv;       %velocity with coherency
Sav=Sc*Sav;     %Cross spectral density
Sva=Sc*Sva;


%Spectral density function of the load vector
Sq=B1*Sa*B1'+B2*Sv*B2'+B1*Sav*B2'+B2*Sva*B1';

%Transformation matrix
H=(K-(w1^2)*M+(1i*w1*C))^(-1);
HT=conj(H);

%Response spectra
Sr(m,n)=H(hp(m),:)*Sq*HT(:,hp(m));
Srv(m,n)=(w1^2)*(H(hp(m),:)*Sq*HT(:,hp(m)))/(2*pi);
Sra(m,n)=((w1^4)*(H(hp(m),:)*Sq*HT(:,hp(m))))/(2*pi)^3;
end

%variance of response spectra
var(m)=sum(real(Sr(m,:)))*dw;
varv(m)=sum(real(Srv(m,:)))*dw;
vara(m)=sum(real(Sra(m,:)))*dw;

%Standard deviation of response spectra
sigmaR(m)=sqrt(var(m));
sigmaRV(m)=sqrt(varv(m));
sigmaRa(m)=sqrt(vara(m));
```

```
80
81 %Peak factor
82 wplus=sigmaRV/sigmaR;
83 N=wplus*Td/(2*pi);          %Number of upcrossings
84 gt=sqrt(2*log(2*N*Td))+0.5772/(sqrt(2*log(2*N*Td)));
85
86 %Expected maximum motions
87 maxDispl=gt*sigmaR;     %Displacement
88 maxvel=gt*sigmaRV;      %Velocity
89 maxacc=gt*sigmaRa;      %Acceleration
90
91 end
```

E.5 Coherency model

```
function [Sc]=Oliveira(B3,a,b,c,w1,beta,V1)

f=w1/(2*pi);    %Frequency in [Hz]

x=zeros(10);

%Distance between supports (in matrix form)
x(1,:)=[0 sqrt(265^2+75^2) sqrt(265^2+75^2) ...
    sqrt((265+264)^2+69^2) ...
     sqrt((265+264)^2+69^2) sqrt((265+264+264)^2+58^2) ...
     sqrt((265+264+264)^2+58^2) sqrt((265+264+264+264)^2+35^2) ...
     sqrt((265+264+264+264)^2+35^2) 1345];

x(2,:)=[sqrt(265^2+75^2) 0 312 sqrt(264^2+(75-69)^2) ...
     sqrt(264^2+(75+69)^2) sqrt((264+264)^2+(75-58)^2) ...
     sqrt((264+264)^2+(75+58)^2) ...
         sqrt((264+264+264)^2+(75-35)^2) ...
     sqrt((264+264+264)^2+(75+35)^2) ...
         sqrt((264+264+264+268)^2+(75)^2)];

x(3,:)=[sqrt(265^2+75^2) 312 0 sqrt(264^2+(75+69)^2) ...
     sqrt(264^2+(75-69)^2) sqrt((264+264)^2+(75+58)^2) ...
     sqrt((264+264)^2+(75-58)^2) ...
         sqrt((264+264+264)^2+(75+35)^2) ...
     sqrt((264+264+264)^2+(75-35)^2) ...
         sqrt((264+264+264+268)^2+(75)^2)];

x(4,:)=[sqrt((265+264)^2+69^2) sqrt(264^2+(75-69)^2) ...
     sqrt(264^2+(75+69)^2) 0 302 sqrt(264^2+(69-58)^2) ...
     sqrt(264^2+(69+58)^2) sqrt((264+264)^2+(69-35)^2) ...
     sqrt((264+264)^2+(69+35)^2) sqrt((264+264+288)^2+(69)^2)];

x(5,:)=[sqrt((265+264)^2+69^2) sqrt(264^2+(75+69)^2) ...
     sqrt(264^2+(75-69)^2) 302 0 sqrt(264^2+(69+58)^2) ...
     sqrt(264^2+(69-58)^2) sqrt((264+264)^2+(69+35)^2) ...
     sqrt((264+264)^2+(69-35)^2) sqrt((264+264+288)^2+(69)^2)];

x(6,:)=[sqrt((265+264+264)^2+58^2) sqrt((264+264)^2+(75-58)^2) ...
     sqrt((264+264)^2+(75+58)^2) sqrt(264^2+(69-58)^2) ...
```

```
35      sqrt(264^2+(69+58)^2) 0 262 sqrt(264^2+(58-35)^2) ...
36      sqrt(264^2+(58+35)^2) sqrt((264+288)^2+(58)^2)];
37
38  x(7,:)=[sqrt((265+264+264)^2+58^2) sqrt((264+264)^2+(75+58)^2) ...
39      sqrt((264+264)^2+(75-58)^2) sqrt(264^2+(69+58)^2) ...
40      sqrt(264^2+(69-58)^2) 262 0 sqrt(264^2+(58+35)^2) ...
41      sqrt(264^2+(58-35)^2) sqrt((264+288)^2+(58)^2)];
42
43  x(8,:)=[sqrt((265+264+264+264)^2+35^2) ...
        sqrt((264+264+264)^2+(75-35)^2) ...
44      sqrt((264+264+264)^2+(75+35)^2) ...
            sqrt((264+264)^2+(69-35)^2) ...
45      sqrt((264+264)^2+(69+35)^2) sqrt(264^2+(58-35)^2) ...
46      sqrt(264^2+(58+35)^2) 0 178 sqrt(288^2+(35)^2)];
47
48  x(9,:)=[sqrt((265+264+264+264)^2+35^2) ...
        sqrt((264+264+264)^2+(75+35)^2) ...
49      sqrt((264+264+264)^2+(75-35)^2) sqrt((264+264)^2+(69+35)^2)...
50       sqrt((264+264)^2+(69-35)^2) sqrt(264^2+(58+35)^2) ...
51       sqrt(264^2+(58-35)^2) 178 0 sqrt(288^2+(35)^2)];
52
53  x(10,:)=[1345 sqrt((264+264+264+268)^2+(75)^2) ...
54      sqrt((264+264+264+268)^2+(75)^2) ...
            sqrt((264+264+288)^2+(69)^2) ...
55      sqrt((264+264+288)^2+(69)^2) sqrt((264+288)^2+(58)^2) ...
56      sqrt((264+288)^2+(58)^2) sqrt(288^2+(35)^2) ...
            sqrt(288^2+(35)^2) 0];
57
58  %Angle (in matrix form)
59  alfa=zeros(10);
60
61  alfa(1,:) = [0 atan(75/265) -atan(75/265) atan(69/(265+264)) ...
62               -atan(69/(265+264)) atan(58/(265+264+264)) ...
63               -atan(58/(265+264+264)) atan(35/(265+264+264+264)) ...
64               -atan(35/(265+264+264+264)) 0];
65
66  alfa(2,:) = [atan(75/265) 0 -(pi/2) -atan((75-69)/264) ...
67      -atan((75+69)/264) -atan((75-58)/(264*2)) ...
68      -atan((75+58)/(264*2)) -atan((75-35)/(264*3)), ...
69      -atan((75+35)/(264*3)) -atan((75)/(264*3+288))];
70
71  alfa(3,:) = [atan(75/265) (pi/2) 0 atan((75+69)/264), ...
```

```
72      atan(5/264), atan((75+58)/(264*2)) atan((75-58)/(264*2)), ...
73      atan((75+35)/(264*3)) atan((75-35)/(264*3))  ...
74      atan((75)/(264*3+288))];
75
76  alfa(4,:) = [atan(69/(265+264)), atan((75-69)/264), ...
77      atan((75+69)/264), 0, -pi/2, -atan(69-58/264), ...
78      -atan((69+58)/264), -atan((69-35)/(264*2)), ...
79      -atan((69+35)/(264*2)) -atan(69/(2*264+288))];
80
81  alfa(5,:) = [atan(69/(265+264)), atan((75+69)/264), ...
82       atan(5/264), pi/2, 0, atan((69+58)/264), atan(69-58/264), ...
83       atan((69+35)/(264*2)), atan((69-35)/(264*2)), ...
84       atan(69/(2*264+288))];
85
86  alfa(6,:) = [atan(58/(265+264+264)), atan((75-58)/(264*2)), ...
87      atan((75+58)/(264*2)), atan((69-58)/264), ...
88      atan((69+58)/264), 0, -pi/2, -atan((58-35)/264), ...
89      -atan((58+35)/264), -atan(58/(264+288))];
90
91  alfa(7,:) = [atan(58/(265+264+264)), atan((75+58)/(264*2)), ...
92       atan((75-58)/(264*2)), atan((69+58)/264), ...
93      atan((69-58)/264), pi/2, 0, atan((58+35)/264), ...
94      atan((58-35)/264),  atan(58/(264+288))];
95
96  alfa(8,:) = [atan(35/(265+264+264+264)), ...
       atan((75-35)/(264*3)), ...
97      atan((75+35)/(264*3)), atan((69-35)/(264*2)), ...
98      atan((69+35)/(264*2)), atan((58-35)/264), ...
99      atan((58+35)/264), 0, -pi/2, -atan(35/288)];
100
101 alfa(9,:) = [atan(35/(265+264+264+264)), ...
       atan((75+35)/(264*3)), ...
102     atan((75-35)/(264*3)), atan((69+35)/(264*2)), ...
103     atan((69-35)/(264*2)), atan((58+35)/264), ...
104     atan((58-35)/264), pi/2, 0,  atan(35/288)];
105
106 alfa(10,:) = [pi, atan((75)/(264*3+288)), ...
107     atan((75)/(264*3+288)), atan(69/(2*264+288)), ...
108     atan(69/(2*264+288)), atan(58/(264+288)), ...
109     atan(58/(264+288)), atan(35/288), atan(35/288), 0];
110
111 alfa = abs(alfa);
```

```
112
113 %Generating longitudinal and tangential distance
114 for n=1:length(x)
115 for m=1:length(x)
116     El(n,m)=abs(x(n,m)*cos(beta-alfa(n,m)));
117     Et(n,m)=abs(x(n,m)*sin(beta-alfa(n,m)));
118 end
119 end
120
121 %Oliveira coherency model
122 for i=1:2
123     alpha(i)=a(i)./f+b(i).*f+c(i);
124 end
125
126 for n=1:length(El)
127 for m=1:length(El)
128
129 Coh(n,m) = ...
       exp(-B3(1).*El(n,m)-B3(2).*Et(n,m)).*exp(-(alpha(1).*...
130     El(n,m).^(1/2)-alpha(2).*Et(n,m).^(1/2)).*(w1/(2*pi)).^2);
131 if Coh(n,m)>1
132     Coh(n,m)=1;
133 end
134
135 end
136 end
137
138 %Inter-component coherency
139 coh_xy=0.3537;
140 coh_xz=0.3506;
141 coh_yz=0.3295;
142
143 %Non-Coherent
144 % Coh=eye(10);
145 % coh_xy=0;
146 % coh_xz=0;
147 % coh_yz=0;
148
149
150 %Fully coherent
151 % Coh=ones(10);
152 % coh_xy=1;
```

```
153 % coh_xz=1;
154 % coh_yz=1;
155
156
157 WP=exp(-(1i*w1*x/V1));       %Wave passage effect
158 CohWP=Coh.*WP;               %Wave passage + incoherence
159
160 %Generating the coherency matrix
161 Sc=zeros(30);
162 for n=1:10
163     for m=1:10
164         Sc(n*3-2:n*3,m*3-2:m*3)=[CohWP(n,m) coh_xy*CohWP(n,m) ...
165             coh_xz*CohWP(n,m); coh_xy*CohWP(n,m) CohWP(n,m) ...
166             coh_yz*CohWP(n,m); coh_xz*CohWP(n,m) ...
                    coh_yz*CohWP(n,m) ...
167             CohWP(n,m)];
168     end
169 end
170
171 end
```

E.6 Ground acceleration spectral density

```
function [Sc]=Oliveira(B3,a,b,c,w1,beta,V1)

f=w1/(2*pi);    %Frequency in [Hz]

x=zeros(10);

%Distance between supports (in matrix form)
x(1,:)=[0 sqrt(265^2+75^2) sqrt(265^2+75^2) ...
    sqrt((265+264)^2+69^2) ...
     sqrt((265+264)^2+69^2) sqrt((265+264+264)^2+58^2) ...
     sqrt((265+264+264)^2+58^2) sqrt((265+264+264+264)^2+35^2) ...
     sqrt((265+264+264+264)^2+35^2) 1345];

x(2,:)=[sqrt(265^2+75^2) 0 312 sqrt(264^2+(75-69)^2) ...
     sqrt(264^2+(75+69)^2) sqrt((264+264)^2+(75-58)^2) ...
     sqrt((264+264)^2+(75+58)^2) ...
         sqrt((264+264+264)^2+(75-35)^2) ...
     sqrt((264+264+264)^2+(75+35)^2) ...
         sqrt((264+264+264+268)^2+(75)^2)];

x(3,:)=[sqrt(265^2+75^2) 312 0 sqrt(264^2+(75+69)^2) ...
     sqrt(264^2+(75-69)^2) sqrt((264+264)^2+(75+58)^2) ...
     sqrt((264+264)^2+(75-58)^2) ...
         sqrt((264+264+264)^2+(75+35)^2) ...
     sqrt((264+264+264)^2+(75-35)^2) ...
         sqrt((264+264+264+268)^2+(75)^2)];

x(4,:)=[sqrt((265+264)^2+69^2) sqrt(264^2+(75-69)^2) ...
     sqrt(264^2+(75+69)^2) 0 302 sqrt(264^2+(69-58)^2) ...
     sqrt(264^2+(69+58)^2) sqrt((264+264)^2+(69-35)^2) ...
     sqrt((264+264)^2+(69+35)^2) sqrt((264+264+288)^2+(69)^2)];

x(5,:)=[sqrt((265+264)^2+69^2) sqrt(264^2+(75+69)^2) ...
     sqrt(264^2+(75-69)^2) 302 0 sqrt(264^2+(69+58)^2) ...
     sqrt(264^2+(69-58)^2) sqrt((264+264)^2+(69+35)^2) ...
     sqrt((264+264)^2+(69-35)^2) sqrt((264+264+288)^2+(69)^2)];

x(6,:)=[sqrt((265+264+264)^2+58^2) sqrt((264+264)^2+(75-58)^2) ...
     sqrt((264+264)^2+(75+58)^2) sqrt(264^2+(69-58)^2) ...
```

```
35      sqrt(264^2+(69+58)^2) 0 262 sqrt(264^2+(58-35)^2) ...
36      sqrt(264^2+(58+35)^2) sqrt((264+288)^2+(58)^2)];
37
38  x(7,:)=[sqrt((265+264+264)^2+58^2) sqrt((264+264)^2+(75+58)^2) ...
39      sqrt((264+264)^2+(75-58)^2) sqrt(264^2+(69+58)^2) ...
40      sqrt(264^2+(69-58)^2) 262 0 sqrt(264^2+(58+35)^2) ...
41      sqrt(264^2+(58-35)^2) sqrt((264+288)^2+(58)^2)];
42
43  x(8,:)=[sqrt((265+264+264+264)^2+35^2) ...
        sqrt((264+264+264)^2+(75-35)^2) ...
44      sqrt((264+264+264)^2+(75+35)^2) ...
            sqrt((264+264)^2+(69-35)^2) ...
45      sqrt((264+264)^2+(69+35)^2) sqrt(264^2+(58-35)^2) ...
46      sqrt(264^2+(58+35)^2) 0 178 sqrt(288^2+(35)^2)];
47
48  x(9,:)=[sqrt((265+264+264+264)^2+35^2) ...
        sqrt((264+264+264)^2+(75+35)^2) ...
49      sqrt((264+264+264)^2+(75-35)^2) sqrt((264+264)^2+(69+35)^2)...
50       sqrt((264+264)^2+(69-35)^2) sqrt(264^2+(58+35)^2) ...
51       sqrt(264^2+(58-35)^2) 178 0 sqrt(288^2+(35)^2)];
52
53  x(10,:)=[1345 sqrt((264+264+264+268)^2+(75)^2) ...
54      sqrt((264+264+264+268)^2+(75)^2) ...
            sqrt((264+264+288)^2+(69)^2) ...
55      sqrt((264+264+288)^2+(69)^2) sqrt((264+288)^2+(58)^2) ...
56      sqrt((264+288)^2+(58)^2) sqrt(288^2+(35)^2) ...
            sqrt(288^2+(35)^2) 0];
57
58  %Angle (in matrix form)
59  alfa=zeros(10);
60
61  alfa(1,:) = [0 atan(75/265) -atan(75/265) atan(69/(265+264)) ...
62              -atan(69/(265+264)) atan(58/(265+264+264)) ...
63              -atan(58/(265+264+264)) atan(35/(265+264+264+264)) ...
64              -atan(35/(265+264+264+264)) 0];
65
66  alfa(2,:) = [atan(75/265) 0 -(pi/2) -atan((75-69)/264) ...
67      -atan((75+69)/264) -atan((75-58)/(264*2)) ...
68      -atan((75+58)/(264*2)) -atan((75-35)/(264*3)), ...
69      -atan((75+35)/(264*3)) -atan((75)/(264*3+288))];
70
71  alfa(3,:) = [atan(75/265) (pi/2) 0 atan((75+69)/264), ...
```

```
72      atan(5/264), atan((75+58)/(264*2)) atan((75-58)/(264*2)), ...
73      atan((75+35)/(264*3)) atan((75-35)/(264*3))  ...
74      atan((75)/(264*3+288))];
75
76  alfa(4,:) = [atan(69/(265+264)), atan((75-69)/264), ...
77      atan((75+69)/264), 0, -pi/2, -atan(69-58/264), ...
78      -atan((69+58)/264), -atan((69-35)/(264*2)), ...
79      -atan((69+35)/(264*2)) -atan(69/(2*264+288))];
80
81  alfa(5,:) = [atan(69/(265+264)), atan((75+69)/264), ...
82       atan(5/264), pi/2, 0, atan((69+58)/264), atan(69-58/264), ...
83       atan((69+35)/(264*2)), atan((69-35)/(264*2)), ...
84       atan(69/(2*264+288))];
85
86  alfa(6,:) = [atan(58/(265+264+264)), atan((75-58)/(264*2)), ...
87      atan((75+58)/(264*2)), atan((69-58)/264), ...
88      atan((69+58)/264), 0, -pi/2, -atan((58-35)/264), ...
89      -atan((58+35)/264), -atan(58/(264+288))];
90
91  alfa(7,:) = [atan(58/(265+264+264)), atan((75+58)/(264*2)), ...
92       atan((75-58)/(264*2)), atan((69+58)/264), ...
93      atan((69-58)/264), pi/2, 0, atan((58+35)/264), ...
94      atan((58-35)/264),  atan(58/(264+288))];
95
96  alfa(8,:) = [atan(35/(265+264+264+264)), ...
       atan((75-35)/(264*3)), ...
97      atan((75+35)/(264*3)), atan((69-35)/(264*2)), ...
98      atan((69+35)/(264*2)), atan((58-35)/264), ...
99      atan((58+35)/264), 0, -pi/2, -atan(35/288)];
100
101 alfa(9,:) = [atan(35/(265+264+264+264)), ...
       atan((75+35)/(264*3)), ...
102     atan((75-35)/(264*3)), atan((69+35)/(264*2)), ...
103     atan((69-35)/(264*2)), atan((58+35)/264), ...
104     atan((58-35)/264), pi/2, 0,  atan(35/288)];
105
106 alfa(10,:) = [pi, atan((75)/(264*3+288)), ...
107     atan((75)/(264*3+288)), atan(69/(2*264+288)), ...
108     atan(69/(2*264+288)), atan(58/(264+288)), ...
109     atan(58/(264+288)), atan(35/288), atan(35/288), 0];
110
111 alfa = abs(alfa);
```

```
112
113 %Generating longitudinal and tangential distance
114 for n=1:length(x)
115 for m=1:length(x)
116     El(n,m)=abs(x(n,m)*cos(beta-alfa(n,m)));
117     Et(n,m)=abs(x(n,m)*sin(beta-alfa(n,m)));
118 end
119 end
120
121 %Oliveira coherency model
122 for i=1:2
123     alpha(i)=a(i)./f+b(i).*f+c(i);
124 end
125
126 for n=1:length(El)
127 for m=1:length(El)
128
129 Coh(n,m) = ...
       exp(-B3(1).*El(n,m)-B3(2).*Et(n,m)).*exp(-(alpha(1).*...
130     El(n,m).^(1/2)-alpha(2).*Et(n,m).^(1/2)).*(w1/(2*pi)).^2);
131 if Coh(n,m)>1
132     Coh(n,m)=1;
133 end
134
135 end
136 end
137
138 %Inter-component coherency
139 coh_xy=0.3537;
140 coh_xz=0.3506;
141 coh_yz=0.3295;
142
143 %Non-Coherent
144 % Coh=eye(10);
145 % coh_xy=0;
146 % coh_xz=0;
147 % coh_yz=0;
148
149
150 %Fully coherent
151 % Coh=ones(10);
152 % coh_xy=1;
```

```
153 % coh_xz=1;
154 % coh_yz=1;
155
156
157 WP=exp(-(1i*w1*x/V1));      %Wave passage effect
158 CohWP=Coh.*WP;              %Wave passage + incoherence
159
160 %Generating the coherency matrix
161 Sc=zeros(30);
162 for n=1:10
163     for m=1:10
164         Sc(n*3-2:n*3,m*3-2:m*3)=[CohWP(n,m) coh_xy*CohWP(n,m) ...
165             coh_xz*CohWP(n,m); coh_xy*CohWP(n,m) CohWP(n,m) ...
166             coh_yz*CohWP(n,m); coh_xz*CohWP(n,m) ...
                    coh_yz*CohWP(n,m) ...
167             CohWP(n,m)];
168     end
169 end
170
171 end
```

E.7 Generation of Acceleration spectral density function

```
function [Sa Sv Sav Sva]=AccelSpectra(w1,wg,wh,Lg,Lh,S0)

%Kanai–Tajimi spectra
%First filter
Hg2=((1+(4*Lg^2)*(w1/wg).^2)./((1-(w1/wg).^2).^2+...
    (4*Lg^2)*(w1/wg).^2));

%Second filter
Hh2=(((w1/wh).^4)./((1-(w1/wh).^2).^2+(4*Lh^2)*(w1/wh).^2)) ;

 Sa= S0*Hg2.*Hh2; %Kanai–Tajimi %Auto–PSD (acceleration)

 Sav= 1i.*Sa./w1;        %Cross spectra
 Sva= -1i.*Sa./w1;
 Sv=Sa./(w1^2);          %Auto–PSD (velocity)
end
```

F Abaqus model

Introduced as an electronic supplement:

Filenames
SFT-model1.CAE - Finite element model of the SFT with inclined tension legs
SFT-model2.CAE - Finite element model of the SFT with vertical tension legs

G Reference Library

Introduced as an electronic supplement:

Filenames
Submerged Tunnels Reference Library.enl - Endnote reference library
Submerged Tunnels Reference Library.Data - PDF articles

References

Andrew, C.E. 1951. Floating tunnel for long water crossings. *Transactions of the american society of civil engineers*, **116**(1), 708–720.

Brandtzæg, A., Arild, A., Folkestad, O., Selberg, A. B., & Ødegård, E. 1971. *Vurdering av dykkede, flytende rørbroer*. Tech. rept. 130100. Selskapet for Industriell og Teknisk Forskning (SINTEF).

Bungum, H., Olesen, O., Pascal, C., Gibbons, S., Lindholm, C., & Vestol, O. 2010. To what extent is the present seismicity of norway driven by post-glacial rebound? *Journal of the geological society*, **167**(2), 373–384.

Cartwright, D. E., & Longuet-Higgins, M. S. 1956. The statistical distribution of the maxima of a random function. *Proceedings of the royal society of london. series a. mathematical and physical sciences*, **237**(1209), 212–232.

Caughey, T. K. 1960. Classical normal modes in damped linear dynamic systems. *Journal of applied mechanics*, **27**(2), 269–271.

Chen, W. J., & Huang, G. J. 2010. Seismic wave passage effect on dynamic response of submerged floating tunnels. *Isab-2010 - first international symposium on archimedes bridge*, **4**, 217–224.

Chopra, Anil K. 2012. *Dynamics of structures : theory and applications to earthquake engineering*. 4th edn. Upper Saddle River, N.J.: Pearson Prentice Hall.

Clough, Ray W., & Penzien, Joseph. 2010. *Dynamics of structures*. 2nd edn. Berkeley, Calif.: Computers and Structures.

Cook, Robert Davis, Malkus, David S., Plesha, Michael E., & Witt, Robert J. 2002. *Concepts and applications of finite element analysis*. 4th edn. Wiley.

Der Kiureghian, Armen. 1996. A coherency model for spatially varying ground motion. *Earthquake engineering & structural dynamics*, **25**(1), 99–111.

Di Pilato, M., Perotti, F., & Fogazzi, P. 2008. 3d dynamic response of submerged floating tunnels under seismic and hydrodynamic excitation. *Engineering structures*, **30**(1), 268–281.

Faltinsen, O. M. 1990. *Sea loads on ships and offshore structures*. Cambridge ocean technology series. Cambridge ; New York: Cambridge University Press.

FEHRL. 1996. *Analysis of the submerged floating tunnel concept*. Tech. rept. 1996/2a. Forum of European Highway Research Laboratories (FEHRL).

Fogazzi, P., & Perotti, F. 2000. The dynamic response of seabed anchored floating tunnels under seismic excitation. *Earthquake engineering & structural dynamics*, **29**(3), 273–295.

Giotta, Joseph (Narrator). 2003. *Transatlantic tunnel*. Extreme engineering, Documentary. Air date: 16 April 2003.

Harichandran, R., & Vanmarcke, E. 1986. Stochastic variation of earthquake ground motion in space and time. *Journal of engineering mechanics*, **112**(2), 154–174.

Hindy, A., & Novak, M. 1980. Pipeline response to random ground motion. *Journal of the engineering mechanics division-asce*, **106**(2), 339–360.

Holmås, T., & Fergestad, D. 1988. *Ikkelineær dynamisk analyse av rørbru*. Tech. rept. 710651. SINTEF.

Jakobsen, B. 2010. Design of the submerged floating tunnel operating under various conditions. *Isab-2010 - first international symposium on archimedes bridge*, **4**, 71–79.

Jøssang, Tor Inge. 2005. *Høgsfjord drømmer*. `http://www.aftenbladet.no/nyheter/lokalt/article173184.ece#.UbFuJ0AweuJ`. Accessed: 2013-06-07.

Kanie, S. 2010. Feasibility studies on various sft in japan and their technological evaluation. *Isab-2010 - first international symposium on archimedes bridge*, **4**, 13–20.

Kunisu, H. 2010. Evaluation of wave force acting on submerged floating tunnels. *Isab-2010 - first international symposium on archimedes bridge*, **4**, 99–105.

Langen, I., & Sigbjörnsson, R. 1979. *Dynamisk analyse av konstruksjoner*. Trondheim: Tapir.

Langen, I., & Sigbjörnsson, R. 1980. On stochastic dynamics of floating bridges. *Engineering structures*, **2**(4), 209–216.

Larssen, R. M., & Jakobsen, S. E. 2010. Submerged floating tunnels for crossing of wide and deep fjords. *Isab-2010 - first international symposium on archimedes bridge*, **4**, 171–178.

Lin, J.H., & Zhang, Y.H. 2007. Seismic random vibration of long-span structures. *Pages 1–41 of: Vibration monitoring, testing, and instrumentation*. Mechanical Engineering Series. CRC Press.

Liu, G. R., & Quek, S. S. 2003. *The finite element method : a practical course*. Oxford ; Boston: Butterworth-Heinemann.

Loh, C.H., & Yeh, G.T. 1988. Spatial variation and stochastic modeling of seismic differential ground movement. *Earthquake engineering & structural dynamics*, **16**(4), 583–596.

Luco, J. E., & Wong, H. L. 1986. Response of a rigid foundation to a spatially random ground motion. *Earthquake engineering & structural dynamics*, **14**(6), 891–908.

Martinelli, L., Barbella, G., & Feriani, A. 2011. A numerical procedure for simulating the multi-support seismic response of submerged floating tunnels anchored by cables. *Engineering structures*, **33**(10), 2850–2860.

Martire, G., Faggiano, B., Mazzolani, F. M., Zollo, A., & Stabile, T. A. 2010. Seismic analysis of a sft solution for the messina strait crossing. *Isab-2010 - first international symposium on archimedes bridge*, **4**, 303–310.

Martire, G., Faggiano, B., Mazzolani, F. M., Zollo, A., & Stabile, T. A. 2012. *A comprehensive study on the performance of submerged floating tunnels during severe seismic events*. Stessa 2012: Proceedings of the 7th International Conference on Behaviour of Steel Structures in Seismic Areas. Boca Raton: Crc Press-Taylor & Francis Group.

MATLAB. 2010. *version 7.10.0 (r2010a)*. Natick, Massachusetts, USA: The MathWorks Inc.

Mazzolani, F. M., Landolfo, R., Faggiano, B., Esposto, M., Perotti, F., & Barbella, G. 2008. Structural analyses of the submerged floating tunnel prototype in qiandao lake (pr of china). *Advances in structural engineering*, **11**(4), 439–454.

Morison, J. R., O'Brien, M. P., Johnson, J. W., & Schaaf, S. A. 1950. The force exerted by surface waves on piles. *Journal of petroleum technology*, **2**(5), 149–154.

Naess, Arvid, & Moan, Torgeir. 2013. *Stochastic dynamics of marine structures*. New York: Cambridge University Press.

NPRA, Norwegian Public Road Administration. 2011. *A feasibility study - how to cross the wide and deep sognefjord*. `http://www.vegvesen.no/_attachment/274047/binary/485789`. Accessed: 2013-06-08.

NPRA, Norwegian Public Road Administration. 2012. *Coastal highway route e39 - project overview*. `http://www.vegvesen.no/Vegprosjekter/ferjefriE39/Konferanse/BransjemoteJan2012/_attachment/301517?_ts=1350fe62b08`. Accessed: 2013-06-07.

Oliveira, Carlos S., Hao, Hong, & Penzien, J. 1991. Ground motion modeling for multiple-input structural analysis. *Structural safety*, **10**(13), 79–93.

Østlid, H. 2010. When is sft competitive? *Isab-2010 - first international symposium on archimedes bridge*, **4**, 81–89.

Priestley, M. B. 1965. Evolutionary spectra and non-stationary processes. *Journal of the royal statistical society. series b (methodological)*, **27**(2), 204–237.

Reed, Sir Edward James. 1886. *An improved sytem of connecting railways which are separated by straits, bays, rivers or other waters, with structures and apparatus for effecting the same*. Vol. 9558. Britain: Darling and Son.

Remseth, Svein, Leira, Bernt J., Okstad, Knut M., Mathisen, Kjell M., & Haukås, Terje. 1999. Dynamic response and fluid/structure interaction of submerged floating tunnels. *Computers and structures*, **72**, 659–685.

Sigbjörnsson, R., Rupakhety, R., Halldorsson, B., Snæbjörnsson, J.T., & Ólafsson, S. 2013. The may 2008 Ölfus earthquake in south iceland: Modelling incoherence of strong ground motion. *Proceedings of the international conference on*

earthquake engineering (se-50eee). 29 to 31 May 2013, Skopje, Republic of Macedonia.

SIMULIA. 2011. *Abaqus version 6.11-1*. Providence, Rhode Island, USA: Dassault Systmes Simulia Corp.

Skorpa, L. 2010. Developing new methods to cross wide and deep norwegian fjords. *Isab-2010 - first international symposium on archimedes bridge*, **4**, 81–89.

Tveit, P. 2010. Submerged floating tunnels (sfts) for norwegian fjords. *Isab-2010 - first international symposium on archimedes bridge*, **4**, 135–143.

Vanmarcke, Erik. 2010. *Random fields : analysis and synthesis*. Rev. and expanded new edn. Singapore ; Hackensack, NJ: World Scientific.

Vanmarcke, Erik H., & Lai, Shih-Sheng P. 1980. Strong-motion duration and rms amplitude of earthquake records. *Bulletin of the seismological society of america*, **70**(4), 1293–1307.

Wilson, E. L., & Penzien, J. 1972. Evaluation of orthogonal damping matrices. *International journal for numerical methods in engineering*, **4**(1), 5–10.

Wilson, Edward L. 2002. *Three-dimensional static and dynamic analysis of structures: A physical approach with emphasis on earthquake engineering*. 3rd edn. Berkley, CA: Computers & Structures.

Wilson, James F. 2003. *Dynamics of offshore structures (2nd edition)*. 2nd edn. John Wiley & Sons.

Xiang, Y., Liu, C., Zhang, K., & Wu, Q. 2010. Risk analysis and management of submerged floating tunnel and its application. *Isab-2010 - first international symposium on archimedes bridge*, **4**, 107–116.

Xiao, J. A., & Huang, G. J. 2010. Transverse earthquake response and design analysis of submerged floating tunnels with various shore connections. *Isab-2010 - first international symposium on archimedes bridge*, **4**, 233–242.

Yang, Q. S., & Chen, Y. J. 2000. A practical coherency model for spatially varying ground motions. *Structural engineering and mechanics*, **9**(2), 141–152.

Zerva, Aspasia. 2009. *Spatial variation of seismic ground motions : modeling and engineering applications*. Advances in engineering. Boca Raton: CRC Press.

Zerva, Aspasia, & Zervas, Vassilios. 2002. Spatial variation of seismic ground motions: An overview. *Applied mechanics reviews*, **55**(3), 271–297.

Zhang, Y. H., Li, Q. S., Lin, J. H., & Williams, F. W. 2009. Random vibration analysis of long-span structures subjected to spatially varying ground motions. *Soil dynamics and earthquake engineering*, **29**(4), 620–629.